Swirling Flow of an Oldroyd-B Fluid over a Rotating Disk

By

Abdul Hafeez

Department of Mathematics

Quaid-i-Azam University
Islamabad, Pakistan
2021

Swirling Flow of an Oldroyd-B Fluid over a Rotating Disk

By

Abdul Hafeez

Supervised By

Prof. Dr. Masood Khan

Department of Mathematics
Quaid-i-Azam University
Islamabad, Pakistan
2021

Swirling Flow of an Oldroyd-B Fluid over a Rotating Disk

By

Abdul Hafeez

A DISSERTATION SUBMITTED IN THE PARTIAL FULFILLMENT OF THE REQUIREMENT FOR

THE DEGREE OF

DOCTOR OF PHILOSOPHY

IN

MATHEMATICS

Supervised by

Prof. Dr. Masood Khan

Department of Mathematics
Quaid-i-Azam University
Islamabad, Pakistan
2021

Author's Declaration

I, **Abdul Hafeez,** hereby state that my PhD thesis titled "**Swirling Flow of an Oldroyd-B Fluid over a Rotating Disk**" is my own work and has not been submitted previously by me for taking any degree from the Quaid-I-Azam University Islamabad, Pakistan or anywhere else in the country/world.

At any time if my statement is found to be incorrect even after my graduate the university has the right to withdraw my PhD degree.

Name of Student: **Abdul Hafeez**

Date: **04-Feb-2022**

Plagiarism Undertaking

I solemnly declare that research work presented in the thesis titled "**Swirling Flow of an Oldroyd-B Fluid over a Rotating Disk**" is solely my research work with no significant contribution from any other person. Small contribution/help wherever taken has been duly acknowledged and that complete thesis has been written by me.

I understand the zero tolerance policy of the HEC and **Quaid-i-Azam University, Islamabad** towards plagiarism. Therefore, I as an Author of the above titled thesis declare that no portion of my thesis has been plagiarized and any material used as reference is properly referred/cited.

I undertake that if I am found guilty of any formal plagiarism in the above titled thesis even afterward of PhD degree, the University reserves the rights to withdraw/revoke my PhD degree and that HEC and the University has the right to publish my name on the HEC/University Website on which names of students are placed who submitted plagiarized thesis.

Student/Author Signature: _____

Name: **Abdul Hafeez**

Swirling Flow of an Oldroyd-B Fluid over a Rotating Disk

By

Abdul Hafeez

CERTIFICATE

A THESIS SUBMITTED IN THE PARTIAL FULFILLMENT OF THE REQUIREMENTS FOR THE DEGREE OF THE
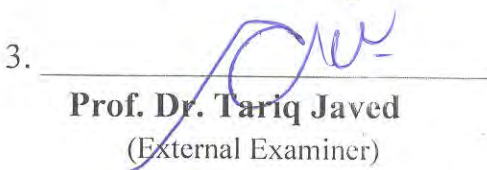
DOCTOR OF PHILOSOPHY IN MATHEMATICS

We accept this thesis as conforming to the required standard

1. _____
   Prof. Dr. Tariq Shah
   (Chairman)

2. _____
   Prof. Dr. Masood Khan
   (Supervisor)

3. _____
   Prof. Dr. Tariq Javed
   (External Examiner)

4. _____
   Dr. Abdullah Shah
   (External Examiner)

Department of Mathematics & Statistics
International Islamic University, Islamabad.

Department of Mathematics, COMSATS
University, Park Road Chak Shahzad,
Islamabad.

Department of Mathematics
Quaid-I-Azam University
Islamabad, Pakistan
2021

Certificate of Approval

This is to certify that the research work presented in this thesis entitled **Swirling Flow of an Oldroyd-B Fluid over a Rotating Disk** was conducted by **Mr. Abdul Hafeez** under the kind supervision of **Prof. Dr. Masood Khan**. No part of this thesis has been submitted anywhere else for any other degree. This thesis is submitted to the Department of Mathematics, Quaid-i-Azam University, Islamabad in partial fulfillment of the requirements for the degree of Doctor of Philosophy in field of Mathematics from Department of Mathematics, Quaid-i-Azam University Islamabad, Pakistan.

Student Name: **Abdul Hafeez**　　　　　　Signature:_____

External committee:

    a) **External Examiner 1**:　　　　　　Signature:_____
       Name: **Prof. Dr. Tariq Javed**
       Designation: Professor
       Office Address: Department of Mathematics & Statistics,
       International Islamic University, Islamabad.

    b) **External Examiner 2**:　　　　　　Signature:_____
       Name: **Dr. Abdullah Shah**
       Designation: Associate Professor
       Office Address: Department of Mathematics, COMSATS University,
       Park Road Chak Shahzad, Islamabad.

    c) **Internal Examiner**　　　　　　Signature:_____
       Name: **Prof. Dr. Masood Khan**
       Designation: Professor
       Office Address: Department of Mathematics, QAU Islamabad.

    Supervisor Name:　　　　　　Signature:_____
    Prof. Dr. Masood Khan

    Name of Dean/ HOD　　　　　　Signature:_____

    Prof. Dr. Tariq Shah

Dedicated to

My beloved parents

Acknowledgement

In the name of **ALLAH**, the Most Glorious and the Most Merciful Lord, the creator and all praises to **ALLAH** who guide me in darkness, helps me in troubles and empowers me to view tentative blocks as stepping stones to the stars to reach the eventual stage with courage. I am nothing without my **ALLAH** but I can achieve everything with assistance. All of my reverence and commitment goes to our **Prophet Hazrat Muhammad SAWW** the source of humanity, kindness and guidance for the whole creatures and who advised the mankind to pursue knowledge from cradle to grave.

First and foremost I would like to express my special appreciation and thanks to my PhD advisor Prof. Dr. Masood Khan, you have been a tremendous mentor for me. I would like to thank you for encouraging my research and for allowing me to grow as a research scientist. Your advice on both research as well as on my career have been invaluable. In short, your tireless work, unique way of research and devotion to your profession cannot be expressed in words.

I would like to thank my mother and father, whose love, prayers and guidance are with me to follow my dreams. I am very thankful to my loving parents for their guidance, support and encouragement. I owe my heartiest gratitude for their assistance and never ending prayers for success. I highly commend the cooperative behavior of my brothers and sisters who endeavored for my edification and betterment.

I gratefully acknowledge the Department of Mathematics, Quaid-i-Azam university Islamabad for this wonderful facilitation sources that made my PhD work possible. My sincere thanks also goes to chairman Department of Mathematics, Prof. Dr. Tariq Shah, who provide me the opportunity for this milestone achievement.

I thank my fellow labmates in for the stimulating discussions, for the sleepless nights we were working together, and for all the fun we have had in the last four years. A very special thank you to Dr. Jawad Ahmed for his invaluable advice and feedback on my research and for always being so supportive of my work. My time at Quaid-i-Azam University was also enriched by the graduates and fellows Dr. Awais Ahmed, Dr. Zahoor Iqbal, Dr. Aamir Hamid, Mahnoor Sarfraz, Muhammad Yasir.

In the end I would like to thank to all my research fellows and to those people who directly and indirectly helped me during my research work.

Best Regards

Abdul Hafeez

Contents

Abstract

Many substances in nature which are capable of flowing but their flow characteristics cannot be effectively described by the classical linearly viscous fluid model. These materials are called non-Newtonian fluids. Such as liquid foams, polymeric fluids, slurries, and food products etc. In order to describe the perplexing rheology of these natural liquids researchers put their efforts adequately, owing to their recently acquired tremendous importance in mechanical, industrial and commercial applications. Further, swirling flows of non-linear fluids due to a rotating geometry has been an advanced area of research due to its wide-ranging applications in technologies, engineering and numerous fields of science.

The main contribution in this thesis is focused on the mathematical modeling and analysis of rotating flows with heat and mass transport mechanisms involving Oldroyd-B fluid, which is a subclass of non-Newtonian viscoelastic fluid. The von Karman transformations are implemented to convert the modeled governing partial differential equations (PDEs) into dimensionless ordinary differential equations (ODEs). The couple system of modeled equations is extremely hard to compute exact solutions. Hence, to handle such flow problems of the rotating disk system, numerical and semi analytical approaches are utilized. The bvp midrich and homotopy analysis methods have been exercised to gain insight into the physics of the considered problems in terms of the flow behavior of Oldroyd-B fluid with thermal and solutal characteristics.

In this research work, the diverse physical phenomena are analyzed and presented graphically. The heat and mass transfer rates are calculated in terms of the Nusselt and Sherwood numbers, respectively. It is found that the higher estimation of magnetic force, in general, reduces the motion of the fluid in the radial and azimuthal directions. Additionally, an in-

crement in the stretching parameter develops the radial velocity component and diminishes the azimuthal velocity component. Further, the Deborah number of retardation time plays an important role in enhancing the thickness of thermal and concentration boundary layers.

Chapter 1

Introduction

This chapter consists of preliminary, literature survey and motivation that encourage us to pursue the current research. Additionally, the outline of the thesis are briefly described at the end.

1.1 Motivation and Literature Survey

The complex rheology of biological and various other fluids utilized in engineering and industries, have inspired the researchers to investigate them with the help of several non-Newtonian fluids models. When the viscosity is variable based, it is classified as non-Newtonian fluid. Recently, for mechanical and industrial applications, non-Newtonian fluids have gained much importance. Materials such as ketchup, mud, blood, shampoos, oils and many other thin and thick substances behave like fluids and are treated as non-Newtonian fluids. Generally, there are three types of non-Newtonian fluids namely, the rate type, the differential type and the integral type. The rate type fluids demonstrate the relaxation and retardation times behavior. The Oldroyd-B

fluid is a rate type material which exhibits both relaxation and retardation times effects of viscoelastic material. This model was proposed by Oldroyd [1]. After that, several researchers have done their work on the properties of Oldroyd-B fluid model. The flow of viscoelastic fluid by a stretching sheet by using an Oldroyd-B fluid model was initially described by Sajid et al. [2]. They developed the mathematical modelling for two dimensional flow of an Oldroyd-B fluid and acquired numerical solutions with the help of finite difference method. Further, the series solutions of three dimensional boundary layer flow of an Oldroyd-B fluid with the impact of heat absorption/generation were discovered by Shehzad et al. [3]. In this study, the flow is generated by a stretching of the surface. Additionally, the study of MHD flow of Oldroyd-B nanofluid induced by a stretching sheet was analyzed by Hayat et al. [4] and calculated the analytical solution of the problem. Mahanthesh et al. [5] discussed the three-dimensional convective flow of an Oldroyd-B fluid. For the numerical solution, the shooting method was used. The steady flow of Oldroyd-B nanofluid with the impact of Joule heating and thermal radiation was studied by Kumar et al. [6]. Moreover, rotating electroosmotic flow of an Oldroyd-B fluid in a microchannel with slip effect was investigated by Liang et al. [7]. This study shows that the slip boundary effect can reduce the boundary stress and promotes the development of flow of the fluid.

Nowadays, the flow over rotating disk has been an advanced area of research for the investigators and engineers due to its wide-range applications in advanced technologies, engineering and numerous fields of science. In real life applications, for instance, centrifugal pumps, aeronautical science, engineering branches as rotating machinery, gas turbine rotors, thermal power generating system, air vacuuming apparatuses and medical equipment and so many others. For this reason, the rotating disk fluid motion has been concentrated with enormous attention

7

and examined by several scientists. The fluid flow by a rotating disk was first studied by von Karman [8]. In this study, he obtained the approximate solution by using the integral method. Afterward, many analysts reported Karman's renowned work with various features for many physical problems. Cochran [9] investigated the fluid flow due to a rotating disk. Three dimensional MHD von Karman flow problem over a rotating disk was discussed by Turkyilmazoglu [10, 11]. Furthermore, Turkyilmazoglu [12] analyzed the nanofluid flow and heat transport by a rotating disk. The flow over a rotating disk with entropy generation was investigated by Rashidi et al. [13]. Additionally, nano-ferroliquid flow, under the influence of a low oscillating stretchable rotating disk discussed by Ellahi et al. [14] and obtained analytical series solution. The recent development in the study of flows over a rotating disk can be viewed via articles [15 − 18].

Due to the presence of suspended nanoparticles with high thermal conductivity, nanofluids are expected to provide better thermal efficiency compared with conventional fluids. Nanofluids have improved properties which potentially make them useful in many heat transfer applications, such as fuel cells, hybrid powered engines, domestic refrigerators, and thermal management in vehicle/engine cooling. Nanofluid, which is a mixture of a base fluid and solid nanoparticles, has recently been studied by many scientists. These composites include nanoparticles with their size ranging from 1 nm to 100 nm embedded in the base fluid and were initially proposed by Choi and Eastman [19]. In their study, they argued that these nanofluids have higher conductive and convective heat transfer relative to the base fluids. Afterwards, several scientists focused on the characteristics of the nanofluid flow. Buongiorno [20] suggested a mathematical model using the thermophoresis and Brownian motion effects to analyze the thermal features of the nanofluids. He found that the conventional fluid with thermophoresis and Brownian

motion effects played a significant role in improving the thermal conductivity of the liquid. The nanofluid over a shrinking surface was investigated by Khan and Pop [21]. Further, the flow and heat transfer of the Carreau fluid in the presence of nanoparticles was studied by Hashim et al. [22]. They used a built-in technique (bvp4c) in MATLAB to acquire the numerical solutions. Additionally, the turbulent nanofluid flow in a pipe was described by Jafaryar et al. [23]. The flow of thermally radiative and magnetized nanofluid flow was described by Hamid et al. [24]. They found dual solutions of the problem. The study of magnetized three-dimensional flow of viscoelastic nanofluid with nonlinear thermal radiation was investigated by Hayat et al. [25]. Recently, swirling flow of Maxwell nanofluid flow over a rotating disk featuring the Cattaneo-Christov double diffusion theory was discussed by Ahmed et al. [26]. They used Buongiorno model to study the thermophoresis diffusion and Brownian motion of the nanoparticles.

The MHD named as magneto-hydro-dynamic is the study of magnetic properties of electrically conducting fluid flow such as, liquid metals, plasmas and salted water. There are some specific uses based on MHD flows include MHD flow control in atomic reactors, MHD pipe flows, drug delivery, biomedicine, cancer therapy, magneto-optical wavelength filters etc. Physically, magnetic field is a resistive force applied on the liquid to control the fluid motion which was initially studied by Hannes Alfvén [27]. Later on, many researchers discussed the fluid flow behavior and heat transfer phenomenon under the influence of magnetic field. Soret and Dufour effects on unsteady MHD flow of Maxwell fluid in a porous medium were explored by Zhao et al. [28]. They concluded that the temperature of the liquid rises by enlargement of magnetic field parameter. Sheikholeslami and Rokni [29] studied the magnetic field effect on the flow of nanofluid and proved that the temperature gradient reduces by the increment of magnetic field. The investigation of external magnetic source on nanofluid flow in cavity was analyzed by

9

Sheikholeslami and Shehzad [30]. The enhancement of heat transfer in MHD nanofluid past a vertical plate was investigated by Sheri and Thummai [31]. Their outcomes demonstrate that the Lorentz force appears to slow down the heat transfer rate. Further, the MHD flow around an electrically conducting heating cylinder with the impact of non-uniform magnetic field was disclosed by Tassone et al. [32]. Most recently, MHD flow of Maxwell nanofluid flow induced by a stretching cylinder was numerically studied by Ahmed et al. [33]. They proved that the velocity of the fluid reduces due to higher magnitude of magnetic force.

Based on the applications in engineering fields and industries like hot rolling, paper making, wire drawing and much more, the stagnation point flow has been extensively investigated by the researchers. The quality of such products may be checked with the flow field and heat transfer rate. Initially in 1911, the stagnation point flow was proposed by Hiemenz [34]. He used the similarity variables to solve the two dimensional stagnation point flow and obtained the exact solution of the problem. After that the study of stagnation point flow towards a stretching plate was disclosed by Chiam [35]. Later on, many researchers have done their work on stagnation point flow of different fluid models. The study of heat transport in a stagnation point flow over a stretching sheet was explored by Chiam [36]. In this investigation, he used regular perturbation technique to obtain the analytical solutions upto second order. Mahapatra and Gupta [37] also investigated the incompressible stagnation point fluid flow over a stretching sheet. The magnetized stagnation point flow towards a stretching sheet was disclosed numerically by Ishak et al. [38]. They found that the temperature of the liquid reduces by enhancing the velocity ratio parameter. Further, the solution of stagnation point flow of nanofluid was claimed by Mustafa et al. [39] and the analytical solution via homotopy analysis method is obtained. The study of two dimensional stagnation point flow of Maxwell fluid over a shrinking sheet was

reported by Motsa et al. [40]. The solution of the governing equations constructed by using successive linearisation method. Moreover, the partial slip effect on stagnation point flow of incompressible fluid by a shrinking sheet was studied by Bhattacharyya et al. [41]. Recently, Khan et al. [42] investigated the stagnation point flow of nanofluid towards a permeable surface with the impact of thermal radiation. They utilized a numerical bvp4c technique and obtained dual nature solutions. Additionally, the stagnation point flow of Williamson fluid with the effect of Ohmic heating was studied by Hamid et al. [43]. They dealt with the problem numerically and discussed the dual nature study.

Heat transfer is a natural process in nature, as it occurs as a result of difference in temperature between the same objects or different two objects. The most important was this can be found in geothermal, petroleum and so forth. Therefore, much attention has been paid to predicting the heat transport mechanism. In order to predict the thermal energy transport mechanism in the fluid flow, Fourier's law of heat conduction is employed. This renowned law was firstly discussed by Fourier [44]. One of the defects pointed out in this law is that it leads to a parabolic equation in the sense that any initial interruption is quickly felt all through the whole substance, that negates the causality principle in continuum which is not a realistic approach. Thus, the instant heat conduction in the medium is a paradox. To resolve this paradox, Cattaneo [45] and Christov [46] proposed a revised model for heat conduction by introducing the thermal relaxation time parameter with an upper convective derivative in Fourier's model. This newly suggested model predicted the heat transport mechanism accurately. Additionally, the structure and uniqueness of the Cattaneo-Christov equation were described by Ciarletta and Straughan [47]. The study of thermal convection with the Cattaneo-Christov model was described by Straughan [48]. Moreover, Han et al. [49] discussed the flow and heat transfer in

the viscoelastic fluid with the Cattaneo-Christov heat flux model. The analysis of the Cattaneo-Christov double diffusion theory on the magnetohydrodynamic (MHD) flow of the micropolar fluid over an oscillatory disk was studied by Rauf et al. [50], and the numerical solutions to the problem were obtained. Some articles based on the investigation of Cattaneo-Christov theory are given in Refs. ([51] and [52]).

1.2   Basic Laws

In fluid dynamics, the conservation laws are the fundamental axioms which are mass conservation, momentum conservation and energy conservation. These laws are used to formulate the fluid flow problems and may be written in integral or differential form.

1.2.1   The Mass Conservation

This law describes that mass is conserved within the control volume for constant density fluids. In this way, the total mass entering in the control volume is equal to the total mass leaving to the control volume in the addition of mass inside the control volume. This law can be stated in mathematical form as:

$$\int_{v(t)} \left(\frac{\partial \rho}{\partial t} + \boldsymbol{\nabla} \cdot (\rho \mathbf{V}) \right) dv = 0. \tag{1.1}$$

As this is true for all $v(t)$, so the integrand vanishes at every point. So, the law of mass conservation is given by

$$\frac{\partial \rho}{\partial t} + \boldsymbol{\nabla} \cdot (\rho \mathbf{V}) = 0. \tag{1.2}$$

The above-mentioned law is also known as the continuity equation. Here, ρ denotes the fluid density, $\mathbf{V}$ the velocity field and t for the time.

12

For steady and incompressible flow, the continuity equation becomes

$$\boldsymbol{\nabla} \cdot \mathbf{V} = 0. \tag{1.3}$$

1.2.2 The Momentum Conservation

According to Newton's second law of motion, which states that the time rate of momentum in a control volume equals the resultant force acting on it. Mathematically as:

$$\int_{v(t)} \left[\frac{\partial \rho \mathbf{V}_\alpha}{\partial t} + \left(\rho \mathbf{V}_\alpha \mathbf{V}_\beta \right)_{,\beta} \right] dv = \int_{v(t)} \left[\rho \mathbf{B} + \boldsymbol{\tau}_{\alpha\beta,\beta} \right] dv. \tag{1.4}$$

It implies that

$$\frac{\partial \rho \mathbf{V}_\alpha}{\partial t} + \left(\rho \mathbf{V}_\alpha \mathbf{V}_\beta \right)_{,\beta} = \rho \mathbf{B} + \boldsymbol{\tau}_{\alpha\beta,\beta}\,, \tag{1.5}$$

which is the momentum conservation law.

Here, $\mathbf{B}$ is the body force per unit volume and $\boldsymbol{\tau}_{\alpha\beta}$ the stress tensor.

Also, expressing the above in more convenient form as:

$$\rho \left[\frac{\partial \mathbf{V}}{\partial t} + \mathbf{V} \cdot \boldsymbol{\nabla} \mathbf{V} \right] = \operatorname{div} \boldsymbol{\tau} + \rho \mathbf{B}. \tag{1.6}$$

1.2.3 The Energy Conservation

From the first law of thermodynamics, the conservation of energy takes the mathematical form as:

$$\rho c_p \frac{dT}{dt} = \boldsymbol{\tau}.\mathbf{L} - \operatorname{div} \mathbf{q_r} - \operatorname{div} \mathbf{q}. \tag{1.7}$$

13

In the above equation, ρ is the fluid density, (c_p, T) denote the specific heat and temperature of fluid, respectively. Further, $\boldsymbol{\tau}$ is the Cauchy stress tensor, $\mathbf{L}$ the velocity gradient, $(\mathbf{q}_r, \mathbf{q})$ depict the radiative and thermal heat flux, respectively, and $\boldsymbol{\tau}.\mathbf{L}$ represents the viscous dissipation.

On the other hand, the energy flux $\mathbf{q}$ for Fourier's law is defined as

$$\mathbf{q} = -k\boldsymbol{\nabla}T, \tag{1.8}$$

with k as the fluid thermal conductivity.

1.2.4 The Concentration Conservation

By this law, the rise in the total mass of species C in control volume is equal to the total net mass flow in control volume with the addition of the development rate of species in control volume. Mathematically, it can be written as

$$\frac{\partial C}{\partial t} + \mathbf{V} \cdot \boldsymbol{\nabla}C = -\boldsymbol{\nabla} \cdot \mathbf{j} + R. \tag{1.9}$$

Here, C is the concentration of the liquid, $\mathbf{j}$ the normal mass flux and R the "source" or "sink" for concentration.

The normal mass flux $\mathbf{j}$ is usually defined by Fick's law as

$$\mathbf{j} = -D\boldsymbol{\nabla}C, \tag{1.10}$$

where D stands for the mass diffusivity.

1.2.5   The Energy Conservation for Nanofluids

For an incompressible nanofluid flow, the energy conservation is defined by

$$\rho c_p \frac{dT}{dt} = -h_p \boldsymbol{\nabla} \cdot \mathbf{j}_p - \operatorname{div} \mathbf{q}_p. \tag{1.11}$$

Here, $(\mathbf{q}_p, h_p, \mathbf{j}_p)$ are the thermal flux of nanofluids, the enthalpy and the total nanoparticle mass flux, respectively.

The mathematical forms of $\mathbf{q}_p$ and $\mathbf{j}_p$ are as follows:

$$\mathbf{q}_p = -k\boldsymbol{\nabla}T + h_p \mathbf{j}_p, \tag{1.12}$$

$$\mathbf{j}_p = -\rho_p \left[D_B \boldsymbol{\nabla}C + D_T \frac{\boldsymbol{\nabla}T}{T_\infty} \right], \tag{1.13}$$

where, $\left(\rho_p, D_B, D_T \right)$ are the density of nanofluid, the Brownian motion and thermophoretic diffusion coefficients, respectively.

After applying the expressions $\mathbf{q}_p$ and $\mathbf{j}_p$ into Eq. (1.11) finally takes the form

$$\rho c_p \frac{dT}{dt} = k\boldsymbol{\nabla}^2 T + \rho_p c_p \left[D_B \boldsymbol{\nabla}C \cdot \boldsymbol{\nabla}T + D_T \frac{\boldsymbol{\nabla}T \cdot \boldsymbol{\nabla}T}{T_\infty} \right]. \tag{1.14}$$

1.2.6   The Mass Conservation for Nanofluids

The concentration equation for nanofluid is written in mathematically as

$$\frac{\partial C}{\partial t} + \mathbf{V} \cdot \boldsymbol{\nabla}C = -\frac{1}{\rho_p} \boldsymbol{\nabla} \cdot \mathbf{j}_p. \tag{1.15}$$

After applying the expression $\mathbf{j}_p$ into Eq. (1.15) result in

$$\frac{\partial C}{\partial t} + \mathbf{V} \cdot \boldsymbol{\nabla} C = D_B \boldsymbol{\nabla}^2 C + D_T \frac{\boldsymbol{\nabla}^2 T}{T_\infty}. \tag{1.16}$$

1.2.7 The Cattaneo-Christov Heat and Mass Fluxes

The generalization of Fourier's and Fick's laws in the form of Cattaneo-Christov model are given by the following mathematical relations:

$$\mathbf{q} + \varepsilon_0 \left(\frac{\partial \mathbf{q}}{\partial t} - \mathbf{q} \cdot \boldsymbol{\nabla} \mathbf{V} + \mathbf{V} \cdot \boldsymbol{\nabla} \mathbf{q} + (\boldsymbol{\nabla} \cdot \mathbf{V}) \mathbf{q} \right) = -k \boldsymbol{\nabla} T, \tag{1.17}$$

$$\mathbf{j} + \varepsilon_1 \left(\frac{\partial \mathbf{J}}{\partial t} - \mathbf{J} \cdot \boldsymbol{\nabla} \mathbf{V} + \mathbf{V} \cdot \boldsymbol{\nabla} \mathbf{J} + (\boldsymbol{\nabla} \cdot \mathbf{V}) \mathbf{J} \right) = -D_B \boldsymbol{\nabla} C, \tag{1.18}$$

where $(\varepsilon_0, \ \varepsilon_1)$ are the thermal and mass relaxation times, respectively. These reduce to classical Fourier's and Fick's laws when $\varepsilon_0 = \varepsilon_1 = 0$.

For steady and incompressible fluid flow, the above equations reduce to

$$\mathbf{q} + \varepsilon_0 \left(\mathbf{V} \cdot \boldsymbol{\nabla} \mathbf{q} - \mathbf{q} \cdot \boldsymbol{\nabla} \mathbf{V} \right) = -k \boldsymbol{\nabla} T, \tag{1.19}$$

$$\mathbf{j} + \varepsilon_1 \left(\mathbf{V} \cdot \boldsymbol{\nabla} \mathbf{J} - \mathbf{J} \cdot \boldsymbol{\nabla} \mathbf{V} \right) = -D_B \boldsymbol{\nabla} C. \tag{1.20}$$

1.3 Homogeneous and Heterogeneous Reactions

The homogeneous and heterogeneous reactions of two chemical species A and B are taken as inspired by Merkin [57]. The homogeneous reaction for cubic autocatalysis is written as

$$A + 2B \rightarrow 3B; \qquad rate = k_c ab^2, \tag{1.21}$$
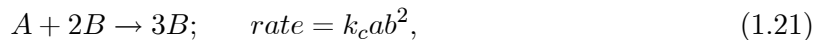
and the heterogeneous reaction is

$$A \rightarrow B; \qquad rate = k_s a. \tag{1.22}$$

Here A and B denote the chemical species, a and b be their concentrations and (k_c and k_s) the rate constants. The reactions mentioned above are assumed to be isothermal.

1.4 The Rate Type Oldroyd-B Fluid Model

Generally, there are three types of non-Newtonian fluids that are the rate type, differential type and integral type. The viscoelastic rate type fluids demonstrate the relaxation and retardation times effects. The Oldroyd-B fluid [1] is a subclass of viscoelastic rate type materials.

The extra stress tensor $\mathbf{S}$ for an Oldroyd-B fluid model is written as

$$\left(1 + \lambda_1 \frac{D}{Dt}\right) \mathbf{S} = \mu \left(1 + \lambda_2 \frac{D}{Dt}\right) \mathbf{A_1}, \tag{1.23}$$

where μ, λ_1 and λ_2 are the dynamic viscosity, the relaxation and retardation times, respectively. Further $\mathbf{A_1} = \boldsymbol{\nabla V} + (\boldsymbol{\nabla V})^t$ with t being transpose, is the first Rivlin-Ericksen tensor and $\frac{D}{Dt}$

17

the upper convected derivative. Moreover, the relation between extra stress tensor and Cauchy stress tensor is defined in the following form

$$\boldsymbol{\tau} + p\mathbf{I} - \mathbf{S} = 0, \tag{1.24}$$

where $\mathbf{I}$ refers the identity tensor and p the fluid pressure.

1.5 Solution Methodologies

1.5.1 Bvp Midrich Scheme (Midpoint Method)

The non-linear system of ordinary differential equations (ODEs) with appropriate boundary conditions (BCs) are extremely hard to compute exact solutions of the problem. So, to handle these non-linear differential equations, there are very helpful and efficient methods such as trapdefer, traprich, middefer and midrich to compute numerical solutions. The methods, trapdefer and traprich are based on trapezoid methods that use Richardson extrapolation enhancement or deferred correction enhancement, respectively. However, the methods, middefer and midrich are the midpoint methods with the same enhancement schemes. Maple software is used to perform the numerical computation. The bvp midrich scheme is specified by the following general algorithm

$$\tilde{X}{}'\left(\tilde{t}\right) = \tilde{F}\left(\tilde{t}, \tilde{X}\left(\tilde{t}\right)\right), \ \tilde{X}\left(\overset{\sim}{t_0}\right) = \tilde{X}_0. \tag{1.25}$$

The term used for the modified Euler method (Explicit mid-point method) is given by

$$\tilde{X}_{n+1} = \tilde{X}_n + h\tilde{F}\left(\tilde{t}_n + \frac{h}{2}, \ \tilde{X}_n + \frac{h}{2}\tilde{F}\left(\tilde{t}_n, \tilde{X}_n\right)\right), \tag{1.26}$$

where h refers the step size and $\tilde{t}_n = \tilde{t}_0 + nh$. The implicit approach of the mid-point method strategy is articulated as

$$\tilde{X}_{n+1} = \tilde{X}_n + h\tilde{F}\left(\tilde{t}_n + \frac{h}{2}, \ \tilde{X}_n + \frac{1}{2}\left(\tilde{X}_n, \tilde{X}_{n+1}\right)\right), \qquad n = 0, 1, 2, \dots \tag{1.27}$$

The local error of the mid-point procedure is of order $O\left(h^3\right)$ and $O\left(h^2\right)$ is the order of global error at each step. With more computational intensive, the algorithm error declines faster as $h \to 0$ and shall be a more stable solution.

1.5.2 Homotopy Analysis Method (HAM)

For solving the non-linear system of ordinary differential equations (ODEs) with suitable boundary conditions are acquired by adopting the well-known semi-analytical technique (HAM). We use the initial guesses $(H_0, G_0, \theta_0, \phi_0)$ and auxiliary linear operators $(\pounds_H, \pounds_G, \pounds_\theta, \pounds_\phi)$ to construct a homotopic series solution using the homotopy approach. Mathematically,

$$
\begin{aligned}
\pounds_H[H(\eta)] &= H''' - H', \ \pounds_G[G(\eta)] = G'' - G, \\
\pounds_\theta[\theta(\eta)] &= \theta'' - \theta, \ \pounds_\phi[\phi(\eta)] = \phi'' - \phi.
\end{aligned}
\tag{1.28}
$$

1.6   Scope of Research

The research in this dissertation contributes to recent scientific and technological developments while considering the non-Newtonian Oldroyd-B fluid flow caused by a rotating disk geometry. For this, the mathematical modelling is developed and discussed the mechanism of swirling flow of non-Newtonian Oldroyd- B fluid. The heat and mass transport in Oldroyd-B fluid flow are of particular interest. In order to describe the physical results, numerical and semi analytical schemes are used for obtaining solutions of the considered problems. Thus, the following objectives are pursued in this study:

- Mathematical modeling of Oldroyd-B fluid flow over a rotating disk is carried out.

- The analysis of heat and mass transport are performed with various physical effects.

- The graphical and tabular results are obtained for the physical interpretation of flow, heat and mass transport phenomena.

1.7   Contribution in Thesis

The aim of this study is to learn more about the heat and mass transport mechanisms for non-Newtonian Oldroyd-B fluid flow over a rotating disk. In this thesis, numerical and analytical approaches are utilized to investigate the flow behavior, heat and mass transfer features for three dimensional axisymmetric flow through a rotating disk geometry. Indeed, no existing studies of Oldroyd-B fluid flow model were carried out in the rotating disk regime earlier to this work.

Therefore, the most significant contributions of this thesis include the development of math-

ematical modelling and their solutions under various physical aspects. The substantial contents of this thesis has already published. This section briefly lists all the research materials produced during this project. The work in this thesis is arranged as follow:

Chapter 2: This chapter presents a mathematical formulation of three dimensional steady, incompressible flow of Oldroyd-B fluid by a rotating disk. An innovative Buongiorno's model is introduced to characterize the heat and mass transport of Oldroyd-B nanofluid considering the impacts of thermophoresis and Brownian diffusion. Consideration is focused on mathematical formulation of momentum equation based on boundary layer approximation theory. For non-dimensionalized of the problem, the von Karman similarity approach is used and then utilizing a numerical technique (bvp midrich) to acquire the solutions. The analysis done in this chapter is published in "**Applied Nanoscience, 10 (2020) 5135-5147**".

Chapter 3: The leading objective of this chapter is to investigate the impact of activation energy in Oldroyd-B fluid flow over a rotating disk. The thermal energy transport analysis is performed with the non-linear thermal radiation. The problem is tackled numerically by bvp midrich scheme. The graphical and tabular results are obtained for the velocity field, thermal and solutal distributions as well as Nusselt and Sherwood numbers, respectively. The findings of this chapter are available in "." **Physica A: Statistical Mechanics and its Applications, (2021) 124085**".

Chapter 4: The prime objective in this chapter is to elaborate the stagnation point flow of Oldroyd-B fluid due to a permeable rotating disk. The impact of non-linear radiation and heat absorption/generation are introduced to visualize the heat transfer behavior. The convective boundary condition is also assumed in order to investigate the fluid thermal characteristics. To acquire results of the problem, a numerical procedure is utilized to handle the problem work.

Additionally, the current results are compared to the previous literature. This research work is published in "**Computer Methods and Programs in Biomedicine, 191 (2020) 105342**".

Chapter 5: The main focus in this chapter is to examine the Darcy flow of an Oldroyd-B fluid. The mechanisms of heat and mass transport are investigated with the significant features of thermal diffusion (Soret) and diffusion thermo (Dufour). Further, the impact of chemical reaction is also assumed on solutal field. To handle the governing problem, the von Karman variables are utilized to get the similarity equations and then integrated numerically via bvp midrich method in Maple. The remarkable results of this chapter are presented in "**Arabian Journal for Science and Engineering, 45 (2020) 5949–5957**".

Chapter 6: This chapter explores the chemically reactive flow of Oldroyd-B fluid by a rotating disk geometry. In this analysis, the Cattaneo-Christov heat flux theory (modified Fourier's law) is used to discuss the fluid thermal features. Moreover, the effect of homogeneous and heterogeneous reactions are considered for the mass transport phenomenon. For obtaining numerical results, a bvp midrich scheme is implemented. The results are available in "**Journal of Thermal Analysis and Calorimetry, 144 (2021) 793-803**".

Chapter 7: An investigation regarding the features of Cattaneo-Christov theory for heat and mass flux in the flow of Oldroyd-B fluid is endorsed in this chapter. The transformed ordinary differential equations are considered for the solutions via an analytical technique (HAM) in Mathematica software. The impacts of physical parameters are illustrated graphically. The work provided in this chapter is published in "**International Communications in Heat and Mass Transfer, 123 (2021) 105179**".

Chapter 8: In this chapter, the presented modeling describes the rotational flow of the viscoelastic Oldroyd-B nanofluid by a rotating disk. A progressive alteration is made in the

heat and concentration equations by exploiting the Cattaneo-Christov heat and mass flux expressions. The Buongiorno model along with the Cattaneo-Christov theory is implemented in the Oldroyd-B nanofluid flow to investigate the mechanisms of heat and mass transport. A link between analytical and numerical results are made via table. The analysis done in this chapter is presented in "**Applied Mathematics and Mechanics (English Edition), 41 (2020) 1083-1094**".

Chapter 9: Finally, this chapter presents the key outcomes of this thesis as well as suggestions for future work.

Chapter 2

Flow of Magnetized Oldroyd-B Nanofluid over a Rotating Disk

In this chapter, the characteristics of an Oldroyd-B nanofluid flow caused by axially symmetric rotating disk are analyzed with the features of vertically applied magnetic field. An innovative Buongiorno model is introduced to characterize the heat and mass transport of Oldroyd-B nanofluid. Consideration is focused on mathematical formulation of momentum equations based on boundary layer approximation theory. The conversion of governing equations into dimensionless forms are based on von Karman similarity variables. The numerical integration of the resultant problem is performed through bvp midrich scheme in Maple. The attained outcomes are exhibited through graphs for flow field, temperature and concentration of nanoparticles distributions as well as numerical values for Nusselt and Sherwood numbers. Results reveal that the presence of magnetic field in the flow region slows down the fluid movement. Also, the thermal and solutal distributions enhance substantially with rising values of retardation time

parameter. Moreover, the temperature of liquid boosts up for growing values of thermophoresis and Brownian motion parameters.

2.1 Development of Mathematical Model

The mathematical relations for conservation of mass and momentum in an incompressible MHD fluid flow are

$$\boldsymbol{\nabla}.\mathbf{V} = 0, \tag{2.1}$$

$$\rho \mathbf{a} = -\boldsymbol{\nabla}p + \boldsymbol{\nabla}.\mathbf{S} + \mathbf{J} \times \mathbf{B}, \tag{2.2}$$

where $\mathbf{a}$ is the material time derivative of velocity vector $\mathbf{V}$ and is given by

$$\mathbf{a} = \frac{d\mathbf{V}}{dt} = \frac{\partial \mathbf{V}}{\partial t} + (\mathbf{V}.\boldsymbol{\nabla})\,\mathbf{V}, \tag{2.3}$$

in which ρ is the density of the fluid and p stands for the pressure. The extra stress tensor $\mathbf{S}$ in Eq. (2.2) is defined in Eq. (1.23) for Oldroyd-B fluid model.

Taking divergence of Eq. (1.23) (cf. **Chapter 1**)on both sides gives

$$\left(1 + \lambda_1 \frac{D}{Dt}\right) \boldsymbol{\nabla}.\mathbf{S} = \mu \left(1 + \lambda_1 \frac{D}{Dt}\right) \boldsymbol{\nabla}.\mathbf{A_1}. \tag{2.4}$$

After applying the operator $\left(1 + \lambda_1 \frac{D}{Dt}\right)$ on Eq. (2.2) and using the result of Eq. (2.4), we finally have

$$\rho \left(1 + \lambda_1 \frac{D}{Dt}\right) \mathbf{a} = -\left(1 + \lambda_1 \frac{D}{Dt}\right) \boldsymbol{\nabla}p + \mu \left(1 + \lambda_2 \frac{D}{Dt}\right) \boldsymbol{\nabla}.\mathbf{A_1} + \left(1 + \lambda_1 \frac{D}{Dt}\right) (\mathbf{J} \times \mathbf{B}), \tag{2.5}$$

where $\frac{D}{Dt}$ is the upper convective derivative and defined for a vector $\mathbf{A}$ as:

$$\frac{D\mathbf{A}}{Dt} = \frac{\partial \mathbf{A}}{\partial t} + (\mathbf{V}.\boldsymbol{\nabla})\,\mathbf{A} - (\boldsymbol{\nabla}\mathbf{V})\,\mathbf{A}. \tag{2.6}$$

For present study, we are taking the cylindrical polar coordinate system (r, φ, z) and assume an axisymmetric three dimensional steady flow, the velocity vector is taken as:

$$\mathbf{V} = [u\,(r, z),\ v\,(r, z),\ w\,(r, z)]\,, \tag{2.7}$$

where (u, v, w) are the radial, azimuthal, and axial velocity components, respectively.

Under the mentioned above assumptions, the system of equations of the problem are given by

$$\frac{\partial u}{\partial r} + \frac{u}{r} + \frac{\partial w}{\partial z} = 0, \tag{2.8}$$

$$
\begin{aligned}
&u\frac{\partial u}{\partial r} - \frac{v^2}{r} + w\frac{\partial u}{\partial z} = -\frac{1}{\rho}\frac{\partial p}{\partial r} - \frac{\sigma}{\rho}B_0^2\left[u + \lambda_1 w\frac{\partial u}{\partial z}\right] \\
&+\nu\left(2\frac{\partial^2 u}{\partial r^2} + \frac{\partial^2 u}{\partial z^2} + \frac{\partial^2 w}{\partial r\partial z} - 2\frac{u}{r^2} + \frac{2}{r}\frac{\partial u}{\partial r}\right) \\
&-\lambda_1\left[u^2\frac{\partial^2 u}{\partial r^2} + w^2\frac{\partial^2 u}{\partial z^2} + 2uw\frac{\partial^2 u}{\partial r\partial z} - 2\frac{uv}{r}\frac{\partial v}{\partial r} - 2\frac{vw}{r}\frac{\partial v}{\partial z} + \frac{uv^2}{r^2} + \frac{v^2}{r}\frac{\partial u}{\partial r}\right] \\
&+\nu\lambda_2\left[
\begin{array}{c}
4\frac{u^2}{r^3} - 2\frac{w}{r^2}\frac{\partial u}{\partial z} - \frac{1}{r}\left(\frac{\partial u}{\partial z}\right)^2 - 2\frac{\partial u}{\partial z}\frac{\partial^2 w}{\partial z^2} + w\frac{\partial^3 u}{\partial z^3} - 2\frac{u}{r^2}\frac{\partial u}{\partial r} - \frac{\partial u}{\partial r}\frac{\partial^2 u}{\partial z^2} \\[2mm]
-\frac{2}{r}\left(\frac{\partial u}{\partial r}\right)^2 - \frac{1}{r}\frac{\partial u}{\partial z}\frac{\partial w}{\partial r} + 2\frac{w}{r}\frac{\partial^2 u}{\partial r\partial z} - \frac{\partial u}{\partial z}\frac{\partial^2 u}{\partial r\partial z} - \frac{\partial u}{\partial r}\frac{\partial^2 w}{\partial r\partial z} + u\frac{\partial^3 u}{\partial r\partial z^2} \\[2mm]
+w\frac{\partial^3 w}{\partial r\partial z^2} + 2\frac{u}{r}\frac{\partial^2 u}{\partial r^2} - 2\frac{\partial u}{\partial r}\frac{\partial^2 u}{\partial r^2} - \frac{\partial u}{\partial z}\frac{\partial^2 w}{\partial r^2} + 2w\frac{\partial^3 u}{\partial r^2\partial z} + u\frac{\partial^3 w}{\partial r^2\partial z} + 2u\frac{\partial^3 u}{\partial r^3},
\end{array}
\right]
\end{aligned}
\tag{2.9}
$$

26

$$u\frac{\partial v}{\partial r} + \frac{uv}{r} + w\frac{\partial v}{\partial z} = \nu\left(\frac{\partial^2 v}{\partial r^2} + \frac{1}{r}\frac{\partial v}{\partial r} - \frac{v}{r^2} + \frac{\partial^2 v}{\partial z^2}\right) - \frac{\sigma}{\rho}B_0^2\left[v + \lambda_1 w\frac{\partial v}{\partial z}\right]$$

$$-\lambda_1\left[u^2\frac{\partial^2 v}{\partial r^2} + w^2\frac{\partial^2 v}{\partial z^2} + 2uw\frac{\partial^2 v}{\partial r\partial z} + 2\frac{uv}{r}\frac{\partial u}{\partial r} + 2\frac{vw}{r}\frac{\partial u}{\partial z} - 2\frac{u^2 v}{r^2} - \frac{v^3}{r^2} + \frac{v^2}{r}\frac{\partial v}{\partial r}\right]$$

$$+\nu\lambda_2\left[\begin{array}{c} u\frac{\partial^3 v}{\partial r^3} + u\frac{\partial^3 v}{\partial r\partial z^2} + 2\frac{v}{r}\frac{\partial^2 u}{\partial r^2} + \frac{v}{r}\frac{\partial^2 u}{\partial z^2} + \frac{v}{r}\frac{\partial^2 w}{\partial r\partial z} + 2\frac{v}{r^2}\frac{\partial u}{\partial r} + w\frac{\partial^3 v}{\partial r^2\partial z} \\[2mm] -\frac{w}{r^2}\frac{\partial v}{\partial z} + \frac{w}{r}\frac{\partial^2 v}{\partial r\partial z} + w\frac{\partial^3 v}{\partial z^3} - 2\frac{\partial v}{\partial r}\frac{\partial^2 u}{\partial r^2} - \frac{\partial v}{\partial r}\frac{\partial^2 u}{\partial z^2} - \frac{\partial v}{\partial r}\frac{\partial^2 w}{\partial r\partial z} - \frac{2}{r}\frac{\partial u}{\partial r}\frac{\partial v}{\partial r} + \frac{uv}{r^3} \\[2mm] -\frac{u}{r^2}\frac{\partial v}{\partial r} - \frac{u}{r}\frac{\partial^2 v}{\partial z^2} - \frac{\partial v}{\partial z}\frac{\partial^2 u}{\partial r\partial z} - \frac{\partial v}{\partial z}\frac{\partial^2 u}{\partial r^2} - \frac{1}{r}\frac{\partial u}{\partial z}\frac{\partial v}{\partial z} - \frac{1}{r}\frac{\partial v}{\partial z}\frac{\partial w}{\partial r} - 2\frac{\partial v}{\partial z}\frac{\partial^2 w}{\partial z^2} \end{array}\right], (2.10)$$

$$u\frac{\partial w}{\partial r} + w\frac{\partial w}{\partial z} = -\frac{1}{\rho}\frac{\partial p}{\partial z} + \nu\left(\frac{\partial^2 u}{\partial r\partial z}\frac{\partial^2 w}{\partial z^2} + \frac{\partial^2 w}{\partial r^2} + \frac{1}{r}\frac{\partial u}{\partial z} + 2\frac{\partial^2 w}{\partial z^2}\right)$$

$$-\frac{\sigma}{\rho}B_0^2\left[0 - \lambda_1 u\frac{\partial w}{\partial r}\right] - \lambda_1\left[u^2\frac{\partial^2 w}{\partial r^2} + w^2\frac{\partial^2 w}{\partial z^2} + 2uw\frac{\partial^2 w}{\partial r\partial z} + \frac{v^2}{r}\frac{\partial w}{\partial r}\right]$$

$$+\nu\lambda_2\left[\begin{array}{c} u\frac{\partial^3 u}{\partial r^2\partial z} + u\frac{\partial^3 w}{\partial r^3} - \frac{u}{r^2}\frac{\partial u}{\partial z} + \frac{u}{r}\frac{\partial^2 u}{\partial r\partial z} + \frac{u}{r^2}\frac{\partial w}{\partial r} + \frac{u}{r}\frac{\partial^2 w}{\partial r^2} + 2u\frac{\partial^3 w}{\partial r\partial z^2} + w\frac{\partial^3 u}{\partial r\partial z^2} \\[2mm] +\frac{\partial^3 w}{\partial r^2\partial z} + \frac{w}{r}\frac{\partial^2 u}{\partial z^2} + \frac{w}{r}\frac{\partial^2 w}{\partial r\partial z} + 2w\frac{\partial^3 w}{\partial z^3} - 2\frac{\partial w}{\partial r}\frac{\partial^2 u}{\partial r^2} - \frac{\partial w}{\partial r}\frac{\partial^2 u}{\partial z^2} - \frac{\partial w}{\partial r}\frac{\partial^2 w}{\partial r\partial z} \\[2mm] -\frac{2}{r}\frac{\partial w}{\partial r}\frac{\partial u}{\partial r} - \frac{\partial w}{\partial z}\frac{\partial^2 u}{\partial r\partial z} - \frac{\partial w}{\partial z}\frac{\partial^2 w}{\partial r^2} - \frac{1}{r}\frac{\partial w}{\partial z}\frac{\partial u}{\partial z} - \frac{1}{r}\frac{\partial w}{\partial z}\frac{\partial w}{\partial r} - 2\frac{\partial w}{\partial z}\frac{\partial^2 w}{\partial z^2} \end{array}\right]. (2.11)$$

In view of the boundary layer approximation, we assumed the order of u, v, r, λ_1 and λ_2 to be one and w, z are of the order δ. Moreover, the other parameter like ν is of the order δ^2, whereas, δ is the boundary layer thickness. After applying the above mentioned approximations, Eqs. (2.9) to (2.11) are simplified as

$$u\frac{\partial u}{\partial r} - \frac{v^2}{r} + w\frac{\partial u}{\partial z} = -\frac{1}{\rho}\frac{\partial p}{\partial r} + \nu\frac{\partial^2 u}{\partial z^2} - \frac{\sigma}{\rho}B_0^2\left[u + \lambda_1 w\frac{\partial u}{\partial z}\right]$$

$$-\lambda_1\left[u^2\frac{\partial^2 u}{\partial r^2} + w^2\frac{\partial^2 u}{\partial z^2} + 2uw\frac{\partial^2 u}{\partial r\partial z} - 2\frac{uv}{r}\frac{\partial v}{\partial r} - 2\frac{vw}{r}\frac{\partial v}{\partial z} + \frac{uv^2}{r^2} + \frac{v^2}{r}\frac{\partial u}{\partial r}\right]$$

$$+\nu\lambda_2\left[w\frac{\partial^3 u}{\partial z^3} - \frac{1}{r}\left(\frac{\partial u}{\partial z}\right)^2 - 2\frac{\partial u}{\partial z}\frac{\partial^2 w}{\partial z^2} - \frac{\partial u}{\partial r}\frac{\partial^2 u}{\partial z^2} - \frac{\partial u}{\partial z}\frac{\partial^2 u}{\partial r\partial z} + u\frac{\partial^3 u}{\partial r\partial z^2}\right], (2.12)$$

27

$$u\frac{\partial v}{\partial r} + \frac{uv}{r} + w\frac{\partial v}{\partial z} = \nu\frac{\partial^2 v}{\partial z^2} - \frac{\sigma}{\rho}B_0^2\left[v + \lambda_1 w\frac{\partial v}{\partial z}\right]$$
$$-\lambda_1\left[u^2\frac{\partial^2 v}{\partial r^2} + w^2\frac{\partial^2 v}{\partial z^2} + 2uw\frac{\partial^2 v}{\partial r\partial z} + \frac{2uv}{r}\frac{\partial u}{\partial r} + \frac{2vw}{r}\frac{\partial u}{\partial z} - 2\frac{u^2v}{r^2} - \frac{v^3}{r^2} + \frac{v^2}{r}\frac{\partial v}{\partial r}\right]$$
$$+\nu\lambda_2\begin{bmatrix} u\frac{\partial^3 v}{\partial r\partial z^2} - \frac{1}{r}\frac{\partial u}{\partial z}\frac{\partial v}{\partial z} - 2\frac{\partial v}{\partial z}\frac{\partial^2 w}{\partial z^2} + w\frac{\partial^3 v}{\partial z^3} \\ -\frac{\partial v}{\partial r}\frac{\partial^2 u}{\partial z^2} - \frac{\partial v}{\partial z}\frac{\partial^2 u}{\partial r\partial z} + \frac{v}{r}\frac{\partial^2 u}{\partial z^2} - \frac{u}{r}\frac{\partial^2 v}{\partial z^2} \end{bmatrix}, \tag{2.13}$$

$$-\frac{1}{\rho}\left(\frac{\partial p}{\partial z}\right) = 0. \tag{2.14}$$

Under the boundary layer approach and using the boundary conditions at infinity, the pressure gradient term can be found as

$$\frac{1}{\rho}\frac{\partial p}{\partial r} = 0. \tag{2.15}$$

Therefore, the final momentum equations reduce to

$$u\frac{\partial u}{\partial r} - \frac{v^2}{r} + w\frac{\partial u}{\partial z} = -\frac{1}{\rho}\frac{\partial p}{\partial r} + \nu\frac{\partial^2 u}{\partial z^2} - \frac{\sigma}{\rho}B_0^2\left[u + \lambda_1 w\frac{\partial u}{\partial z}\right]$$
$$-\lambda_1\left[u^2\frac{\partial^2 u}{\partial r^2} + w^2\frac{\partial^2 u}{\partial z^2} + 2uw\frac{\partial^2 u}{\partial r\partial z} - 2\frac{uv}{r}\frac{\partial v}{\partial r} - 2\frac{vw}{r}\frac{\partial v}{\partial z} + \frac{uv^2}{r^2} + \frac{v^2}{r}\frac{\partial u}{\partial r}\right]$$
$$+\nu\lambda_2\left[w\frac{\partial^3 u}{\partial z^3} - \frac{1}{r}\left(\frac{\partial u}{\partial z}\right)^2 - 2\frac{\partial u}{\partial z}\frac{\partial^2 w}{\partial z^2} - \frac{\partial u}{\partial r}\frac{\partial^2 u}{\partial z^2} - \frac{\partial u}{\partial z}\frac{\partial^2 u}{\partial r\partial z} + u\frac{\partial^3 u}{\partial r\partial z^2}\right], \tag{2.16}$$

$$u\frac{\partial v}{\partial r} + \frac{uv}{r} + w\frac{\partial v}{\partial z} = \nu\frac{\partial^2 v}{\partial z^2} - \frac{\sigma}{\rho}B_0^2\left[v + \lambda_1 w\frac{\partial v}{\partial z}\right]$$
$$-\lambda_1\left[u^2\frac{\partial^2 v}{\partial r^2} + w^2\frac{\partial^2 v}{\partial z^2} + 2uw\frac{\partial^2 v}{\partial r\partial z} + \frac{2uv}{r}\frac{\partial u}{\partial r} + \frac{2vw}{r}\frac{\partial u}{\partial z} - 2\frac{u^2v}{r^2} - \frac{v^3}{r^2} + \frac{v^2}{r}\frac{\partial v}{\partial r}\right]$$
$$+\nu\lambda_2\begin{bmatrix} u\frac{\partial^3 v}{\partial r\partial z^2} - \frac{1}{r}\frac{\partial u}{\partial z}\frac{\partial v}{\partial z} - 2\frac{\partial v}{\partial z}\frac{\partial^2 w}{\partial z^2} + w\frac{\partial^3 v}{\partial z^3} \\ -\frac{\partial v}{\partial r}\frac{\partial^2 u}{\partial z^2} - \frac{\partial v}{\partial z}\frac{\partial^2 u}{\partial r\partial z} + \frac{v}{r}\frac{\partial^2 u}{\partial z^2} - \frac{u}{r}\frac{\partial^2 v}{\partial z^2} \end{bmatrix}. \tag{2.17}$$
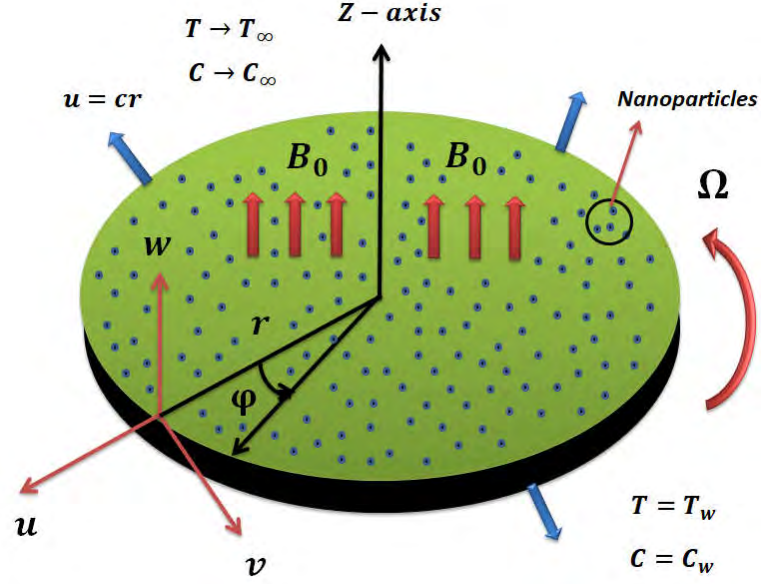
28

2.2 Model Sketch

Fig 2.1: A physical model of the problem.

2.3 Problem Formulation

In this section, a steady, incompressible and three-dimensional flow of Oldroyd-B fluid is analyzed in the presence of nanoparticles. The flow is assumed to be generated by a stretchable rotating disk. The disk at $z = 0$ rotates with uniform angular velocity Ω. Here, the magnetic field acts along the $z-$direction. For small magnetic Reynolds number, the induced magnetic field is assumed as zero. The analysis of heat and mass transport are performed by the classical Fourier's and Fick's laws, respectively. A physical model of the problem is presented in **Fig**. **2.1**. The disk is maintained at uniform temperature T_w and concentration C_w. Here T_∞, C_∞ are the ambient temperature and concentration, respectively.

From the above stated assumptions, the governing non-linear equations for the given prob-

lem are

$$\frac{\partial u}{\partial r} + \frac{u}{r} + \frac{\partial w}{\partial z} = 0, \tag{2.18}$$

$$
u\frac{\partial u}{\partial r} - \frac{v^2}{r} + w\frac{\partial u}{\partial z} = -\frac{1}{\rho}\frac{\partial p}{\partial r} + \nu\frac{\partial^2 u}{\partial z^2} - \frac{\sigma}{\rho}B_0^2\left[u + \lambda_1 w\frac{\partial u}{\partial z}\right]
$$
$$
-\lambda_1\left[u^2\frac{\partial^2 u}{\partial r^2} + w^2\frac{\partial^2 u}{\partial z^2} + 2uw\frac{\partial^2 u}{\partial r\partial z} - 2\frac{uv}{r}\frac{\partial v}{\partial r} - 2\frac{vw}{r}\frac{\partial v}{\partial z} + \frac{uv^2}{r^2} + \frac{v^2}{r}\frac{\partial u}{\partial r}\right]
$$
$$
+\nu\lambda_2\left[w\frac{\partial^3 u}{\partial z^3} - \frac{1}{r}\left(\frac{\partial u}{\partial z}\right)^2 - 2\frac{\partial u}{\partial z}\frac{\partial^2 w}{\partial z^2} - \frac{\partial u}{\partial r}\frac{\partial^2 u}{\partial z^2} - \frac{\partial u}{\partial z}\frac{\partial^2 u}{\partial r\partial z} + u\frac{\partial^3 u}{\partial r\partial z^2}\right], \tag{2.19}
$$

$$
u\frac{\partial v}{\partial r} + \frac{uv}{r} + w\frac{\partial v}{\partial z} = \nu\frac{\partial^2 v}{\partial z^2} - \frac{\sigma}{\rho}B_0^2\left[v + \lambda_1 w\frac{\partial v}{\partial z}\right]
$$
$$
-\lambda_1\left[u^2\frac{\partial^2 v}{\partial r^2} + w^2\frac{\partial^2 v}{\partial z^2} + 2uw\frac{\partial^2 v}{\partial r\partial z} + \frac{2uv}{r}\frac{\partial u}{\partial r} + \frac{2vw}{r}\frac{\partial u}{\partial z} - 2\frac{u^2v}{r^2} - \frac{v^3}{r^2} + \frac{v^2}{r}\frac{\partial v}{\partial r}\right]
$$
$$
+\nu\lambda_2\begin{bmatrix} u\frac{\partial^3 v}{\partial r\partial z^2} - \frac{1}{r}\frac{\partial u}{\partial z}\frac{\partial v}{\partial z} - 2\frac{\partial v}{\partial z}\frac{\partial^2 w}{\partial z^2} + w\frac{\partial^3 v}{\partial z^3} \\ -\frac{\partial v}{\partial r}\frac{\partial^2 u}{\partial z^2} - \frac{\partial v}{\partial z}\frac{\partial^2 u}{\partial r\partial z} + \frac{v}{r}\frac{\partial^2 u}{\partial z^2} - \frac{u}{r}\frac{\partial^2 v}{\partial z^2} \end{bmatrix}, \tag{2.20}
$$

$$
u\frac{\partial T}{\partial r} + w\frac{\partial T}{\partial z} = \alpha\frac{\partial^2 T}{\partial z^2} + \tau_1\left[D_B\frac{\partial T}{\partial z}\frac{\partial C}{\partial z} + \frac{D_T}{T_\infty}\left(\frac{\partial T}{\partial z}\right)^2\right], \tag{2.21}
$$

$$
u\frac{\partial C}{\partial r} + w\frac{\partial C}{\partial z} = D_B\frac{\partial^2 C}{\partial z^2} + \frac{D_T}{T_\infty}\frac{\partial^2 T}{\partial z^2}. \tag{2.22}
$$

The relevant boundary conditions are

$$u = cr, \quad v = \Omega r, \quad w = 0, \quad T = T_w, \quad C = C_w \qquad \text{at } z = 0,$$

$$u \to 0, \quad v \to 0, \quad T \to T_\infty, \quad C \to C_\infty \qquad \text{as } z \to \infty. \tag{2.23}$$

Here, Ω indicates the swirl rate and c the stretch rate of the disk. Further, ν is the kinematic

30

viscosity, τ_1 the heat capacities ratio, σ the electrical conductivity, B_0 the strength of magnetic field, λ_1 the relaxation time, λ_2 the retardation time, T the temperature of the fluid, α the thermal diffusivity and C the concentration of the fluid.

Introducing the following von Karman transformations

$$\eta = \sqrt{\frac{\Omega}{\nu}}z, \ u = \Omega r F, \ v = \Omega r G, \ w = \sqrt{\Omega \nu}H, \ \theta = \frac{T - T_\infty}{T_w - T_\infty}, \ \phi = \frac{C - C_\infty}{C_w - C_\infty}. \tag{2.24}$$

After putting the mentioned transformations (2.24) into governing Eqs. (2.18) to (2.22), we have

$$H' + 2F = 0, \tag{2.25}$$

$$F^2 - G^2 + F'H - F'' + \beta_1 \left(F''H^2 + 2FF'H - 2GG'H \right)$$

$$+ \beta_2 \left(2F'^2 + 2F'H'' - F'''H \right) + M \left(F + \beta_1 F'H \right) = 0, \tag{2.26}$$

$$2FG + G'H - G'' + \beta_1 \left(G''H^2 + 2 \left(FG' + F'G \right) H \right)$$

$$- \beta_2 \left(G'''H - 2F'G' - 2G'H'' \right) + M \left(G + \beta_1 G'H \right) = 0, \tag{2.27}$$

$$\frac{1}{\mathrm{Pr}}\theta'' - H\theta' + Nb\theta'\phi' + Nt\theta'^2 = 0, \tag{2.28}$$

$$\phi'' - ScH\phi' + \frac{Nt}{Nb}\theta'' = 0. \tag{2.29}$$

31

The boundary conditions are transformed as below

$$F(\eta) = \omega, \quad G(\eta) = 1, \quad H(\eta) = 0, \quad \theta(\eta) = 1, \quad \phi(\eta) = 1 \quad \text{at } \eta = 0,$$

$$F(\eta) \to 0, \quad G(\eta) \to 0, \quad \theta(\eta) \to 0, \quad \phi(\eta) \to 0 \quad \text{as} \quad \eta \to \infty, \tag{2.30}$$

where, prime refers differentiation w.r.t η.

Further, (F, G, H) are the dimensionless velocity in radial, azimuthal and axial directions, respectively. Also, (θ, ϕ) are the dimensionless temperature and concentration of the liquid, respectively.

The different flow parameters appearing in Eqs. $(2.26) - (2.30)$ are characterized by:

$M = \frac{\sigma B_0^2}{\rho \Omega}$ is the magnetic field parameter, $\omega = \frac{c}{\Omega}$ the stretching parameter, $\beta_1 = \lambda_1 \Omega$ the relaxation time parameter, $\beta_2 = \lambda_2 \Omega$ the retardation time parameter, $\Pr = \frac{\nu}{\alpha}$ the Prandtl number, $Sc = \frac{\nu}{D_B}$ the Schmidt number, $\left(Nt = \frac{\tau D_T (T_w - T_\infty)}{\nu T_\infty}, \ Nb = \frac{\tau D_B (C_w - C_\infty)}{\nu}\right)$ for the Brownian motion and thermophoresis parameters, respectively.

2.4 Physical Parameters

2.4.1 Heat Transfer Performance

The efficiency of transfer of heat from surface to fluid can be characterized by Nusselt number Nu. In Physical point of view, Fourier's law and Newton's law of cooling are used to defined the Nusselt number Nu. Mathematically, it is given as

$$Nu = \frac{R q_w}{k(T_w - T_\infty)}, \tag{2.31}$$

32

in which

$$q_w = -k \left(\frac{\partial T}{\partial z} \right) \bigg|_{z=0}. \tag{2.32}$$

In non-dimensional form, we have

$$\mathrm{Re}^{-\frac{1}{2}} Nu = -\theta'(0). \tag{2.33}$$

2.4.2   Mass Transfer Performance

The rate of mass transport at the disk surface can be stated by Sherwood number Sh, which can be defined by Fick's law. Mathematically,

$$Sh = \frac{R j_w}{D_B (C_w - C_\infty)}, \tag{2.34}$$

with

$$j_w = -D_B \left(\frac{\partial C}{\partial z} \right) \bigg|_{z=0}. \tag{2.35}$$

In non-dimensional form, we get

$$\mathrm{Re}^{-\frac{1}{2}} Sh = -\phi'(0), \tag{2.36}$$

where R is the characteristic radius and the Reynolds number is $\mathrm{Re} \left(= \frac{R^2 \Omega}{\nu} \right)$.

2.5   Validation of Numerical Outcomes

To ensure that the numerical results obtained using the bvp midrich scheme in Maple are accurate, a comparison of $F'(0)$, $-G'(0)$ and $-\theta'(0)$ is made for the limiting case, i.e. in the

33

absence of β_1, β_2, ω, M and also without taking the nanoparticles. These comparisons to those of Bachok *et al*. [53], Turkyilmazoglu [54] and (Kelson and Desseaux) [55] with the present numerical results can be noticed in **Table 2**.1. This table demonstrates a decent assertion among the existing results and the previous outcomes. This gives the reliability of our numerical scheme.

2.6 Results and Discussion

Our basic goal in this section is to understand the physics about the various physical parameters via tables and graphical structures. To illustrate the impact of these parameters on the fluid flow behavior, heat and mass transfer, results are drawn in figures 2.2 to 2.8. The differential system in Eqs. (2.25) to (2.29) with conditions (2.30) are extremely non-linear in nature. To handle these non-linear differential equations, we use a numerical method called bvp midrich scheme on Maple. Impacts of involved parameters like, magnetic field parameter M, relaxation time parameter β_1, stretching parameter ω, retardation time parameter β_2, Schmidt number Sc,, thermophoresis parameter Nt, Prandtl number Pr and Brownian motion parameter Nb are discussed. The whole analysis is performed with fixed values of $M = 1.0$, $\omega = 1.3$, $\beta_1 = 0.05$, $\beta_2 = 0.05$, $Nt = Nb = 0.1$, $\text{Pr} = 5.0$ and $S_c = 5.0$. It is worth mentioning that each one plot is approaching the far-field boundary conditions asymptotically.

Figs. 2.2 $(\mathbf{a-e})$ describe the effect of magnetic field parameter M on the velocities $(F(\eta)$, $G(\eta)$ and $H(\eta))$, temperature $\theta(\eta)$ and concentration $\phi(\eta)$ of the fluid. The influence of magnetic field parameter M on radial velocity $F(\eta)$ is reported in **Fig. 2**.2 $(\mathbf{a})$. Here, M is a dimensionless parameter used to control the motion of the fluid. It can be noticed that the

higher values of $M (= 1.0,\ 3.0,\ 5.0, 7.0)$ reduce the radial velocity $F(\eta)$ of the fluid. To see the impact of M on azimuthal velocity $G(\eta)$, result is shown through **Fig. 2.2 (b)**. In this figure, we see that the velocity of the fluid also declines with enlargement of M. Additionally, the higher estimations of M cause the reduction of the boundary layer thickness in this situation. Physically, magnetic field is a Lorentz force and this force is a resistive force which decelerates the motion of fluid. Moreover, the curves of axial velocity $H(\eta)$ are plotted with various values of M in **Fig. 2.2 (c)**. It can be scrutinized that the velocity $H(\eta)$ is negative, showing the fluid flows in downward direction and flow in vertical way is reduced due to higher magnitude of magnetic parameter. For the particular set of physical parameters, it is sighted that the temperature of fluid $\theta(\eta)$ is enhanced with enlarging of M as seen in **Fig. 2.2 (d)**. The physical phenomenon of Lorentz force corresponds to the enhancement of the heat transport phenomenon and hence the thickness of the thermal boundary layer is also boosted. From **Fig. 2.2 (e)**, the concentration of nanoparticles $\phi(\eta)$ improves for larger values of $M (= 1.0,\ 3.0,\ 5.0, 7.0)$ and default parameters are fixed. In addition, during this invasion, the thickness of the concentration boundary layer increases.

Figs. **2.3 (a)** to **(c)** are plotted to observed the variation in azimuthal velocity $G(\eta)$, temperature $\theta(\eta)$ and concentration $\phi(\eta)$ distributions, respectively under the action of relaxation time parameter β_1. From **Fig. 2.3 (a)**, the azimuthal velocity declines for large values of $\beta_1 (= 0.1,\ 0.3,\ 0.5,\ 0.7)$. Additionally, at this intrusion, the reduction in the thickness of boundary layer is seen. This feature is described as, the Deborah number β_1 is the ratio of material relaxation time to the material observation time. So the estimation in relaxation time parameter β_1 infers the stress relaxation is higher or the observation time is shorter showing that the fluid behave like solid response. Thus, the fluid flow is confronted with a higher re-

sistance that reduces the fluid motion. **Fig**. **2.3** (b) displays the temperature $\theta(\eta)$ variation against η for numerous values of relaxation time parameter β_1. As is obvious in this figure, the temperature decline for higher values of β_1. The influence of β_1 on the concentration distribution $\phi(\eta)$ is pictured through **Fig**. **2.3** (c) with non-zero values of other supervising parameters. It can be shown that the nanoparticle volume friction $\phi(\eta)$ is decreased with the up growing values of relaxation time parameter $\beta_1 (= 0.1, \ 0.3, \ 0.5, \ 0.7)$.

To discuss the velocities (radial, azimuthal and axial), temperature and concentration of the Oldroyd-B liquid flow against the effect of Deborah number of retardation time parameter β_2, the graphs are sketched in **Figs. 2.4** (a)-(e). Retardation parameter describes the retardation time when strain at constant stress reduces, as a result, the velocity decreases on increasing trend of retardation time parameter. The effect of β_2 on radial velocity $F(\eta)$ is presented in **Fig. 2.4** (a). With the enlargement of $\beta_2 (= 0.1, 0.3, 0.6, 0.9)$, the radial fluid's velocity is decreased. Moreover, **Fig. 2.4** (b) is captured to clarify the features of β_2 on the azimuthal velocity. It is noted that the azimuthal velocity of the fluid enhances with the increment in $\beta_2 (= 0.1, 0.3, 0.6, 0.9)$. **Fig. 2.4** (c) represents the influence of retardation time parameter β_2 on axial velocity $H(\eta)$. **Figs. 2.4** (d) and (e) are displayed to watch the impact of β_2 on temperature $\theta(\eta)$ and nanoparticle volume friction $\phi(\eta)$, respectively. These figures depict that the fluid's temperature as well as the concentration of nanoparticles are boosted up by the growing value of $\beta_2 (= 0.1, 0.3, 0.6, 0.9)$.

The influence of ω on velocity field, temperature and concentration distributions is illustrated through **Figs. 2.5** (a − e). It is concluded from **Fig. 2.5** (a) that the radial velocity $F(\eta)$ rises with the increment in stretching parameter $\omega (= 1.0, 1.3, 1.5, 1.7)$. This is primarily because of the fact that the stretching parameter ω is the ratio of stretch c to the swirl Ω

rate. By enlarging $\omega \left(=1.0, 1.3, 1.5, 1.7\right)$, the radial velocity of the fluid rises due to increases in the disk stretching rate. On the other hand, the contrary effect on azimuthal velocity $G\left(\eta\right)$ is seen in **Fig. 2**.**5** (**b**). This is because of the reduction in the velocity of rotation of the disk as compared to the stretching rate. Further, to watch the effect of ω on axial velocity $H\left(\eta\right)$, results are obtained through **Fig. 2**.**5** (**c**). The curves of temperature distribution $\theta\left(\eta\right)$ aligned with various values of ω are achieved in **Fig. 2**.**5** (**d**). It is remarked that the thermal boundary layer thickness declines as stretching parameter ω changes from 1.0 to 1.7. Moreover, the temperature of fluid decreases with a higher trend of ω. A similar observation can be observed for $\phi\left(\eta\right)$ as shown in **Fig. 2**.**5** (**e**).

To see the impact of Nt (thermophoresis parameter) on heat and mass transport phenomena, **Figs. 2**.**6** (**a, b**) are sketched. Here, higher rate of $Nt\left(=0.1, 0.16, 0.24, 0.3\right)$ increases the temperature distribution $\theta\left(\eta\right)$. In terms of physics, higher values of Nt increase the thermophoretic force, which improves heat transport in the liquid. Additionally, to see the variation in concentration distribution via Nt, curves are drawn in **Fig. 2**.**6** (**b**). From this figure, it reveals that the concentration distribution as well as related boundary layer thickness enhances by enlarging the values of thermophoresis parameter.

The influence on temperature and concentration distributions of Brownian motion parameter Nb is shown in **Figs. 2**.**7** (**a, b**). In these sketches, the temperature distribution $\theta\left(\eta\right)$ rises for increasing values of Nb. It's because by taking larger estimation of Brownian motion parameter Nb creates a higher diffusion rate, which boosts up collisions between the solid particles. As a result, the fluid's temperature rises which is shown in **Fig. 2**.**7** (**a**). Further, the impact of Nb on the concentration distribution in decreasing manner is observed. In simple terms, taking the larger values of Nb causes more collisions between the fluid particles. As a result,

mass moves at a very slow rate, which results in a decrease in the concentration distribution.

The effect of Pr on thermal distribution $\theta(\eta)$ is displayed in **Fig. 2.8 (a)**. It is remarked that the temperature drops down with the increasing values of $\Pr(= 5.0,\ 8.0,\ 12.0,\ 15.0)$. Further, a reduction in the mass transport is reported through **Fig. 2.8 (b)**, due to enhancement of Schmidt number Sc. Physically, higher values of Schmidt number Sc declines the diffusion coefficient because of the existence of an inverse relation between Schmidt number Sc and diffusion coefficient D_B. Thus in consequence, concentration distribution $\phi(\eta)$ is reduced in this situation.
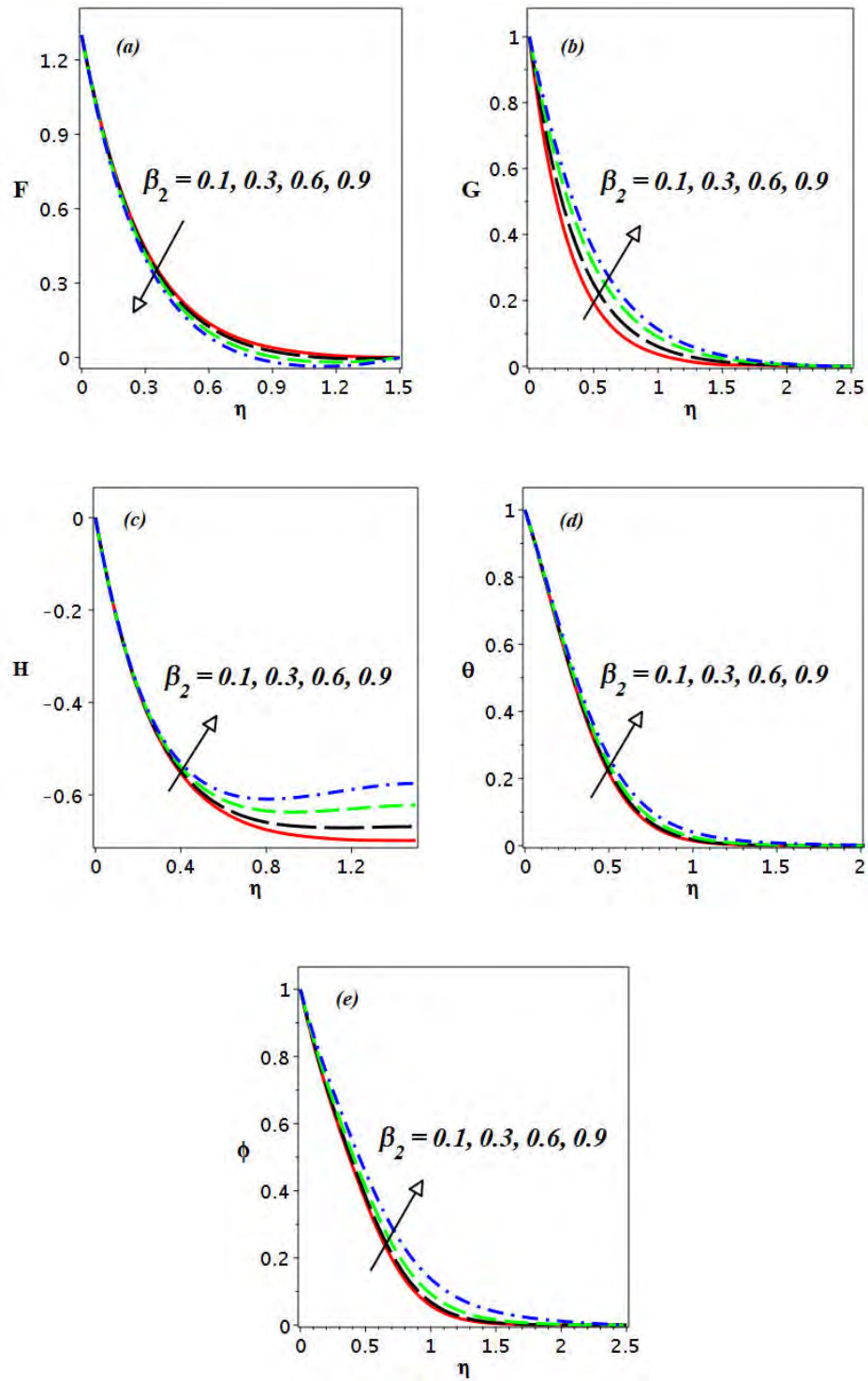
In **Table 2.2**, the values of Nusselt $\{-\theta'(0)\}$ and Sherwood $\{-\phi'(0)\}$ numbers are calculated numerically against different values of Nt, Nb, β_1, and β_2. Observations reveal that $-\theta'(0)$ decreases for increasing Nt, Nb, β_1, and β_2, respectively. The mass transfer rate $-\phi'(0)$ declines against Nt, β_1, and β_2, respectively while an opposite trends are noticed against Nb.
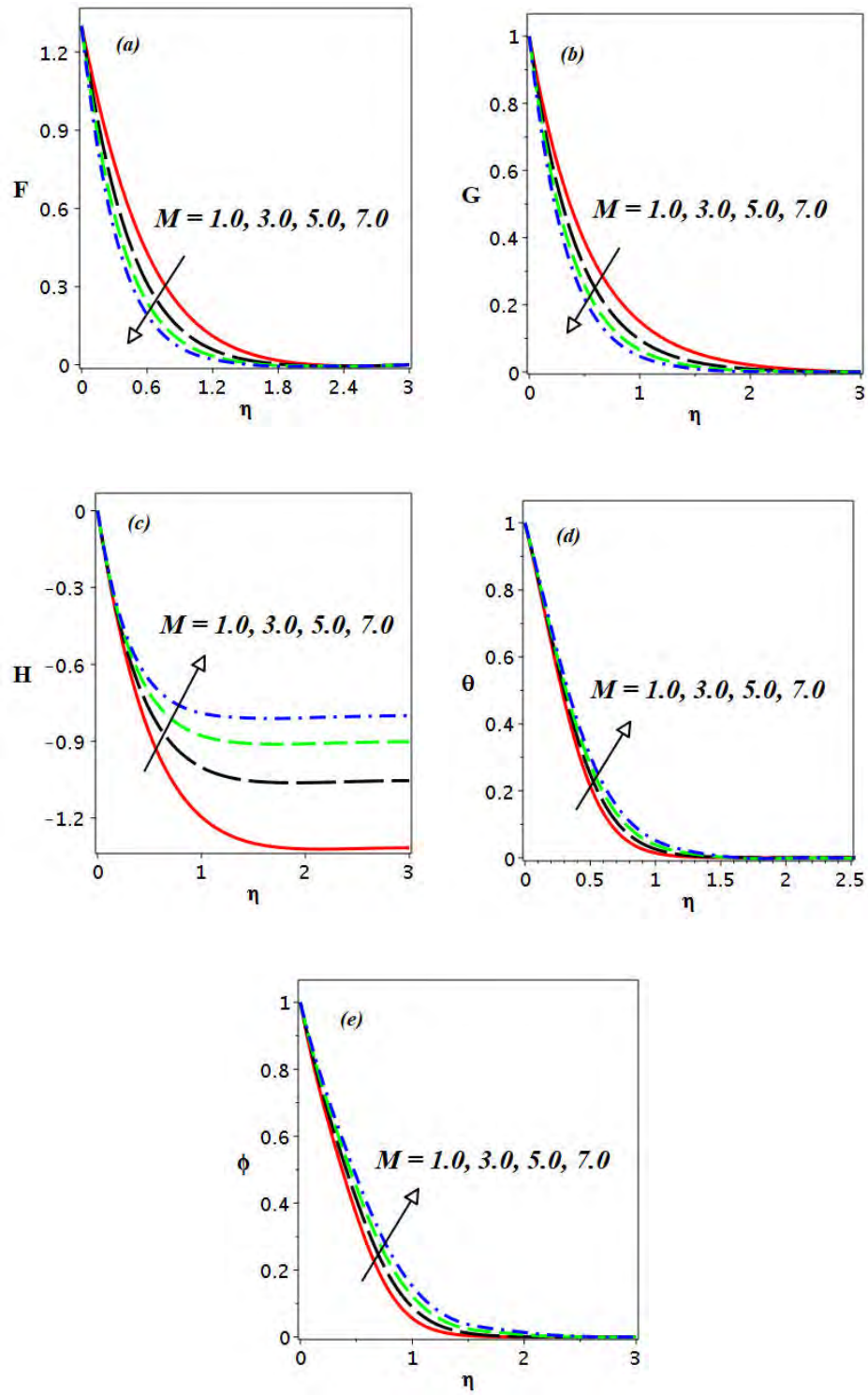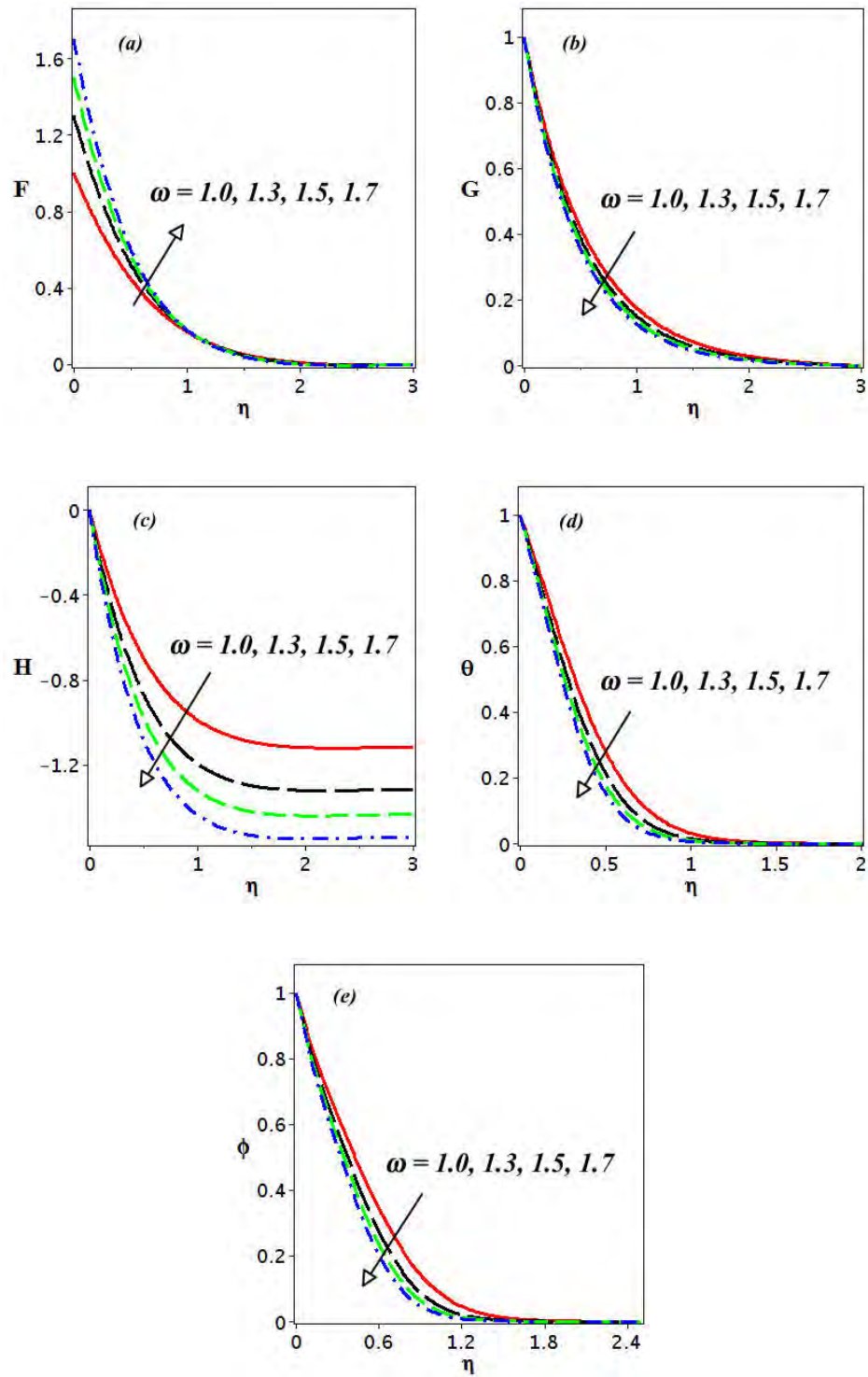
Figs. 2.2: Impact of M on $F(\eta)$, $G(\eta)$, $H(\eta)$, $\theta(\eta)$ and $\phi(\eta)$.
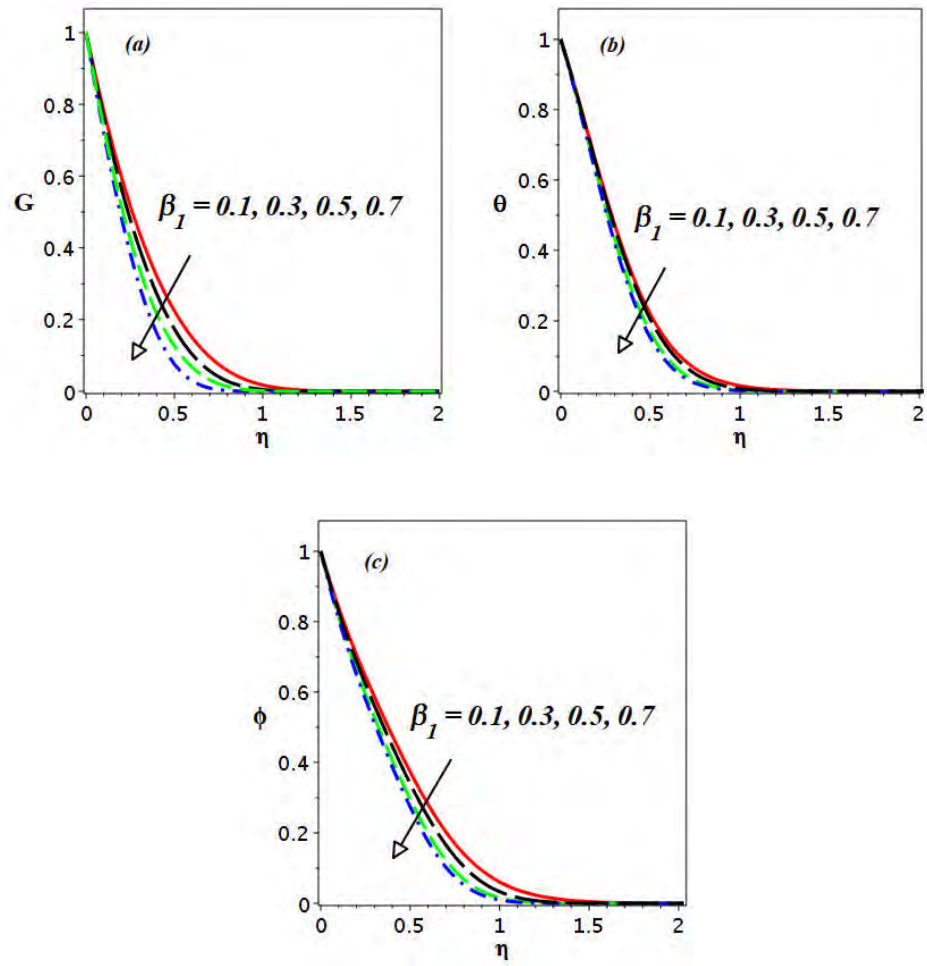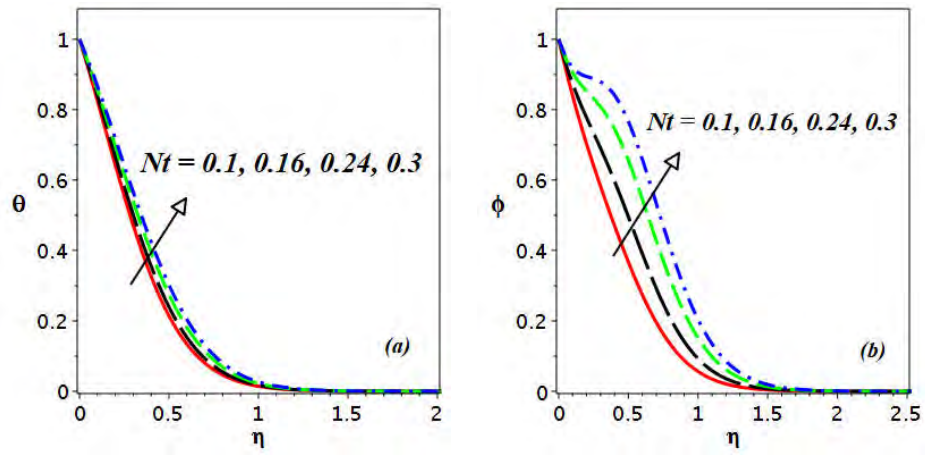
Figs. 2.3: Impact of β_1 on $G(\eta)$, $\theta(\eta)$ and $\phi(\eta)$.
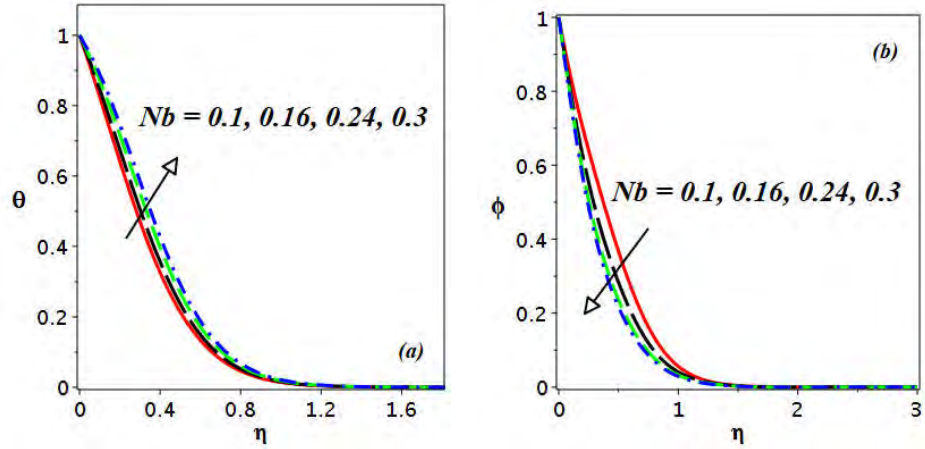
Figs. 2.4: Impact of β_2 on $F(\eta)$, $G(\eta)$, $H(\eta)$, $\theta(\eta)$ and $\phi(\eta)$.

41

Figs. 2.5: Impact of ω on $F(\eta)$, $G(\eta)$, $H(\eta)$, $\theta(\eta)$ and $\phi(\eta)$.

Figs. 2.6: Impact of Nt on $\theta\left(\eta\right)$ and $\phi\left(\eta\right)$.

Figs. 2.7: Impact of Nb on $\theta\left(\eta\right)$ and $\phi\left(\eta\right)$.
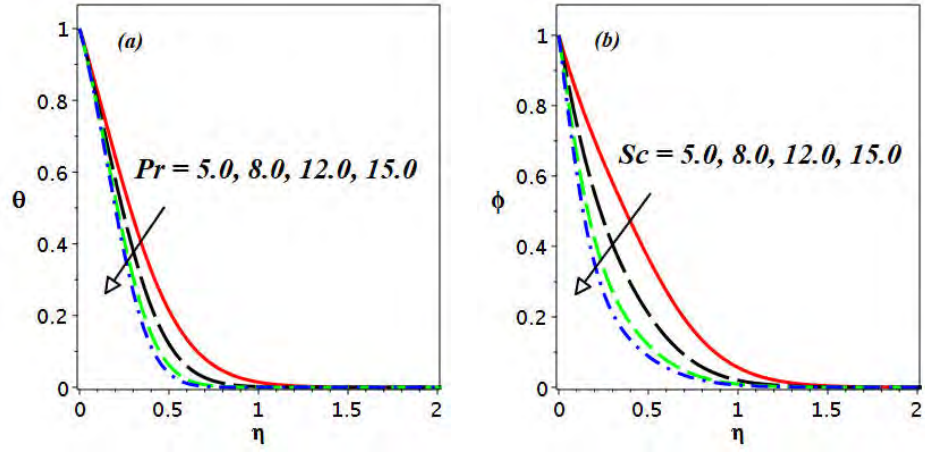
Figs. 2.8: Impact of Pr on $\theta(\eta)$ and impact of Sc on $\phi(\eta)$.

Table 2.1: An overview of the $F'(0)$, $-G'(0)$ and $-\theta'(0)$ with those of previously published articles.

	Bachok *et al*. [53]	Turkyilmazoglu [54]	Kelson & Desseaux [55]	Present results
$F'(0)$	0.5102	0.51023262	0.510233	0.51023
$-G'(0)$	0.6159	0.61592201	0.615922	0.61592
$-\theta'(0)$	0.9337	0.93387794	–	0.93386

Table 2.2: The numerical results of $-\theta'(0)$ and $-\phi'(0)$ for fixed $Pr = 5.0 = Sc$, $M = 1.0$,

$\omega = 1.3$.

Nt	Nb	β_1	β_2	$-\theta'(0)$	$-\phi'(0)$
0.1	0.1	0.03	0.03	1.642439	1.767962
0.2				1.400994	1.378959
0.3				1.202406	1.228859
0.3	0.2			0.897917	2.218264
	0.3			0.659153	2.489121
	0.4			0.476081	2.588055
0.3	0.4	0.05		0.475536	2.578542
		0.1		0.474154	2.554745
		0.15		0.472739	2.530992
0.3	0.4	0.15	0.1	0.472088	2.517484
			0.2	0.470591	2.473393
			0.3	0.468955	2.421493

Chapter 3

Activation Energy Impacts on Rotating and Radiative Flow of Oldroyd-B Fluid

This chapter focuses on the examination of heat and mass transportation in Oldroyd-B fluid flow influenced by non-linear radiation, heat absorption/generation and Arrhenius chemical reaction with activation energy. The fluid flow is controlled by vertically applied magnetic flux over a rotating disk configuration. The numerical integration is performed through bvp midrich scheme on Maple for the governing non-linear ordinary differential equations. Significant consequences with some dynamic physical constraints are prepared for the velocity profile, temperature and concentration distributions. Results reveal that the occurrence of radiative heat flux enhances the thermal profile efficiently. Moreover, concentration distribution is detected to be an increasing function of activation energy parameter.

3.1 Mathematical Formulation

A steady and incompressible boundary layer flow of Oldroyd-B fluid over a rotating disk is assumed. The disk at $z = 0$ rotates with uniform angular velocity Ω and stretches with constant rate c. Here, the magnetic field acts in $z-$direction. The heat transfer analysis is performed with the impact of heat absorption/generation and nonlinear thermal radiation. Moreover, the impact of activation energy on mass transport is also considered here. Equations for heat and mass transport are constructed with the help of classical Fourier's and Fick's laws, respectively.

Form the above stated assumptions, the governing equations for an Oldroyd-B fluid flow are (Eqs. ((2.18), (2.19), (2.20) cf. Chapter **2**)

$$\frac{\partial u}{\partial r} + \frac{u}{r} + \frac{\partial w}{\partial z} = 0, \tag{3.1}$$

$$
\begin{aligned}
&u\frac{\partial u}{\partial r} - \frac{v^2}{r} + w\frac{\partial u}{\partial z} = \nu\frac{\partial^2 u}{\partial z^2} - \frac{\sigma}{\rho}B_0^2\left[u + \lambda_1 w\frac{\partial u}{\partial z}\right] \\
&-\lambda_1\left[u^2\frac{\partial^2 u}{\partial r^2} + w^2\frac{\partial^2 u}{\partial z^2} + 2uw\frac{\partial^2 u}{\partial r\partial z} - \frac{2uv}{r}\frac{\partial v}{\partial r} - \frac{2vw}{r}\frac{\partial v}{\partial z} + \frac{uv^2}{r^2} + \frac{v^2}{r}\frac{\partial u}{\partial r}\right] \\
&+\nu\lambda_2\left[-\frac{1}{r}\left(\frac{\partial u}{\partial z}\right)^2 - 2\frac{\partial u}{\partial z}\frac{\partial^2 w}{\partial z^2} + w\frac{\partial^3 u}{\partial z^3} - \frac{\partial u}{\partial r}\frac{\partial^2 u}{\partial z^2} - \frac{\partial u}{\partial z}\frac{\partial^2 u}{\partial r\partial z} + u\frac{\partial^3 u}{\partial r\partial z^2}\right],
\end{aligned} \tag{3.2}
$$

$$
\begin{aligned}
&u\frac{\partial v}{\partial r} + \frac{uv}{r} + w\frac{\partial v}{\partial z} = \nu\frac{\partial^2 v}{\partial z^2} - \frac{\sigma}{\rho}B_0^2\left[v + \lambda_1 w\frac{\partial v}{\partial z}\right] \\
&-\lambda_1\left[u^2\frac{\partial^2 v}{\partial r^2} + w^2\frac{\partial^2 v}{\partial z^2} + 2uw\frac{\partial^2 v}{\partial r\partial z} + \frac{2uv}{r}\frac{\partial u}{\partial r} + \frac{2vw}{r}\frac{\partial u}{\partial z} - 2\frac{u^2v}{r^2} - \frac{v^3}{r^2} + \frac{v^2}{r}\frac{\partial v}{\partial r}\right] \\
&+\nu\lambda_2\left[\begin{array}{l} u\frac{\partial^3 v}{\partial r\partial z^2} - \frac{1}{r}\frac{\partial u}{\partial z}\frac{\partial v}{\partial z} - 2\frac{\partial v}{\partial z}\frac{\partial^2 w}{\partial z^2} + w\frac{\partial^3 v}{\partial z^3} \\[2mm] -\frac{\partial v}{\partial r}\frac{\partial^2 u}{\partial z^2} - \frac{\partial v}{\partial z}\frac{\partial^2 u}{\partial r\partial z} + \frac{v}{r}\frac{\partial^2 u}{\partial z^2} - \frac{u}{r}\frac{\partial^2 v}{\partial z^2} \end{array}\right],
\end{aligned} \tag{3.3}
$$

$$u\frac{\partial T}{\partial r} + w\frac{\partial T}{\partial z} = \frac{k}{\rho c_p}\left(\frac{\partial^2 T}{\partial z^2}\right) + \frac{Q}{\rho c_p}\left(T - T_\infty\right) - \frac{1}{\rho c_p}\frac{\partial q_r}{\partial z}, \tag{3.4}$$

$$u\frac{\partial C}{\partial r} + w\frac{\partial C}{\partial z} = D_B\left(\frac{\partial^2 C}{\partial z^2}\right) - K_r^2\left[\frac{T}{T_\infty}\right]^n \exp\left[\frac{-E_a}{k_1 T}\right]\left(C - C_\infty\right). \tag{3.5}$$

The boundary conditions are

$$u = cr, \quad v = \Omega r, \quad w = 0, \quad T = T_w, \quad C = C_w, \quad \text{at } z = 0,$$

$$u \to 0, \quad v \to 0, \quad T \to T_\infty, \quad C \to C_\infty, \quad \text{as } z \to \infty. \tag{3.6}$$

Here, K_r is the reaction rate, n the fitted rate constant $(-1 < n < 1)$, E_a the activation energy, k_1 the Boltzmann constant and k the thermal conductivity.

Adopting the Rosseland's diffusion approximation [56] for the radiative heat flux q_r and the expression is given by

$$q_r = -\frac{4}{3}\frac{\sigma^*}{k^*}\frac{\partial T^4}{\partial z} = -\frac{16}{3}\frac{\sigma^* T^3}{k^*}\frac{\partial T}{\partial z}, \tag{3.7}$$

where k^* is the Rosseland mean spectral absorption coefficient and σ^* the Stefan-Boltzmann constant. We designate $T = T_\infty\left(1 + (\theta_w - 1)\right)\theta$, where $\theta_w\left(=\frac{T_w}{T_\infty}\right) > 1$ is the temperature ratio parameter.

After applying the transformations (Eq. (2.24) cf. Chapter **2**) into Eqs. $(3.1) - (3.5)$, we acquire

$$H' + 2F = 0, \tag{3.8}$$

$$F^2 - G^2 + F'H - F'' + \beta_1\left(F''H^2 + 2FF'H - 2GG'H\right)$$

$$+\beta_2\left(2F'^2 + 2F'H'' - F'''H\right) + M^2\left(F + \beta_1 F'H\right) = 0, \tag{3.9}$$

$$2FG + G'H - G'' + \beta_1 \left(G''H^2 + 2\left(FG' + F'G\right)H\right)$$

$$-\beta_2 \left(G'''H - 2F'G' - 2G'H''\right) + M^2 \left(G + \beta_1 G'H\right) = 0, \tag{3.10}$$

$$\theta'' \left(1 + \frac{4}{3}Rd\right) + \frac{4}{3}Rd \left[\begin{array}{c} \left(\theta^3\theta'' + 3\theta^2\theta'^2\right)(\theta_w - 1)^3 \\ +3\left(\theta^2\theta'' + 2\theta\theta'^2\right)(\theta_w - 1)^2 + 3\left(\theta\theta'' + \theta'^2\right)(\theta_w - 1) \end{array} \right] - \Pr H\theta' + \gamma \Pr \theta = 0, \tag{3.11}$$

$$\phi'' - ScH\phi' - \sigma RSc\left[1 + \delta\theta\right]^n \exp\left[\frac{-E}{1 + \delta\theta}\right]\phi(\eta) = 0. \tag{3.12}$$

The transformed boundary conditions are

$$F(\eta) = \omega, \quad G(\eta) = 1, \quad H(\eta) = 0, \quad \theta(\eta) = 1, \quad \phi(\eta) = 1, \quad \text{at } \eta = 0,$$

$$F(\eta) \to 0, \quad G(\eta) \to 0, \quad \theta(\eta) \to 0, \quad \phi(\eta) \to 0, \quad \text{as} \quad \eta \to \infty. \tag{3.13}$$

In the above expressions, the involved dimensionless parameters, which are presented in governing equations are $\gamma \left(= \frac{Q}{\rho c_p \Omega}\right)$ the heat absorption/generation parameter, $Rd \left(= \frac{16\sigma^*T_\infty^3}{3k^*k}\right)$ the radiation parameter, $E \left(= \frac{E_a}{k_1 T_\infty}\right)$ the activation energy, $\sigma \left(= \frac{K_r^2}{c}\right)$ the reaction parameter and $\delta \left(= \frac{T_w - T_\infty}{T_\infty}\right)$ the temperature difference parameter.

The Nusselt number Nu and Sherwood number Sh are defined by

$$Nu = -\left(1 + \frac{16}{3}\frac{\sigma^*T^3}{kk^*}\right)\frac{k\,R\left(\frac{\partial T}{\partial z}\right)\big|_{z=0}}{k\,(T_w - T_\infty)}, \tag{3.14}$$

and

$$Sh = -\frac{D_B\,R\left(\frac{\partial C}{\partial z}\right)\big|_{z=0}}{D_B\,(C_w - C_\infty)}. \tag{3.15}$$

Making use of the transformations (Eq. (2.24) cf. Chapter **2**) in Eq. (3.14) and (3.15), we

obtain

$$\mathrm{Re}^{-\frac{1}{2}} Nu = -\left\{1 + \frac{4Rd}{3}\left[1 + (\theta_w - 1)\,\theta\,(0)\right]^3\right\}\theta'\,(0)\,, \tag{3.16}$$

$$\mathrm{Re}^{-\frac{1}{2}} Sh = -\phi'\,(0)\,, \tag{3.17}$$

where Re is the Reynolds number defined in Chapter **2**.

3.2 Results and Discussion

In this part, the main focus is to illustrate the physical behavior of the present problem via graphical structures and tables. The system of ordinary differential equations (3.8) to (3.12) along with BCs (3.13) are solved numerically by numerical technique called bvp midrich scheme in Maple. To discuss the different parameters that are involved in the set of equations for the fluid flow behavior, heat and mass transport, results are drawn in figures **3.1** to **3.5**. The effect of involved parameters like, relaxation time parameter β_1, stretching parameter ω, magnetic field parameter M, retardation time parameter β_2, activation energy E, reaction parameter σ, Prandtl number Pr, temperature difference parameter δ and Schmidt number Sc are discussed via figures and tables. For the graphical results, we fixed the flow parameters that are $M = 0.5$, $\omega = 1.3$, $\beta_1 = 0.2$, $\beta_2 = 0.2$, $\gamma = 1.5$, $Rd = 0.1$, $\theta_w = 1.1$, $\mathrm{Pr} = 5.0$, $E = 0.1$, $n = 0.5$, $\delta = 0.1$, $\sigma = 0.1$ and $Sc = 5.0$. Additionally, the obtained solutions through graphical structures are specified for the involved parameters in the ranges, $0.1 \leq \beta_2 \leq 0.9$, $1.3 \leq \omega \leq 1.8$, $0.0 \leq Rd \leq 0.3$, $0.0 \leq \gamma \leq 0.9$, $0.1 \leq E \leq 1.5$, $0.0 \leq \sigma \leq 1.5$, $0.1 \leq \delta \leq 1.5$, $4.0 \leq \mathrm{Pr} \leq 9.0$, $4.0 \leq Sc \leq 9.0$.

To verify the validity of numerical results which are achieved by Maple software, a com-

parison of $F'(0)$, $-G'(0)$ and $-\theta'(0)$ is made for limiting case. These comparisons to those of Bachok *et al.* [53] and Turkyilmazoglu [54] can be noticed in **Table 3.1**. This table shows that there is a reasonable correlation between current and previous results. This allows us the reliability of our numerical results and problem.

Figs. 3.1 (a) $-$ (c) depict the variation of radial $F(\eta)$, azimuthal $G(\eta)$ and axial $H(\eta)$ velocities, temperature $\theta(\eta)$ and concentration $\phi(\eta)$ distributions under the action of Deborah number of retardation time parameter β_2. **Fig. 3.1 (a)** demonstrates the effect of β_2 on radial velocity $F(\eta)$ against η. It can be found that the higher rate of $\beta_2 (= 0.1, 0.3, 0.6, 0.9)$ declines the radial velocity $F(\eta)$ of the fluid. Meanwhile, a converse relation can be seen for azimuthal velocity $G(\eta)$ when retardation time parameter β_2 increases. To see the impact of β_2 on axial velocity $H(\eta)$, results are shown via **Fig. 3.1 (c)**. We see that the values of axial velocity $H(\eta)$ are negative, which shows the flow of the fluid in downward directions. It means that, due to taking the effect of β_2, the flow intensity in vertical downward direction is decreased. Moreover, the magnitude of axial velocity drops off on different values of β_2. **Figs. 3.1 (d)** and (**e**) display the influence of β_2 on temperature $\theta(\eta)$ and concentration $\phi(\eta)$ distributions, respectively, when the other parameters are fixed. It is shown that the temperature $\theta(\eta)$ as well as the concentration $\phi(\eta)$ distributions are boosted up by higher values of $\beta_2 (= 0.1, 0.3, 0.6, 0.9)$. Moreover, the thickness of both thermal and concentration boundary layers is increased as the retardation parameter β_2 changes from 0.1 to 0.9.

To see the change in the velocity field, temperature and concentration distributions by taking effect of stretching parameter ω, the results are graphically illustrated in **Figs. 3.2 (a)** to (**e**). As the stretching parameter ω is the ratio of stretch to the swirl rates. So, by enlarging $\omega (= 1.3, 1.4, 1.6, 1.8)$, the radial fluid velocity increases due to an increase in the disk's stretching

rate. Meanwhile, for the azimuthal velocity $G(\eta)$, a converse effect is found as seen in **Fig. 3.2 (b)**. This is due to a decrease in the disk's rotation rate. Additionally, to see the graphical structure of axial velocity $H(\eta)$ against different stretching rates, curves can be observed in **Fig. 3.2 (c)**. The distribution of temperature $\theta(\eta)$ against different values of stretching parameter ω is obtained in **Fig. 3.2 (d)**. It can be found that the fluid temperature is reduced by taking the higher stretching rate $\omega (= 1.3 \text{ to } 1.8)$. The same result can be observed for the concentration distribution $\phi(\eta)$ as pictured in **Fig. 3.2 (e)**.

The variation of temperature distribution $\theta(\eta)$ via radiation parameter Rd and heat generation/absorption parameter γ, respectively, is shown through **Figs. 3.3 (a)** and **(b)** with default values of other fixed parameters. One can observe from the distributions given in these figures that all the solutions satisfy the far field boundary conditions asymptotically. As we can see from **Fig. 3.3 (a)** that the dimensionless liquid temperature $\theta(\eta)$ is boosted up by the radiation parameter Rd with respect to η. Physically, strength of the radiative source described by radiation dimensionless parameter Rd which enhances the temperature due to extra heat that is provided to the fluid. Moreover, the influence of heat generation/absorption parameter γ on $\theta(\eta)$ is examined via **Fig. 3.3 (b)**. These curves show that the fluid temperature improves as the heat generation parameter γ changes from 0.0 to 0.9. Additionally, the enlargement of γ causes the thermal boundary layer thickness to be raised in this situation.

In order to show the impact of different parameters such as, activation energy E, reaction parameter σ and temperature difference parameter δ on concentration distribution $\phi(\eta)$, some results are shown. In this regard, **Figs. 3.4 (a)** to **(c)** are pictured to see the variation in concentration distribution $\phi(\eta)$ with respect to mentioned parameters against η. From **Fig. 3.4 (a)**, the concentration distribution $\phi(\eta)$ as well as the thickness of concentration layer in-

creases with the augmentation in activation energy $E\,(=0.1, 0.5, 1.0, 1.5)$. Furthermore, for the particular set of physical parameters, the concentration volume fraction drops off as an increment in reaction parameter σ. The same outcomes can be seen for the temperature difference parameter δ in **Fig. 3**.**5** (**c**).

The impact of Pr on temperature of the fluid is discussed with default values of other fixed physical parameters in **Fig. 3**.**5** (**a**). This figure shows that the temperature drops down by varying the Prandtl number in four steps $(4.0, 5.0, 7.0, 9.0)$. Physically, the enlargement of $\mathrm{Pr}\,(>1)$ reduces the thermal diffusivity, hence the reduction of the temperature $\theta\,(\eta)$ is noticed in this manner. Moreover, **Fig. 3**.**5** (**b**) illustrates mass transport with the impact of Schmidt number Sc in the flow of Oldroyd-B fluid over a rotating disk. The analysis is done for various values of Schmidt number $Sc\,(=4.0, 5.0, 7.0, 9.0)$. It is remarked that the Schmidt number Sc causes the concentration distribution $\phi\,(\eta)$ to decline as seen in **Fig. 3**.**5** (**b**). Physically, higher rate of Schmidt number decreases the diffusion coefficients, hence as a result, the concentration reduces in this situation.

To see the change in Nusselt number $\mathrm{Re}^{-\frac{1}{2}}\,Nu$ and Sherwood number $\mathrm{Re}^{-\frac{1}{2}}\,Sh$ for different physical parameters are discussed through **Tables 3.2** and **3.3**. The values of $\mathrm{Re}^{-\frac{1}{2}}\,Nu$ and $\mathrm{Re}^{-\frac{1}{2}}\,Sh$ are calculated numerically with respect to different physical parameters like, β_1, β_2 and M shown in **Table 3.2**. These results show that the Nusselt number and Sherwood number are enhanced with the enhancement in β_1. An opposite outcomes can be seen for β_2 and M. Moreover, in **Table 3.3**, the impact of Rd, γ and Pr, respectively on $\mathrm{Re}^{-\frac{1}{2}}\,Nu$ are analyzed. It is be observed that the heat transfer rate reduces with an increment in Rd. A similar observation is seen for the γ. While the Nusselt number are boosted up as Pr changes from 6.0 to 7.0.
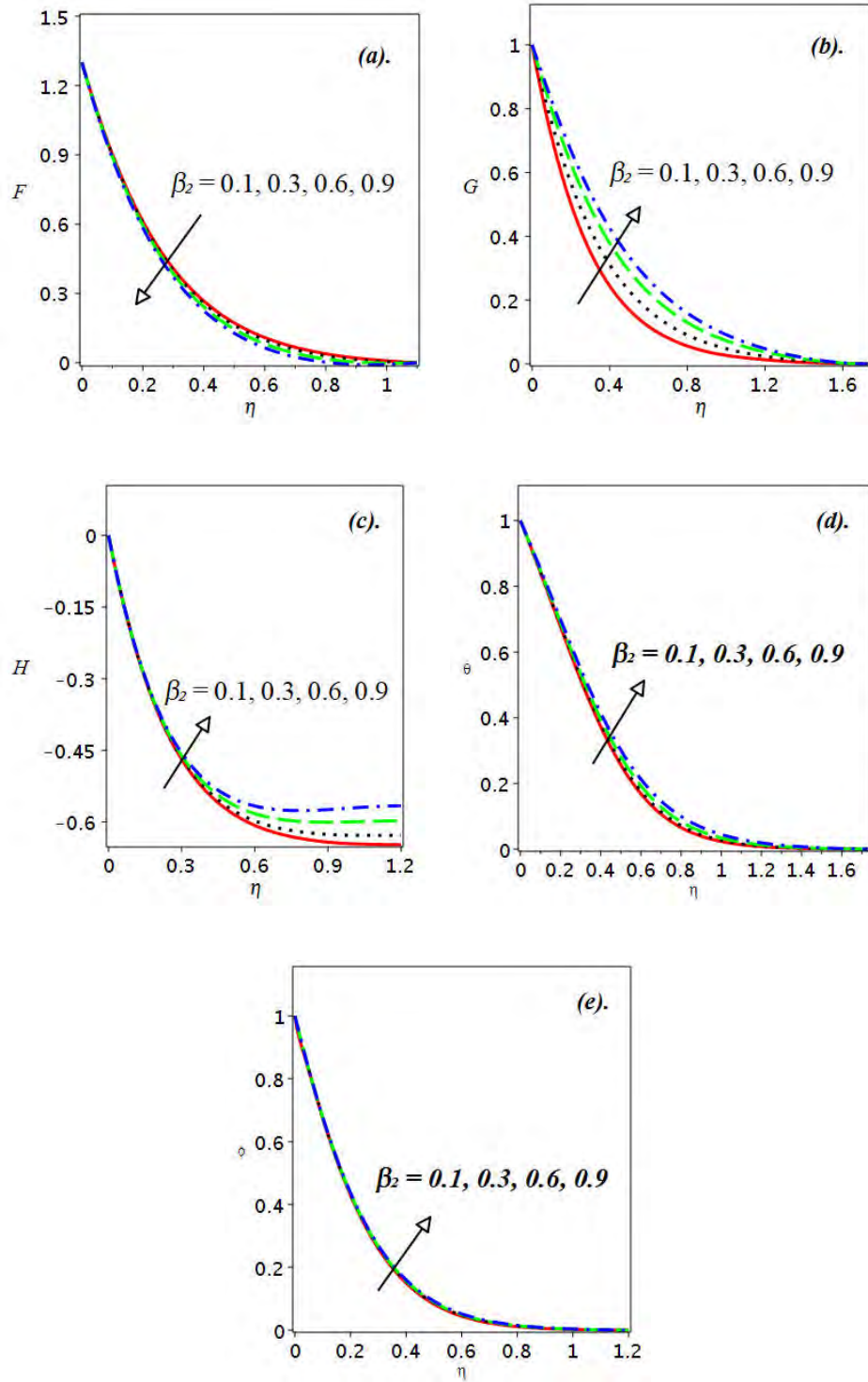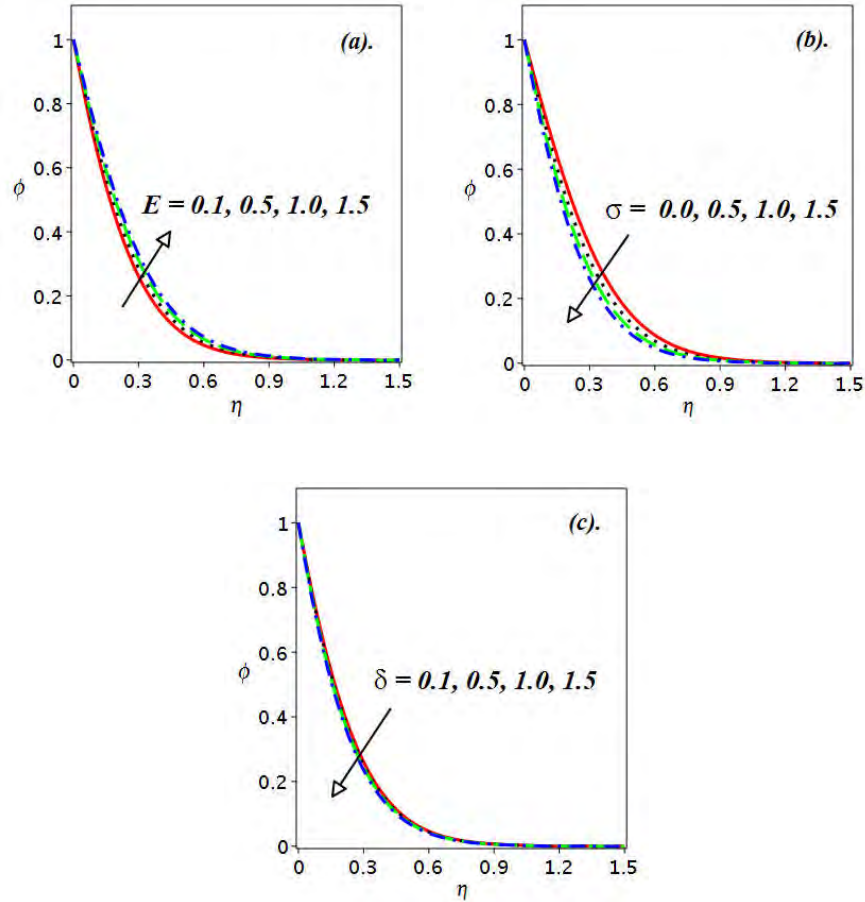
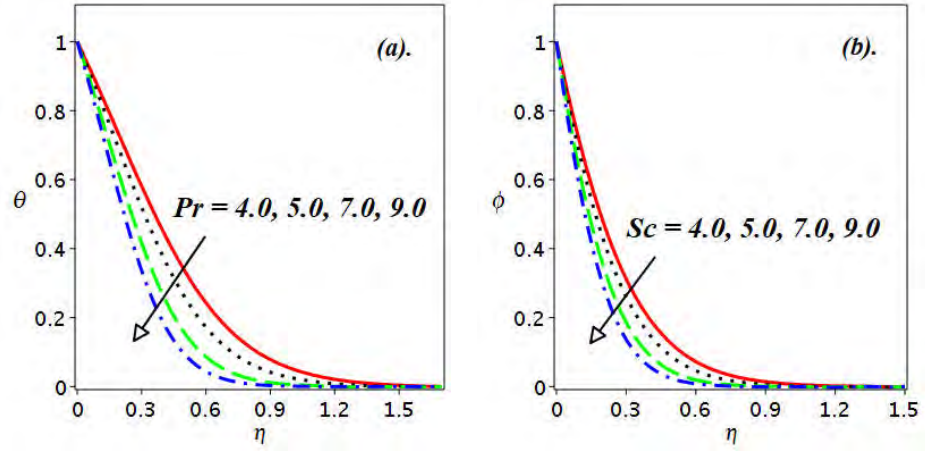**Figs. 3.1**: Impact of β_2 on $F(\eta)$, $G(\eta)$, $H(\eta)$, $\theta(\eta)$ and $\phi(\eta)$.
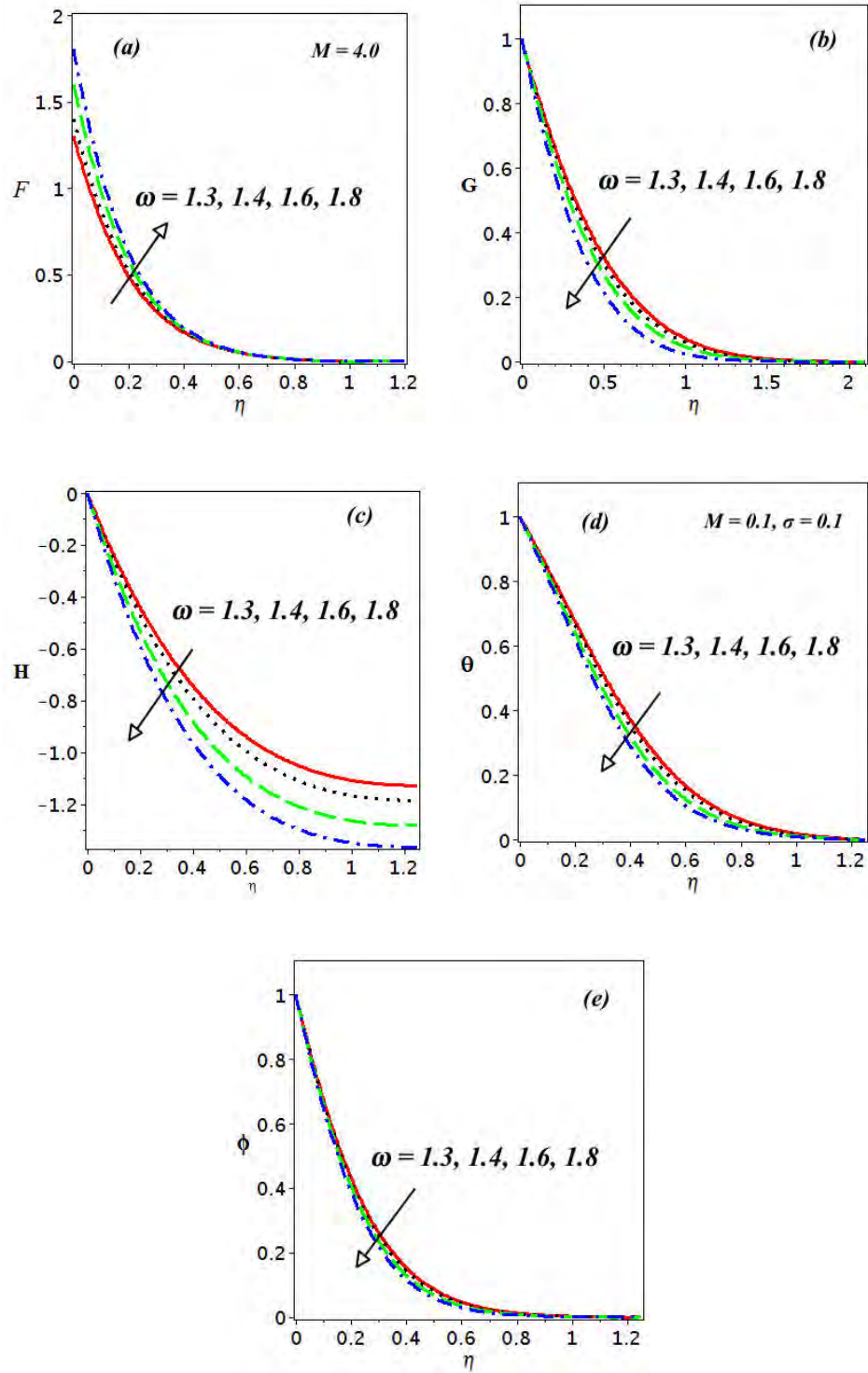
Figs. 3.2: Impact of ω on $F(\eta)$, $G(\eta)$, $H(\eta)$, $\theta(\eta)$ and $\phi(\eta)$.
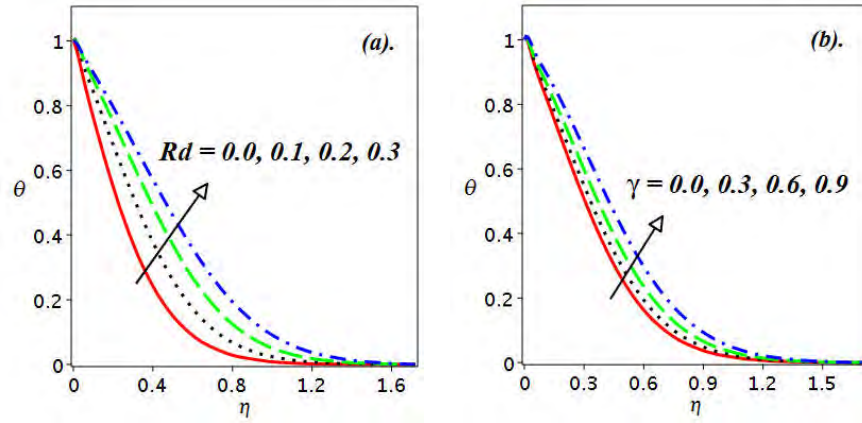
Figs. 3.3: Variation in $\theta(\eta)$ on Rd and γ.

Figs. 3.4: Variation in $\phi(\eta)$ on E, σ and δ.

Figs. 3.5: Variation in $\theta(\eta)$ on Pr and variation in $\phi(\eta)$ on Sc.

Table 3.1: A comparison of the $F'(0)$, $-G'(0)$ and $-\theta'(0)$ on fixed $\text{Pr} = 6.2$ and $\beta_1 = 0 = \beta_2 = M = \omega = \gamma = Rd$ with past outcomes.

	Turkyilmazoglu [54]	Bachok *et al.* [53]	bvp midrich results
$F'(0)$	0.51023262	0.5102	0.5101162643
$-G'(0)$	0.61592201	0.6159	0.6158492796
$-\theta'(0)$	0.93387794	0.9337	0.9336941128

Table 3.2: The numerical values of $\mathrm{Re}^{-\frac{1}{2}} Nu$ and $\mathrm{Re}^{-\frac{1}{2}} Sh$ on various values of β_1, β_2 and

M and the other parameters are fixed.

β_1	β_2	M	$\mathrm{Re}^{-\frac{1}{2}} Nu$	$\mathrm{Re}^{-\frac{1}{2}} Sh$
0.2	0.2	0.5	1.7683091993	2.2276477609
0.3			1.9780494438	2.3355715514
0.4			2.0335341066	2.3680021632
0.2	0.2		1.7954361264	2.2424495253
	0.3		1.7831406023	2.2371290254
	0.4		1.7698931330	2.2315134573
0.2	0.2	0.5	1.7683091993	2.2276477609
		0.6	1.7597401551	2.2240388941
		0.7	1.7497844668	2.2198909343
		0.8	1.7385208744	2.2152553852

Table 3.3: The numerical values of $\mathrm{Re}^{-\frac{1}{2}} Nu$ for various values of Rd, γ and Pr and the default parameters are fixed.

Rd	γ	Pr	$\mathrm{Re}^{-\frac{1}{2}} Nu$
0.1	0.1	5.0	1.7683091993
0.2			1.5467477587
0.3			1.4377191461
0.3	0.2		1.3565981679
	0.3		1.2709140344
	0.4		1.1799367091
0.3	0.1	6.0	1.6185916354
		6.5	1.7041687711
		7.0	1.7866720833

Chapter 4

Stagnation Point Flow of Radiative Oldroyd-B Nanofluid

This chapter reports the MHD boundary layer stagnation point flow of an Oldroyd-B nanofluid over a porous rotating disk. The impact of non-linear radiation and heat generation/absorption are studied on heat transfer behavior. The features of Brownian motion and thermophoresis during the nanoparticles movement in fluid motion are studied with Buongiorno model.

The governing partial differential equations (PDEs) are transformed into dimensionless ordinary differential equations (ODEs) using the von Karman transformations. The bvp midrich technique utilized to obtain the numerical solution of the governing problem. The results reveal that the concentration gradient at the wall reduces with an increment in mass transfer parameter.

4.1 Mathematical Formulation

In this portion, an incompressible steady three-dimensional boundary layer flow of Oldroyd-B fluid over a permeable disk subject to magnetic field applied in the axial direction is considered. The flow is generated due to stretching velocity $u = cr$, and rotating velocity $v = \Omega r$ of the disk as shown in **Fig**. **2.1** (cf. Chapter **2**). The stagnation point is at the surface $(z = 0)$ and the liquid flows at $(z \geqslant 0)$ the upper half plane. The disk is assumed porous with mass flux velocity w_0 with $w_0 > 0$ for injection and $w_0 < 0$ for suction. By the Fourier's law of heat conduction, the heat transfer analysis is performed with the influence of nonlinear radiation and heat generation/absorption. Here, T_f is the convective fluid temperature and h_f the convective heat transfer coefficient because the surface temperature is of the convective heating process. From the above discussion, the governing equations for the considered non-linear problem are (Eqs.(2.18) to (2.20) cf. Chapter **2**, Eqs. (1.7), $(1.11) - (1.14)$, $(1.15) - (1.16)$ cf. Chapter **1**)

$$\frac{\partial u}{\partial r} + \frac{u}{r} + \frac{\partial w}{\partial z} = 0, \tag{4.1}$$

$$
u\frac{\partial u}{\partial r} - \frac{v^2}{r} + w\frac{\partial u}{\partial z} = \nu\frac{\partial^2 u}{\partial z^2} - \frac{\sigma}{\rho}B_0^2\left[u + \lambda_1 w\frac{\partial u}{\partial z} - u_e\right]
$$
$$
+ u_e\frac{\partial u_e}{\partial r} - \lambda_1\left[u^2\frac{\partial^2 u}{\partial r^2} + w^2\frac{\partial^2 u}{\partial z^2} + 2uw\frac{\partial^2 u}{\partial r\partial z} - \frac{2uv}{r}\frac{\partial v}{\partial r} - \frac{2vw}{r}\frac{\partial v}{\partial z} + \frac{uv^2}{r^2} + \frac{v^2}{r}\frac{\partial u}{\partial r}\right]
$$
$$
+ \nu\lambda_2\left[-\frac{1}{r}\left(\frac{\partial u}{\partial z}\right)^2 - 2\frac{\partial u}{\partial z}\frac{\partial^2 w}{\partial z^2} + w\frac{\partial^3 u}{\partial z^3} - \frac{\partial u}{\partial r}\frac{\partial^2 u}{\partial z^2} - \frac{\partial u}{\partial z}\frac{\partial^2 u}{\partial r\partial z} + u\frac{\partial^3 u}{\partial r\partial z^2}\right], \tag{4.2}
$$

$$u\frac{\partial v}{\partial r} + \frac{uv}{r} + w\frac{\partial v}{\partial z} = \nu\frac{\partial^2 v}{\partial z^2} - \frac{\sigma}{\rho}B_0^2\left[v + \lambda_1 w\frac{\partial v}{\partial z}\right]$$

$$-\lambda_1\left[u^2\frac{\partial^2 v}{\partial r^2} + w^2\frac{\partial^2 v}{\partial z^2} + 2uw\frac{\partial^2 v}{\partial r\partial z} + 2\frac{uv}{r}\frac{\partial u}{\partial r} + 2\frac{vw}{r}\frac{\partial u}{\partial z} - 2\frac{u^2 v}{r^2} - \frac{v^3}{r^2} + \frac{v^2}{r}\frac{\partial v}{\partial r}\right]$$

$$+\nu\lambda_2\begin{bmatrix} u\frac{\partial^3 v}{\partial r\partial z^2} - 2\frac{\partial v}{\partial z}\frac{\partial^2 w}{\partial z^2} + w\frac{\partial^3 v}{\partial z^3} - \frac{1}{r}\frac{\partial u}{\partial z}\frac{\partial v}{\partial z} \\ -\frac{\partial v}{\partial r}\frac{\partial^2 u}{\partial z^2} + \frac{v}{r}\frac{\partial^2 u}{\partial z^2} - \frac{\partial v}{\partial z}\frac{\partial^2 u}{\partial r\partial z} - \frac{u}{r}\frac{\partial^2 v}{\partial z^2} \end{bmatrix}, \tag{4.3}$$

$$u\frac{\partial T}{\partial r} + w\frac{\partial T}{\partial z} = \frac{k}{\rho c_p}\left(\frac{\partial^2 T}{\partial z^2}\right) - \frac{1}{\rho c_p}\frac{\partial q_r}{\partial z} + \tau_1\left(D_B\frac{\partial T}{\partial z}\frac{\partial C}{\partial z} + \frac{D_T}{T_\infty}\left(\frac{\partial T}{\partial z}\right)^2\right) + \frac{Q}{\rho c_p}(T - T_\infty), \tag{4.4}$$

$$u\frac{\partial C}{\partial r} + w\frac{\partial C}{\partial z} = D_B\frac{\partial^2 C}{\partial z^2} + \frac{D_T}{T_\infty}\frac{\partial^2 T}{\partial z^2}. \tag{4.5}$$

The BCs are

$$u = cr, \quad v = \Omega r, \quad w = w_0, \quad -k\frac{\partial T}{\partial z} = h_f(T_f - T), \quad C = C_w \text{ at } z = 0,$$

$$u \to u_e = ar, \quad v \to 0, \quad w = w_e = -2az, \quad T \to T_\infty, \quad C \to C_\infty \text{ as } z \to \infty. \tag{4.6}$$

The expression for the radiative heat flux q_r is (Eq. (3.7) cf. Chapter **3**)

$$q_r = -\frac{4}{3}\frac{\sigma^*}{k^*}\frac{\partial T^4}{\partial z} = -\frac{16}{3}\frac{\sigma^* T^3}{k^*}\frac{\partial T}{\partial z}, \tag{4.7}$$

After applying the transformations (Eq. (2.24) cf. Chapter **2**) into Eqs. (4.1) − (4.5), we get

$$H' + 2F = 0, \tag{4.8}$$

$$F^2 - G^2 + F'H - F'' + \beta_1 \left(F''H^2 + 2FF'H - 2GG'H \right)$$

$$+\beta_2 \left(2F'^2 + 2F'H'' - F'''H \right) + M \left(F + \beta_1 F'H - A \right) - A^2 = 0, \tag{4.9}$$

$$2FG + G'H - G'' + \beta_1 \left(G''H^2 + 2 \left(FG' + F'G \right) H \right)$$

$$-\beta_2 \left(G'''H - 2F'G' - 2G'H'' \right) + M \left(G + \beta_1 G'H \right) = 0, \tag{4.10}$$

$$\theta'' \left(1 + \frac{4}{3} Rd \right) + \frac{4}{3} Rd \left[\begin{array}{c} \left(\theta^3 \theta'' + 3\theta^2 \theta'^2 \right) \left(\theta_w - 1 \right)^3 \\ +3 \left(\theta^2 \theta'' + 2\theta \theta'^2 \right) \left(\theta_w - 1 \right)^2 + 3 \left(\theta \theta'' + \theta'^2 \right) \left(\theta_w - 1 \right) \end{array} \right]$$

$$- \Pr H\theta' + \Pr \left(Nb\theta'\phi' + Nt\theta'^2 \right) + \gamma \Pr \theta = 0, \tag{4.11}$$

$$\phi'' - ScH\phi' + \frac{Nt}{Nb}\theta'' = 0. \tag{4.12}$$

The transformed BCs are

$$F\left(\eta \right) = \omega, \ G\left(\eta \right) = 1, \ H\left(\eta \right) = s, \ \theta'\left(\eta \right) = -Bi\left(1 - \theta\left(\eta \right) \right), \ \phi\left(\eta \right) = 1 \quad \text{at } \eta = 0,$$

$$F\left(\eta \right) \to A, \ G\left(\eta \right) \to 0, \ \theta\left(\eta \right) \to 0, \ \phi\left(\eta \right) \to 0 \quad \text{as } \eta \to \infty. \tag{4.13}$$

The dimensionless physical parameters are as follow:

$A \left(= \frac{a}{\Omega} \right)$ the velocity ratio parameter, $s \left(= \frac{w_o}{\sqrt{\Omega \nu}} \right)$ the mass transfer parameter and $Bi \left(= \frac{h_f}{k} \sqrt{\frac{\nu}{\Omega}} \right)$

the Biot number and rest of the parameters are similar as defined in the previous chapter.

63

4.2 Physical Parameters

The physical parameters defined as follows:

(i) The Nusselt number Nu is defined by

$$Nu = -\left(1 + \frac{16}{3}\frac{\sigma^* T^3}{kk^*}\right)\frac{R\,k\left(\frac{\partial T}{\partial z}\right)\big|_{z=0}}{k\left(T_f - T_\infty\right)}. \tag{4.14}$$

Making use of the transformations (Eq. (2.24) cf. Chapter **2**) in Eq. (4.14) gives

$$\mathrm{Re}^{-\frac{1}{2}}Nu = -\left\{1 + \frac{4Rd}{3}\left[1 + (\theta_w - 1)\,\theta\,(0)\right]^3\right\}\theta'(0). \tag{4.15}$$

(ii) The Sherwood number Sh is

$$Sh = -\frac{R\,D_B\left(\frac{\partial C}{\partial z}\right)\big|_{z=0}}{D_B\left(C_w - C_\infty\right)}. \tag{4.16}$$

After using the similarity variables (Eq. (2.24) cf. Chapter **2**) in Eq. (4.16), we obtain

$$\mathrm{Re}^{-\frac{1}{2}}Sh = -\phi'(0), \tag{4.17}$$

where Re is the Reynolds number defined in Chapter **2**.

4.3 Results and Discussion

In the present investigation, our aim is to interpret the characteristics of swirling stagnation point flow of Oldroyd-B nanofluid over a permeable rotating disk. In order to describe the flow behavior, heat and mass transfers in terms of various involved parameters, results are drawn in figures **4.1** to **4.6**. For this, we fixed various physical parameters which are $M = 1.0$, $\omega = 1.3$, $s = 0.1$, $\beta_1 = 0.05$, $\beta_2 = 0.2$, $A = 1.5$, $\theta_w = 1.1$, $Rd = 0.03$, $Bi = 0.8$, $\gamma = 0.5$, $Nt = 0.1$, $Nb = 0.1$, $\Pr = 5.0$ and $Sc = 5.0$ to illustrate physical reasoning of the problem.

The influence of stretching parameter ω on velocity in radial $F(\eta)$ and azimuthal $G(\eta)$ directions, temperature $\theta(\eta)$ and concentration $\phi(\eta)$ distributions, respectively is sketched in **Figs. 4.1 (a)−(d)** with the specified values of other parameters. **Fig. 4.1 (a)** shows the impact of ω on fluid velocity in radial direction. In this figure, the radial velocity $F(\eta)$ shows a rising behavior with an increase in ω in the range 0.1 to 2.0. Basically, the stretching parameter ω is the ratio of stretch c to swirl Ω rates of the disk. So, by higher estimation of stretching parameter $\omega (= 0.1, 1.0, 1.5, 2.0)$, the fluid velocity in radial direction $F(\eta)$ increases due to an increase in the disk stretching rate. On the other hand, the contrary variation on velocity in azimuthal direction is noticed in **Fig. 4.1 (b)**. This is because of the decrease in the swirl rate of the disk as compared to stretching rate. Moreover, the change in temperature for higher values of ω is discussed through **Fig. 4.1 (c)** with the default values of other parameters. It is remarked that the temperature $\theta(\eta)$ declines with the enlargement of ω. For solutal distribution $\phi(\eta)$, similar results can be seen (see **Fig. 4.1 (d)**).

Figs. 4.2 (a − b) are sketched to see the effect of velocity ratio parameter A on radial velocity $F(\eta)$ and azimuthal velocity $G(\eta)$ against η. It is noted that as the value of

$A (= 0.0, 0.1, 0.3, 0.5)$ increases, so does the radial velocity $F(\eta)$. As A is the ratio of free stream velocity rate to rotation rate of the disk. Physically, it can be perceived that when the values of $A < 1$, the rotating disk velocity will be dominant than the free stream velocity. As rotation of disk is also contributes in the radial velocity of the fluid and the disk rotation accelerates with more speed, the development of centrifugal force will become more stronger which as a result, push the fluids particles in the radial direction, so, enhancement of the radial flow velocity is noticed. Furthermore, the reduction of the velocity in azimuthal direction is seen in **Fig. 4.2 (b)**. This is due to a decrease in the rotation rate of the disk. **Figs. 4.3 (a) − (c)** depict the effect of suction parameter s on $F(\eta)$, $\theta(\eta)$ and $\phi(\eta)$, respectively. In **Fig. 4.3 (a)**, we seen that the velocity of the fluid enhances by the enlargement of mass transfer parameter $s (= 0.0, 0.1, 0.3, 0.5)$ with $A = 0.1$. Enlargement in temperature field $\theta(\eta)$ is noticed for the case of injection which changes from 0.0 to 0.5 that is displayed in **Fig. 4.3 (b)**. Furthermore, the concentration distribution for mass transfer parameter s is pictured in **Fig. 4.3 (c)**. It is scrutinized that the concentration of the fluid enhances as s changes from 0.0 to 0.5.

In order to see the change in fluid temperature on thermal radiation parameter Rd, Biot number Bi and heat absorption/generation parameter δ, respectively, results are sketched via **Figs. 4.4 (a) − (c)**. Here, distributions given in these sketches show that all results are satisfied boundary conditions asymptotically. It is sighted that the temperature of the fluid $\theta(\eta)$ is boosted up under the action of radiation parameter Rd against η. Basically, the process of radiation described by dimensionless radiation parameter Rd which raises the fluid temperature due to providing of extra heat to the fluid. Furthermore, the impact of Biot number Bi on temperature distribution is discussed via **Fig. 4.4 (b)**. As we seen that the temperature within the fluid flow is boosted up with an increment in Biot number $Bi (= 0.1, 0.3, 0.5, 0.8)$. From the

definition of Biot number Bi, the increasing values of Bi implies that the convective heat transfer coefficient increases which allows more heat to be transferred from the surface. Furthermore, the temperature distribution $\theta(\eta)$ is also influenced by heat generation/absorption parameter γ (see **Fig. 4.4 (c)**). This figure highlighted that the temperature of the fluid is enhanced by enlarging values of $\gamma (= 0.0, 0.3, 0.6, 0.9)$. Additionally, the thermal boundary layer thickness becomes thicker with the enlargement of γ in this manner.

The effect of thermophoresis parameter Nt on $\theta(\eta)$ and $\phi(\eta)$ Oldroyd-B liquid is illustrated in **Figs. 4.5 (a)** and **(b)**. According to the results, the temperature of the fluid rises as Nt goes from 0.1 to 0.7. The same behavior is seen for concentration of nanoparticle as shown in **Fig. 4.5 (b)**. Basically, the thermophoretic force produces in the fluid by taking the higher values of Nt and consequently, heat and mass transport enhance in the fluid. To see the effect of Brownian motion parameter (Nb) on $\theta(\eta)$ and $\phi(\eta)$, respectively, results are drawn in **Figs. 4.6 (a)** to **(b)**. From **Fig. 4.6 (a)**, it is rendered that the temperature rises when the values of Nb increases. Moreover, the concentration distribution $\phi(\eta)$ declines as Nb changes form 0.1 to 0.7 with $Bi = 0.2$. As, the resistance to the mass transport phenomenon is produced by higher Brownian motion which leads to a reduction in the concentration distribution.

To see the variations in Nusselt number and Sherwood number on different physical parameters, results are drawn in **Tables 4.1** and **4.2**, respectively. In **Table 4.1**, we seen that the enlargement of s, β_1 and β_2, respectively, the Nusselt number reduces, while a converse results can be noticed for Biot number Bi. Additionally, the heat transfer at the wall shows decreasing results for Rd, Nt and Nb, respectively. Furthermore, the variation of Sherwood number $Re^{-1/2} Sh$ with respect to s, β_1, β_2, Nt, Nb and Sc, respectively, numerical results of Oldroyd-B fluid over a porous disk are presented in **Table 4.2**. It can be observed that, the
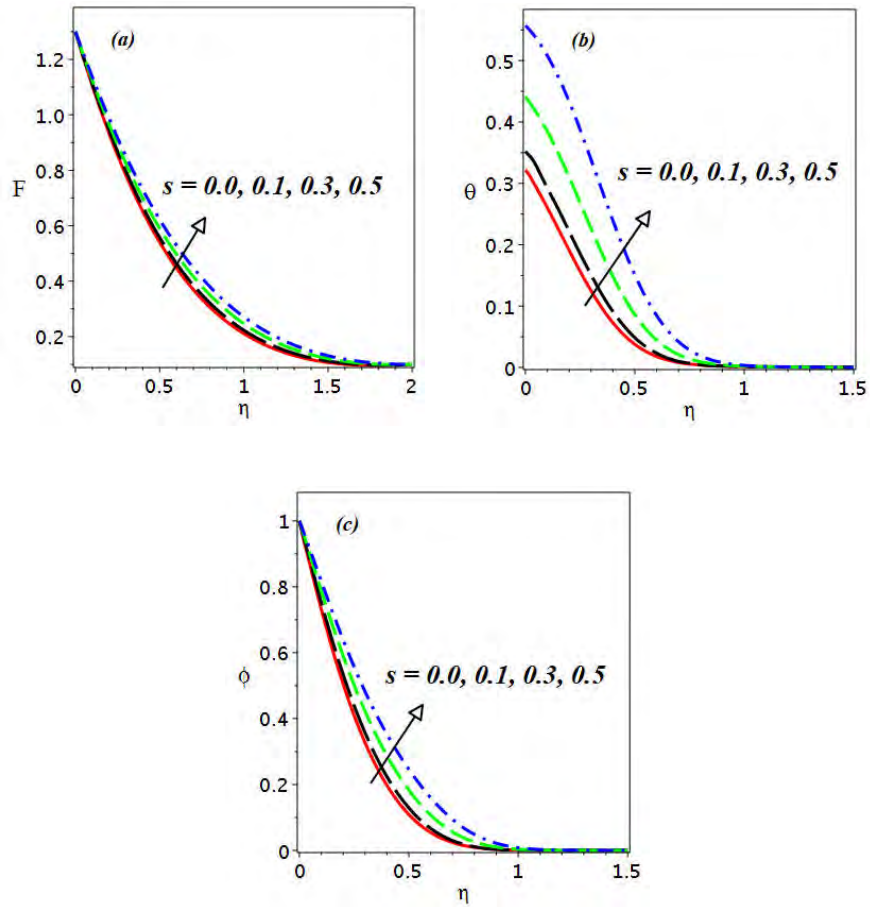
mass transfer at the well declines with respect to s, β_1 and β_2, respectively. On the other hand, results show the higher trend of Sherwood number against Nt, Nb and Sc, respectively.
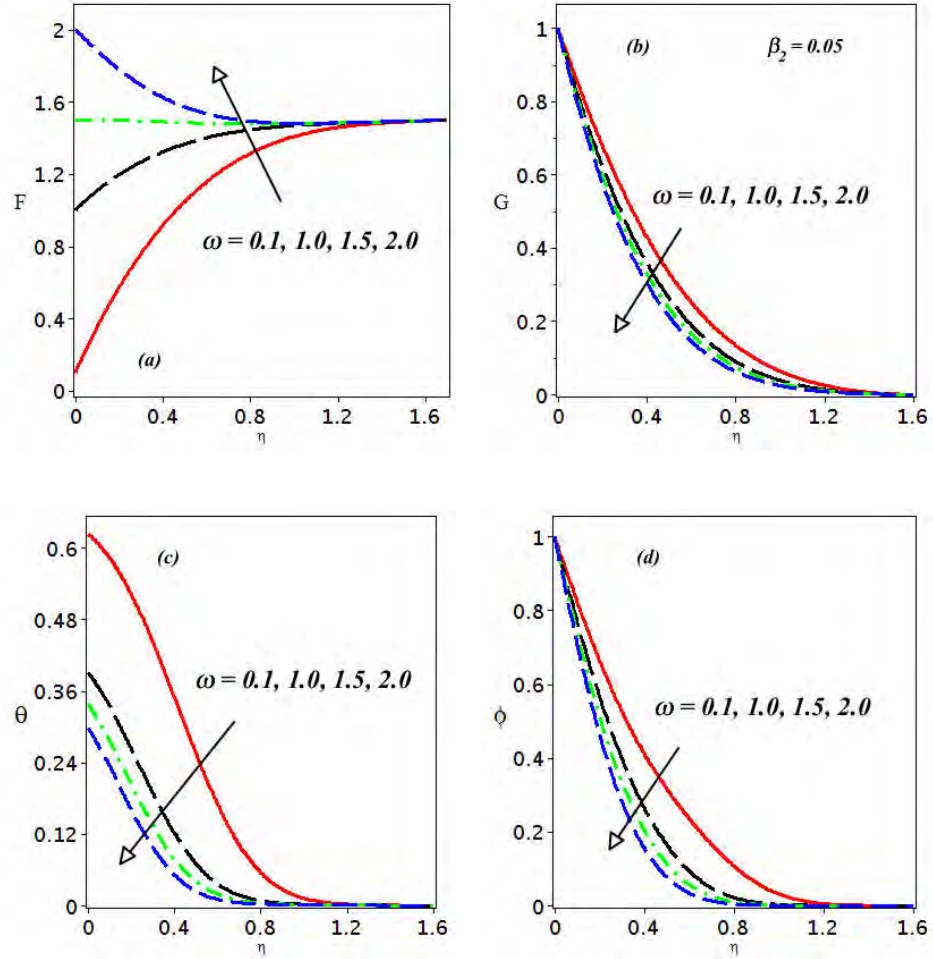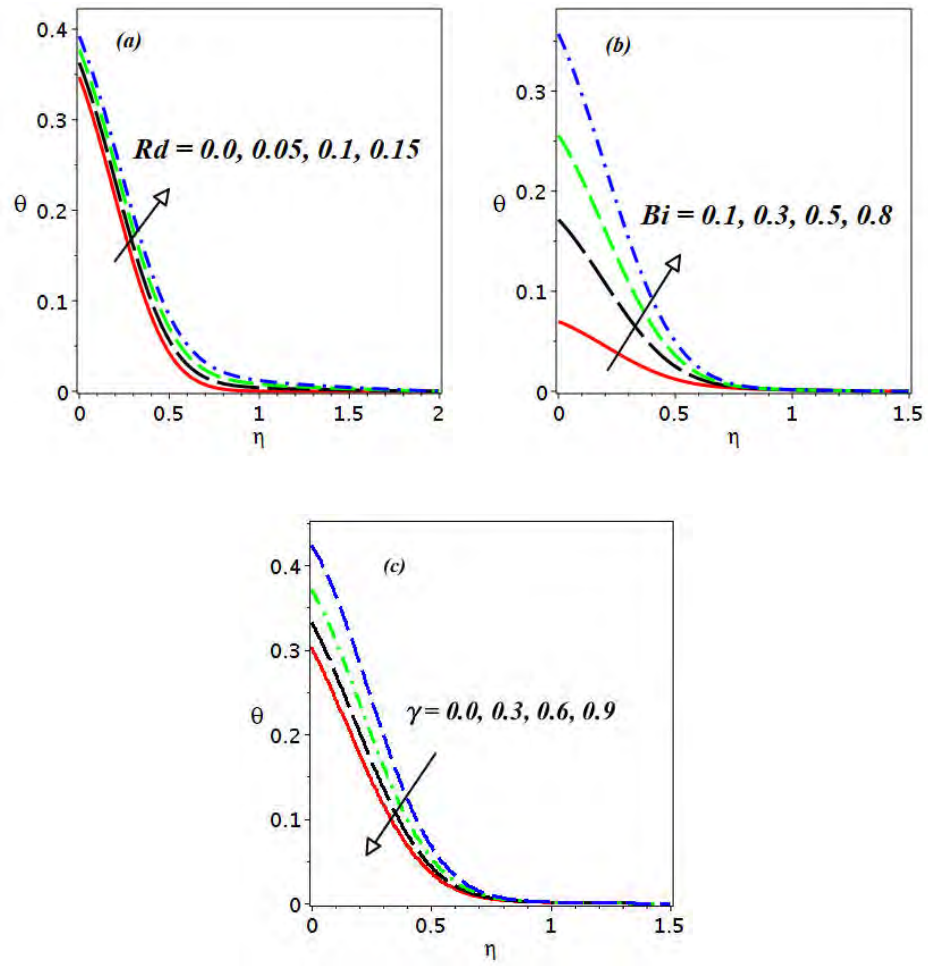

Figs. 4.1: Impact of ω on $F(\eta)$, $G(\eta)$, $\theta(\eta)$ and $\phi(\eta)$.
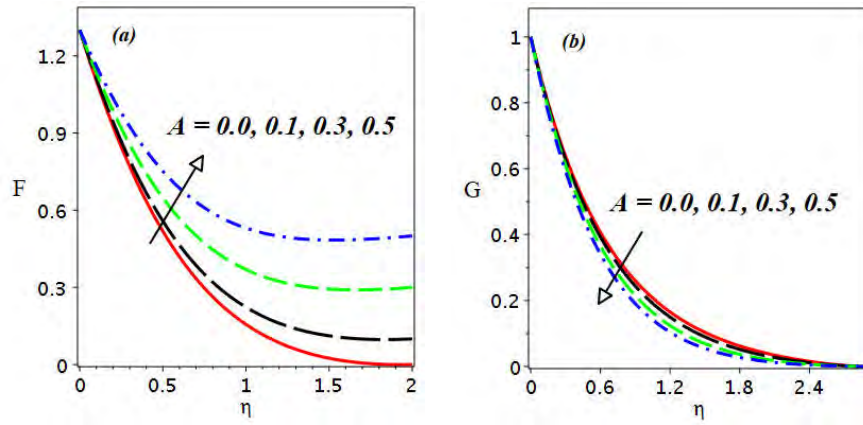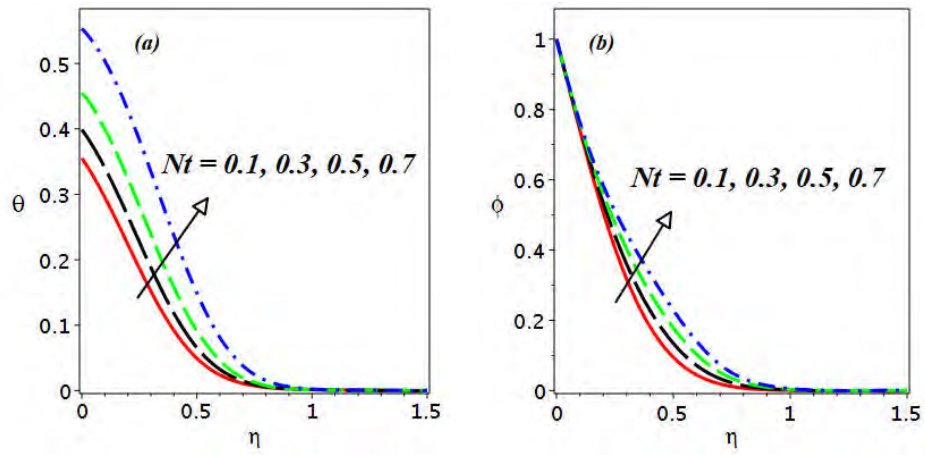
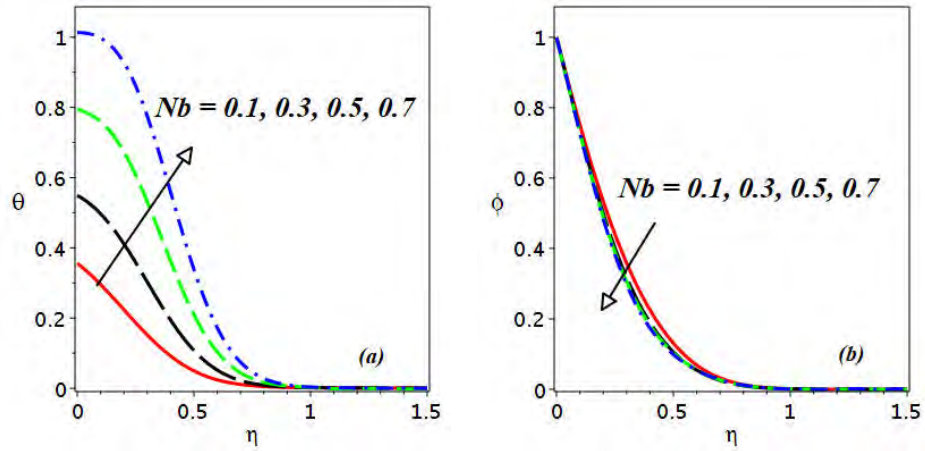**Figs. 4.2**: Impact of A on $F(\eta)$ and $G(\eta)$.

Figs. 4.3: Impact of s on $F(\eta)$, $\theta(\eta)$ and $\phi(\eta)$.

Figs. 4.4: Variation of $\theta(\eta)$ on Rd, Bi and γ.

Figs. 4.5: Impact of Nt on $\theta(\eta)$ and $\phi(\eta)$.

Figs. 4.6: Impact of Nb on $\theta(\eta)$ and $\phi(\eta)$.

Table 4.1: Influence of physical parameters s, β_1, β_2, Bi, Rd, Nt and Nb on $\mathrm{Re}^{-1/2}\,Nu$ with $\omega = 1.3$, $M = 1$, $A = 0.5$, $\theta_w = 1.1$, $Sc = 5.0 = \mathrm{Pr}$ and $\gamma = 0.5$.

s	β_1	β_2	Bi	Rd	Nt	Nb	$\mathrm{Re}^{-1/2}\,Nu$
0.1	0.03	0.2	0.5	0.1	0.1	0.1	0.32869670
0.2							0.30445296
0.3							0.27164688
0.3	0.05						0.27142563
	0.08						0.27003383
0.3	0.1	0.1					0.27147688
		0.3					0.26767199
0.3	0.1	0.5	0.5				0.26242469
			0.55				0.27614758
			0.6				0.28880341
0.3	0.1	0.5	0.7	0.3			0.25893435
				0.5			0.21710155
				0.7			0.18330227
0.3	0.1	0.5	0.7	0.6	0.1		0.19931250
					0.2		0.17118192
					0.3		0.13864581
0.3	0.1	0.5	0.7	0.6	0.2	0.1	0.17132248
						0.2	0.11515603
						0.3	0.05633411

Table 4.2: Influence of physical parameters s, β_1, β_2, Nt, Nb and Sc on $\mathrm{Re}^{-1/2} Sh$ with $\omega = 1.3$, $M = 1$, $A = 0.5$, $Pr = 5$, $Rd = 0.1$, $Bi = 0.5$ and $\gamma = 0.5$.

s	β_1	β_2	Nt	Nb	Sc	$\mathrm{Re}^{-1/2} Sh$
0.1	0.03	0.2	0.1	0.1	3.0	2.30389026
0.2						2.07722109
0.3						1.86641287
0.3	0.05					1.86447322
	0.08					1.86148902
	0.1					1.85943551
0.3	0.1	0.3				1.85286187
		0.4				1.84598114
		0.5				1.81700298
0.3	0.1	0.1	0.3			2.24122884
			0.4			2.61593126
			0.5			3.21403998
0.3	0.1	0.1	0.3	0.3		2.29779179
				0.4		2.32245478
				0.5		2.31603409
0.3	0.1	0.1	0.3	0.3	5.0	2.29779179
					7.0	2.48750201
					9.0	2.65290729

Chapter 5

Swirling Flow of Oldroyd-B Fluid with Soret-Dufour Effects

In this chapter, a mathematical investigation of the Darcy flow of an Oldroyd-B fluid due to a permeable rotating disk is discussed. The mechanisms of heat and mass transport are investigated with the significant features of thermal diffusion (Soret) and diffusion thermo (Dufour). Further, the impact of chemical reaction is also assumed on solutal field. To handle the governing problem, the von Karman variables are utilized to produce the similarity equations which are then numerically integrated via bvp midrich method in Maple. A parametric survey is undertaken and the results are displayed in both graphical and tabular formats. It is proved that the velocity of the fluid reduces with the impact of the porosity parameter. The rate of heat transfer accelerates substantially with the decreasing values of Soret number.

5.1 Mathematical Formulation

We assume the axisymmetric flow of an Oldroyd-B fluid influenced by stretchable rotating porous disk. The flow about $z-$axis is axisymmetric so that all physical quantities are independent to φ. The magnetic field is applied normally to the disk in this problem. The disk is assumed to be porous with mass flow rate w_0 ($w_0 > 0$ for injection and $w_0 < 0$ for suction). The assessments of heat and mass transport are performed with the addition of Soret and Dufour effects. The effect of chemical reaction is also taken to measure the performance of mass transport. The schematic view of the rotating disk is displayed in **Fig**. **2.1** (cf. Chapter **2).**

Within the assumptions specified above, the governing equations of the problem are given by

$$\frac{\partial u}{\partial r} + \frac{u}{r} + \frac{\partial w}{\partial z} = 0, \tag{5.1}$$

$$
\begin{aligned}
u\frac{\partial u}{\partial r} - \frac{v^2}{r} + w\frac{\partial u}{\partial z} &= \nu\frac{\partial^2 u}{\partial z^2} - \frac{\sigma}{\rho}B_0^2\left[u + \lambda_1 w\frac{\partial u}{\partial z}\right] - \frac{\phi_1 \nu}{K_a}u \\
&- \lambda_1\left[u^2\frac{\partial^2 u}{\partial r^2} + w^2\frac{\partial^2 u}{\partial z^2} + 2uw\frac{\partial^2 u}{\partial r\partial z} - \frac{2uv}{r}\frac{\partial v}{\partial r} - \frac{2vw}{r}\frac{\partial v}{\partial z} + \frac{uv^2}{r^2} + \frac{v^2}{r}\frac{\partial u}{\partial r}\right] \\
&+ \nu\lambda_2\left[-\frac{1}{r}\left(\frac{\partial u}{\partial z}\right)^2 - 2\frac{\partial u}{\partial z}\frac{\partial^2 w}{\partial z^2} + w\frac{\partial^3 u}{\partial z^3} - \frac{\partial u}{\partial r}\frac{\partial^2 u}{\partial z^2} - \frac{\partial u}{\partial z}\frac{\partial^2 u}{\partial r\partial z} + u\frac{\partial^3 u}{\partial r\partial z^2}\right],
\end{aligned} \tag{5.2}
$$

$$
\begin{aligned}
u\frac{\partial v}{\partial r} + \frac{uv}{r} + w\frac{\partial v}{\partial z} &= \nu\frac{\partial^2 v}{\partial z^2} - \frac{\sigma}{\rho}B_0^2\left[v + \lambda_1 w\frac{\partial v}{\partial z}\right] - \frac{\phi_1 \nu}{K_a}v \\
&- \lambda_1\left[u^2\frac{\partial^2 v}{\partial r^2} + w^2\frac{\partial^2 v}{\partial z^2} + 2uw\frac{\partial^2 v}{\partial r\partial z} + 2\frac{uv}{r}\frac{\partial u}{\partial r} + 2\frac{vw}{r}\frac{\partial u}{\partial z} - 2\frac{u^2 v}{r^2} - \frac{v^3}{r^2} + \frac{v^2}{r}\frac{\partial v}{\partial r}\right] \\
&+ \nu\lambda_2\left[\begin{array}{l} u\frac{\partial^3 v}{\partial r\partial z^2} - 2\frac{\partial v}{\partial z}\frac{\partial^2 w}{\partial z^2} + w\frac{\partial^3 v}{\partial z^3} - \frac{1}{r}\frac{\partial u}{\partial z}\frac{\partial v}{\partial z} \\[2mm] -\frac{\partial v}{\partial r}\frac{\partial^2 u}{\partial z^2} + \frac{v}{r}\frac{\partial^2 u}{\partial z^2} - \frac{\partial v}{\partial z}\frac{\partial^2 u}{\partial r\partial z} - \frac{u}{r}\frac{\partial^2 v}{\partial z^2} \end{array}\right],
\end{aligned} \tag{5.3}
$$

$$u\frac{\partial T}{\partial r} + w\frac{\partial T}{\partial z} = \frac{k}{\rho c_p}\left(\frac{\partial^2 T}{\partial z^2}\right) + \frac{Dk_T}{c_s c_p}\frac{\partial^2 C}{\partial z^2}, \tag{5.4}$$

$$u\frac{\partial C}{\partial r} + w\frac{\partial C}{\partial z} = D\frac{\partial^2 C}{\partial z^2} + \frac{Dk_T}{T_m}\frac{\partial^2 T}{\partial z^2} - K^*\left(C - C_\infty\right). \tag{5.5}$$

The boundary conditions are

$$u = cr, \quad v = \Omega r, \quad w = w_0, \quad T = T_w, \quad C = C_w \quad \text{at} \quad z = 0,$$

$$u \to 0, \quad v \to 0, \quad T \to T_\infty, \quad C \to C_\infty \quad \text{as} \quad z \to \infty. \tag{5.6}$$

Considering the variables (cf. Chapter **2**)

$$\eta = \sqrt{\frac{\Omega}{\nu}}z, \; u = \Omega r F, \; v = \Omega r G, \; w = \sqrt{\Omega\nu}H, \; \theta = \frac{T - T_\infty}{T_w - T_\infty}, \; \phi = \frac{C - C_\infty}{C_w - C_\infty}. \tag{5.7}$$

Substituting the above variables into Eqs. $(5.1)-(5.5)$ reduce to the following non-dimensional form

$$H' + 2F = 0, \tag{5.8}$$

$$F^2 - G^2 + F'H - F'' + \lambda F + \beta_1\left(F''H^2 + 2FF'H - 2GG'H\right)$$

$$+\beta_2\left(2F'^2 + 2F'H'' - F'''H\right) + M\left(F + \beta_1 F'H\right) = 0, \tag{5.9}$$

$$2FG + G'H - G'' + \lambda G + \beta_1\left(G''H^2 + 2\left(FG' + F'G\right)H\right)$$

$$-\beta_2\left(G'''H - 2F'G' - 2G'H''\right) + M\left(G + \beta_1 G'H\right) = 0, \tag{5.10}$$

76

$$\theta'' - \Pr H\theta' + \Pr Du\phi'' = 0, \tag{5.11}$$

$$\phi'' - ScH\phi' + ScS_r\theta'' - ScK\phi = 0. \tag{5.12}$$

The transformed BCs are

$$F(\eta) = \omega, \ G(\eta) = 1, \ H(\eta) = s, \ \theta(\eta) = 1, \ \phi(\eta) = 1 \text{ at } \eta = 0,$$

$$F(\eta) \to 0, \ G(\eta) \to 0, \ \theta(\eta) \to 0, \ \phi(\eta) \to 0 \quad \text{as } \eta \to \infty, \tag{5.13}$$

The controlling parameters are $\lambda \left(= \frac{\nu\phi_1}{\Omega K_a}\right)$ the porosity parameter, $Du \left(= \frac{Dk_T}{c_s c_p \nu} \frac{C_w - C_\infty}{T_w - T_\infty}\right)$ the Dufour number, $S_r \left(= \frac{Dk_T}{\nu T_m} \frac{T_w - T_\infty}{C_w - C_\infty}\right)$ the Soret number, $K \left(= \frac{K^*}{\Omega}\right)$ the chemical reaction parameter, $Sc \left(= \frac{\nu}{D}\right)$ the Schmidt number and the remaining parameters are similar as defined in the previous chapters.

5.2 Physical Parameters of Interest

The Nusselt number (Nu) is defined by

$$Nu = \frac{Rq_w}{k(T_w - T_\infty)}, \tag{5.14}$$

with

$$q_w = -k\left(\frac{\partial T}{\partial z}\right)\bigg|_{z=0}. \tag{5.15}$$

The dimensionless form

$$\mathrm{Re}^{-\frac{1}{2}} Nu = -\theta'(0). \tag{5.16}$$

The Sherwood number (Sh) is

$$Sh = -\frac{Rj_w}{D\left(C_w - C_\infty\right)}, \tag{5.17}$$

where

$$j_w = D\left(\frac{\partial C}{\partial z}\right)\bigg|_{z=0}. \tag{5.18}$$

In non-dimensional form is

$$\mathrm{Re}^{-\frac{1}{2}} Sh = -\phi'(0), \tag{5.19}$$

where, Re is the Reynolds number defined in previous chapter.

5.3 Problem Discussion

The numerical outcomes are plotted and tabulated in order to see the impact of various parameters on the velocity field, liquid temperature, concentration distribution. The numerical scheme (bvp midirch) is followed to characterize the flow, temperature and concentration of the liquid in the form of graphs. The current analysis which involves the non-dimensional parameters are M, ω, s, β_1, β_2, λ, Du, Sr, γ, Pr and Sc. The whole analysis is performed by fixing the values of parameters as $M = 1.0$, $\omega = 1.3$, $s = 0.1$, $\beta_1 = 0.05$, $\beta_2 = 0.05$, $\lambda = 0.1$, $Du = 0.1$, $Sr = 0.1$, $\gamma = 0.1$, Pr $= 5.0$ and $Sc = 5.0$.

In order to show the variations of velocity profiles in different directions, temperature as well as concentration of the fluid under the action of porosity parameter λ, results are traced by **Figs. 5.1 (a − e)**. The enlargement of porosity parameter $\lambda\,(0.1 − 0.5)$ leads to reduced magnitude of the velocity field (see **Figs. 5.1 (a − c)**). As, the existence of porous media essentially increases the flow resistance therefore reduces the movement of the fluid. Moreover, in **Figs. 5.1 (d − e)**,

78

the liquid temperature as well as concentration distribution are enhanced by the increment of λ. As the presence of porous media arises the resistance in the liquid, resulting in an increase in fluid temperature and concentration. The influence of β_2 (retardation time parameter) on the flow field is presented in **Figs. 5.2. (a − c)**. It is concluded from these graphs that raising of $\beta_2 \, (= 0.05, 0.1, 0.15, 0.2)$ increases the azimuthal velocity and decreases the magnitude of velocity in the radial and axial directions.

The variation of temperature and concentration distributions via Soret Sr and Dufour Du numbers, are shown through **Figs. 5.3 (a)** and **(b)** with default values of other fixed parameters. One can observe from the distributions given in these figures that all the solutions satisfied the far field boundary conditions asymptotically. As we can see from these figures that the dimensionless liquid temperature $\theta(\eta)$ declines and concentration $\phi(\eta)$ distribution boosted by the Soret Sr and Dufour Du numbers. Moreover, the effect of chemical reaction parameter on concentration distribution $\phi(\eta)$ is examined through **Fig. 5.4**. These curves show that the concentration distribution falls down as the chemical reaction parameter changes from 0.0 to 0.9. From a physical perspective, the chemical reaction creates additional resistance to the molecular motion of the liquid, resulting in a decrease in concentration distribution. Further, the variation of Nusselt number and Sherwood numbers on the impact of porosity parameter λ is plotted in **Figs. 5.5 (a − b)** against different values of stretching parameter. As obvious in this plot, the Nusselt number diminishes by increasing $\lambda \, (= 0.0, 1.0, 3.0, 5.0)$ and enhances against $\omega (= 0.8 \text{ to } 2.0)$. The same behavior is noted for Sherwood number (see **Fig. 5.5 (b)**).

To watch the change in Nusselt and Sherwood numbers for different physical parameters, results are done in **Tables 5.1** and **5.2**. The variation of Nusselt number on s, β_1, β_2, Du, and Pr, numerical results are calculated in **Table 5.1**. In this table, it is noted that for higher

estimation of s, β_2 and Du, respectively, the Nusselt number $\{-\theta'(0)\}$ reduces gradually and rises for β_1 and Pr, respectively. Further, from **Table 5.2** represents that variation of Sherwood number $\{-\phi'(0)\}$ against distinct values of s, β_1, β_2, Sr, γ and Sc. From this table, an increment in mass transfer rate is observed under the action of K and Sc, respectively. On the other hand, the converse result is noticed against s, β_1, β_2 and Sr, respectively.

Table 5.1: Influence of physical parameters (s, β_1, β_2, Du and Pr) on $\text{Re}^{-1/2}Nu$ with other fixed parameters.

s	β_1	β_2	Du	Pr	$\text{Re}^{-1/2}Nu$
0.1	0.03	0.03	0.1	5.0	1.70252272
0.2					1.50425573
0.3					1.31795786
0.3	0.05				1.31421459
	0.08				1.30861779
	0.1				1.30489738
0.3	0.1	0.05			1.30255102
		0.08			1.29905964
		0.1			1.29656603
0.3	0.1	0.1	0.13		1.19915648
			0.15		1.13217867
			0.2		0.95909851
0.3	0.1	0.1	0.2	6.0	1.00746229
				7.0	1.04122868
				8.0	1.06025442

Table 5.2: Influence of physical parameters s, β_1, β_2, Sr, K and Sc on $\mathrm{Re}^{-1/2}\,Sh$ with fixed values of other parameters.

s	β_1	β_2	Sr	K	Sc	$\mathrm{Re}^{-1/2}\,Sh$
0.1	0.03	0.03	0.1	0.1	5.0	1.90263505
0.2						1.70268819
0.3						1.51283970
0.3	0.05					1.50970351
	0.08					1.50502678
	0.1					1.50192512
0.3	0.1	0.05				1.49996670
		0.08				1.49698803
		0.1				1.49492053
0.3	0.1	0.1	0.13			1.43139736
			0.15			1.38928656
			0.2			1.28847545
0.3	0.1	0.1	0.2	0.2		1.47564879
				0.3		1.65305420
				0.4		1.82180421
0.3	0.1	0.1	0.2	0.4	6.0	2.04495337
					7.0	2.27626930
					8.0	2.51397531
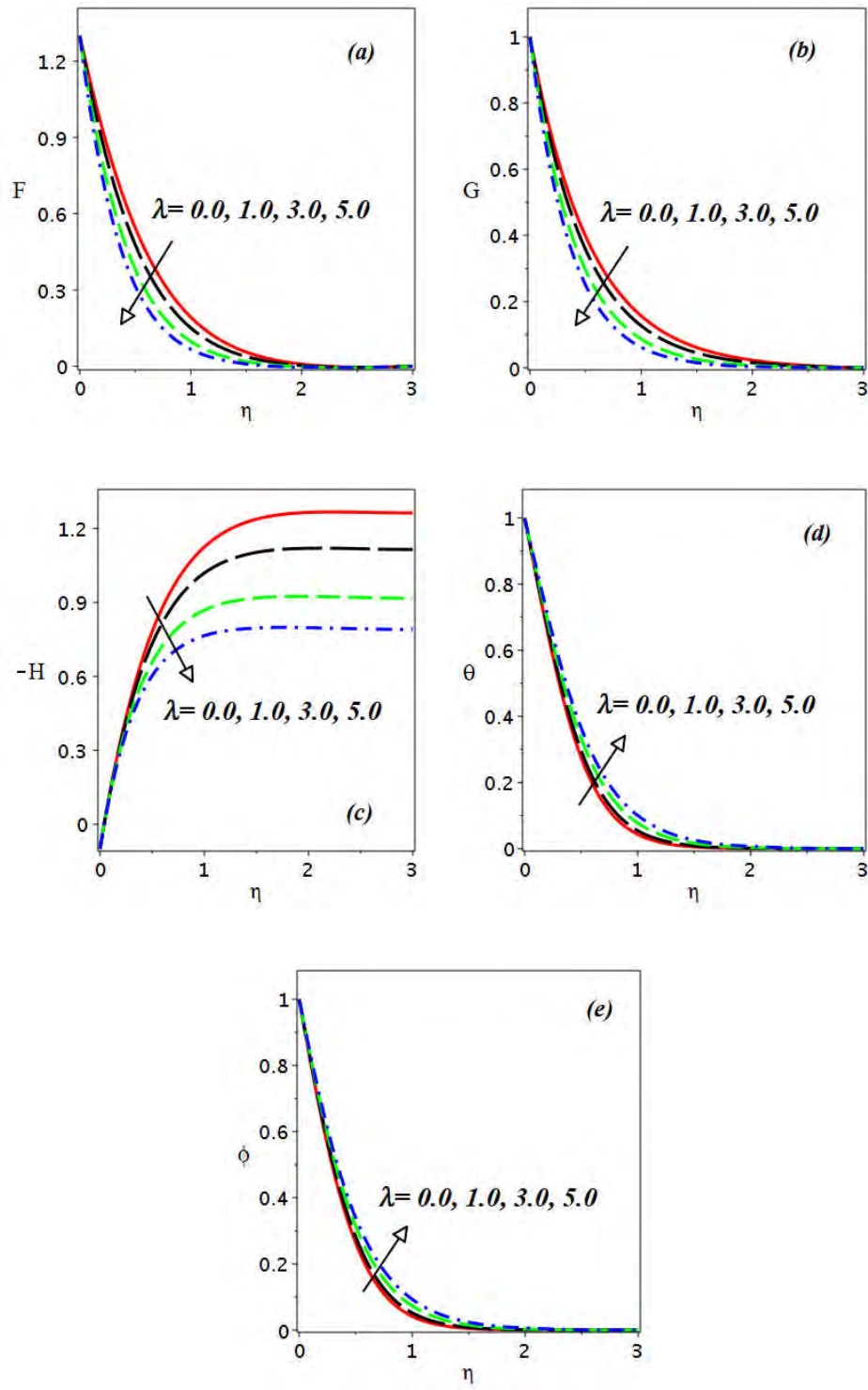
Figs. 5.1: Impact of λ on $F(\eta)$, $G(\eta)$, $-H(\eta)$, $\theta(\eta)$ and $\phi(\eta)$.
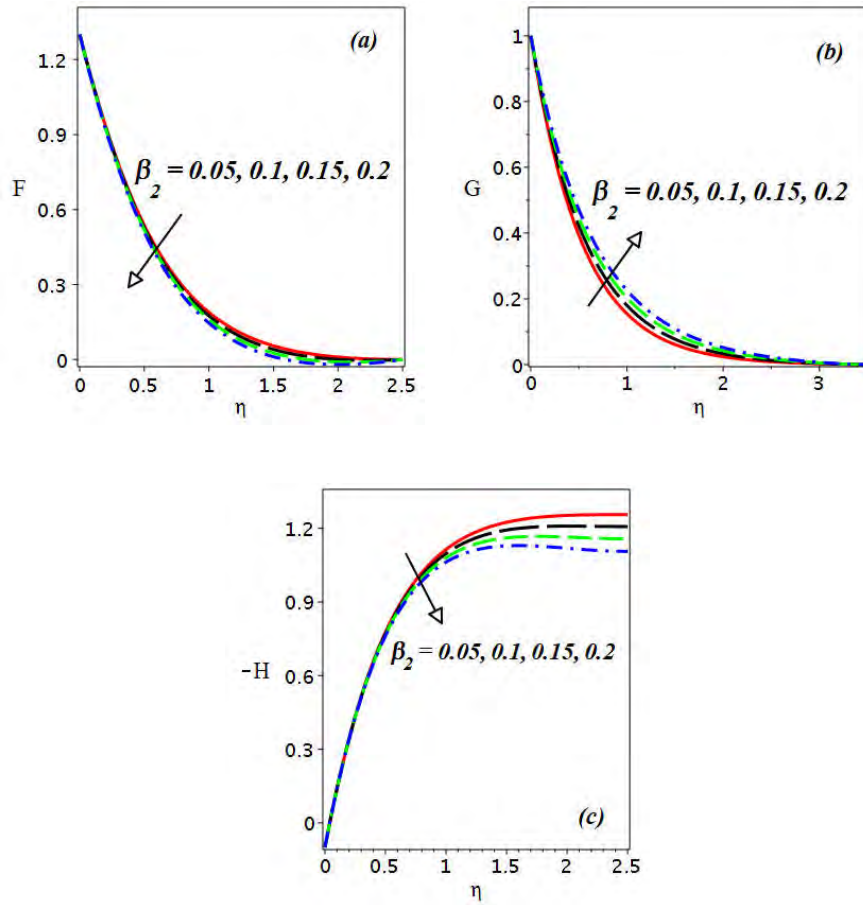
Figs. 5.2: Impact of β_2 on $F(\eta)$, $G(\eta)$ and $-H(\eta)$.
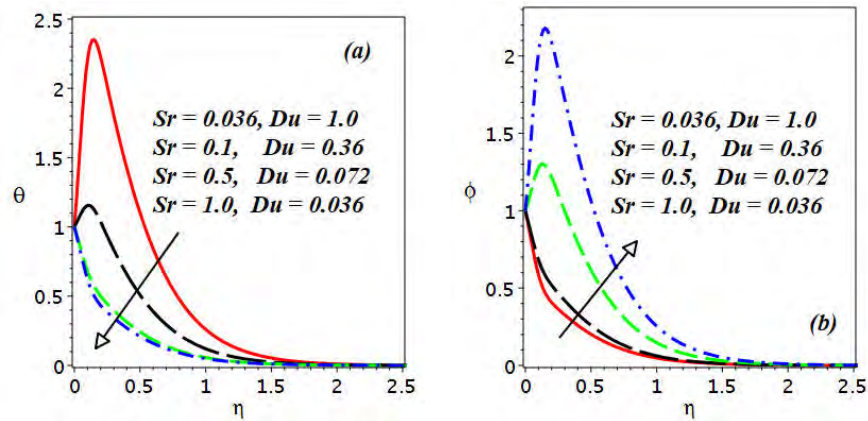
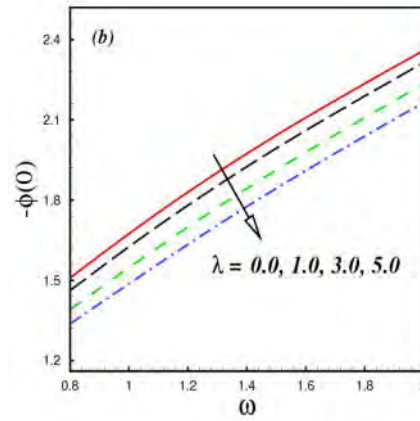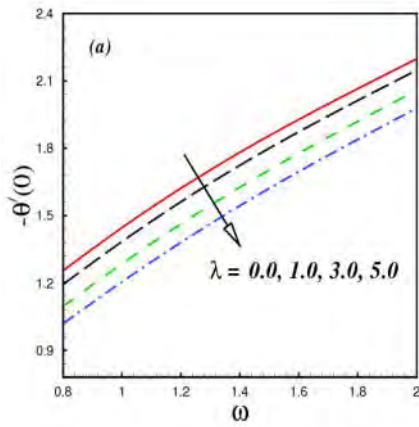**Figs. 5.3**: Impact of $(Sr$ and $Du)$ on $\theta(\eta)$ and $\phi(\eta)$.
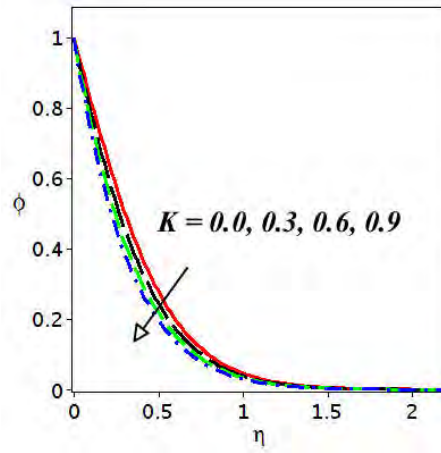
Fig. 5.4: Impact of K on $\phi(\eta)$.

Figs. 5.5: Impact of λ on $-\theta'(\eta)$ and $-\phi'(\eta)$ against ω.

Chapter 6

Chemically Reactive Flow of Oldroyd-B Fluid with non-Fourier's Heat Flux Theory

The current chapter investigates the magnetized flow of an Oldroyd-B fluid over a rotating disk under various physical perspectives. To investigate the fluid thermal transport features in this analysis, we employ the modified Fourier's law rather than the classical Fourier's law. The influence of homogeneous-heterogeneous reactions on mass transport is also studied. The governing continuity, momentum, heat and concentration partial differential equations (PDEs) are reduced into a set of non-dimensional ordinary differential equations (ODEs) by utilizing the von Karman variables. In order to obtain numerical solutions, the bvp midrich approach is used. Diverse effects of different involved parameters on the velocity profiles, temperature and concentration of the fluid are discussed. The comparison table is also designed to determine

whether our numerical results are valid with previous results.

6.1 Problem Formulation

The current work focuses on the magnetized swirling flow of Oldroyd-B fluid with homogeneous and heterogeneous reactions. The Catteneo-Christov heat flux theory (modified Fourier's law) is utilized here for carrying out the heat transport analysis. In addition, the impact of homogeneous and heterogeneous reactions is considered to control mass transportation. The flow is generated by the spinning with uniform angular velocity Ω and radially stretching disk as shown in flow setup **Fig. 2.1** (cf. Chapter **2**). The governing equations for steady incompressible and magnetized three dimensional flow of an Oldroyd-B fluid are (Eqs. (1.3), (1.6), (1.19), (1.21), (1.22) cf. Chapter **1**)

$$\frac{\partial u}{\partial r} + \frac{1}{r}u + \frac{\partial w}{\partial z} = 0, \tag{6.1}$$

$$
\begin{aligned}
u\frac{\partial u}{\partial r} - \frac{1}{r}v^2 + w\frac{\partial u}{\partial z} &= \nu\frac{\partial^2 u}{\partial z^2} - \frac{\sigma}{\rho}B_0^2\left[u + \lambda_1 w\frac{\partial u}{\partial z}\right] \\
&- \lambda_1\left[u^2\frac{\partial^2 u}{\partial r^2} + w^2\frac{\partial^2 u}{\partial z^2} + 2uw\frac{\partial^2 u}{\partial r\partial z} - \frac{2}{r}uv\frac{\partial v}{\partial r} - \frac{2}{r}vw\frac{\partial v}{\partial z} + \frac{1}{r^2}uv^2 + \frac{1}{r}v^2\frac{\partial u}{\partial r}\right] \\
&+ \nu\lambda_2\left[-\frac{1}{r}\left(\frac{\partial u}{\partial z}\right)^2 - 2\frac{\partial u}{\partial z}\frac{\partial^2 w}{\partial z^2} + w\frac{\partial^3 u}{\partial z^3} - \frac{\partial u}{\partial r}\frac{\partial^2 u}{\partial z^2} - \frac{\partial u}{\partial z}\frac{\partial^2 u}{\partial r\partial z} + u\frac{\partial^3 u}{\partial r\partial z^2}\right],
\end{aligned}
\tag{6.2}
$$

$$
\begin{aligned}
u\frac{\partial v}{\partial r} + \frac{1}{r}uv + w\frac{\partial v}{\partial z} &= \nu\frac{\partial^2 v}{\partial z^2} - \frac{\sigma}{\rho}B_0^2\left[v + \lambda_1 w\frac{\partial v}{\partial z}\right] \\
&- \lambda_1\left[u^2\frac{\partial^2 v}{\partial r^2} + w^2\frac{\partial^2 v}{\partial z^2} + 2uw\frac{\partial^2 v}{\partial r\partial z} + \frac{2}{r}uv\frac{\partial u}{\partial r} + \frac{2}{r}vw\frac{\partial u}{\partial z} - \frac{2}{r^2}u^2v - \frac{1}{r^2}v^3 + \frac{1}{r}v^2\frac{\partial v}{\partial r}\right] \\
&+ \nu\lambda_2\left[\begin{array}{l} u\frac{\partial^3 v}{\partial r\partial z^2} - 2\frac{\partial v}{\partial z}\frac{\partial^2 w}{\partial z^2} + w\frac{\partial^3 v}{\partial z^3} - \frac{1}{r}\frac{\partial u}{\partial z}\frac{\partial v}{\partial z} \\[4pt] + \frac{1}{r}v\frac{\partial^2 u}{\partial z^2} - \frac{\partial v}{\partial r}\frac{\partial^2 u}{\partial z^2} - \frac{\partial v}{\partial z}\frac{\partial^2 u}{\partial r\partial z} - \frac{1}{r}u\frac{\partial^2 v}{\partial z^2} \end{array}\right],
\end{aligned}
\tag{6.3}
$$

87

$$\frac{\partial T}{\partial r} + w\frac{\partial T}{\partial z} = \alpha\frac{\partial^2 T}{\partial z^2}$$

$$-\varepsilon_0 \left[u^2\frac{\partial^2 T}{\partial r^2} + 2uw\frac{\partial^2 T}{\partial r\partial z} + w^2\frac{\partial^2 T}{\partial z^2} + u\frac{\partial w}{\partial r}\frac{\partial T}{\partial z} + u\frac{\partial u}{\partial r}\frac{\partial T}{\partial r} + w\frac{\partial u}{\partial z}\frac{\partial T}{\partial r} + w\frac{\partial w}{\partial z}\frac{\partial T}{\partial z} \right], \quad (6.4)$$

$$u\frac{\partial a}{\partial r} + w\frac{\partial a}{\partial z} = D_A\frac{\partial^2 a}{\partial z^2} - k_c ab^2, \quad (6.5)$$

$$u\frac{\partial b}{\partial r} + w\frac{\partial b}{\partial z} = D_B\frac{\partial^2 b}{\partial z^2} + k_c ab^2. \quad (6.6)$$

The relevant BCs are

$$u = cr, \quad v = \Omega r, \quad w = 0, \quad T = T_w, \quad D_A\frac{\partial a}{\partial z} = k_s a, \quad D_B\frac{\partial b}{\partial z} = -k_s a, \quad \text{at} \ \ z = 0,$$

$$u \to 0, \ v \to 0, \ T \to T_\infty, \ a \to a_0, \quad b \to 0, \quad as \ z \to \infty. \quad (6.7)$$

In the above equations, ε_0 is the thermal relaxation time, (k_c, k_s) the rate constants and (D_A, D_B) the diffusion coefficients of species.

Familiarizing the von Karman transformations (Eq. (2.24) cf. Chapter **2**) into Eqs. (6.1) − (6.6), we finally get

$$H' + 2F = 0, \quad (6.8)$$

$$F^2 - G^2 + F'H - F'' + \beta_1 \left(F''H^2 + 2FF'H - 2GG'H \right)$$

$$+\beta_2 \left(2F'^2 + 2F'H'' - F'''H \right) + M \left(F + \beta_1 F'H \right) = 0, \quad (6.9)$$

88

$$2FG + G'H - G'' + \beta_1 \left(G''H^2 + 2 \left(FG' + F'G \right) H \right)$$

$$-\beta_2 \left(G'''H - 2F'G' - 2G'H'' \right) + M \left(G + \beta_1 G'H \right) = 0, \tag{6.10}$$

$$\frac{1}{\Pr}\theta'' - H\theta' - \varepsilon_t \left[H^2\theta'' + HH'\theta' \right] = 0, \tag{6.11}$$

$$\frac{1}{Sc}\phi'' - H\phi' - K_1\phi h^2 = 0, \tag{6.12}$$

$$\frac{\delta^*}{Sc}h'' - Hh' + K_1\phi h^2 = 0. \tag{6.13}$$

The transformed BCs are

$$F\left(\eta\right) = \omega, \ G\left(\eta\right) = 1, \ H\left(\eta\right) = 0, \ \theta\left(\eta\right) = 1, \ \phi'\left(\eta\right) = K_2\phi\left(\eta\right), \quad \delta^*h'\left(\eta\right) = -K_2\phi\left(\eta\right) \ \text{at} \ \eta = 0,$$

$$F\left(\eta\right) \to 0, \ G\left(\eta\right) \to 0, \ \theta\left(\eta\right) \to 0, \ \phi\left(\eta\right) \to 1, \ h\left(\eta\right) \to 0 \ \text{as} \ \eta \to \infty, \tag{6.14}$$

where, $\varepsilon_t \left(= \varepsilon_0 \Omega \right)$ is the thermal relaxation time, $K_1 \left(= K_c \frac{a_0^2}{\Omega} \right)$ the homogeneous reaction rate, $Sc \left(= \frac{\nu}{D_A} \right)$ the Schmidt number, $K_2 \left(= \frac{K_s}{D_A} \sqrt{\frac{\nu}{\Omega}} \right)$ the heterogeneous reaction rate, $\Pr \left(= \frac{\nu}{\alpha} \right)$ the Prandtl number, $\delta^* \left(= \frac{D_B}{D_A} \right)$ the ratio of diffusion coefficients and the rest parameters are similar as defined in previous chapters.

The species A and B are not equal generally, although it may be expected that their size will be similar. In the occasion, we presume that the diffusion species coefficients D_B and D_A are identical, i.e., $\delta^* = 1$, hence

$$\phi\left(\eta\right) + h\left(\eta\right) = 1. \tag{6.15}$$

Now using the above condition (6.15), Eqs. (6.12)-(6.13) and their respective boundary condi-

tions take the form

$$\frac{1}{Sc}\phi'' - H\phi' - K_1 [1 - \phi]^2 \phi = 0, \qquad (6.16)$$

$$\phi'(0) = K_2\phi(0) \quad \text{and} \quad \phi(\infty) \to 1. \qquad (6.17)$$

6.2 Results and Discussion

The primary goal of this study is to investigate the physics of Oldroyd-B fluid flow with energy transport under the modified Fourier's law. The effect of the controlling parameters are graphically presented to provide an understanding into the physics of the problem. The findings are presented in **Figs. 6.1-6.5** in order to explain the fluid flow behavior, heat and mass transportation by different parameters. The solutions are investigated numerically using bvp midrich scheme on Maple programming. We set different parameters for describing physical structure which are $\omega = 0.8$, $M = 10$, $\beta_1 = 0.05$, $\beta_2 = 0.05$, $\varepsilon_c = 0.1$, $K_1 = 0.3$, $K_2 = 0.3$, $Sc = 10.0$ and $\Pr = 10.0$. Here, numerical computations has been made with emerging parameters in the ranges, $0.05 \leq \beta_1 \leq 0.7$, $0.05 \leq \beta_2 \leq 0.7$, $0.0 \leq \varepsilon_t \leq 0.3$, $0.3 \leq K_1 \leq 7.0$, $0.3 \leq K_2 \leq 0.9$, $3.0 \leq \Pr \leq 9.0$, $3.0 \leq Sc \leq 9.0$.

The curves of velocities ($F(\eta)$, $G(\eta)$ and $H(\eta)$), respectively are drawn in **Figs. 6.1(a-e)** for varying values of β_1. **Fig. 6.1(a)** discloses the change in radial velocity $F(\eta)$ with respect to relaxation time parameter β_1. It shows that the radial velocity declines by taking values of β_1 from $0.05 - 0.7$. Because the relaxation time is the ratio of material relaxation time to material observation time. Hence, for larger estimation of relaxation time parameter imply the stress relaxation is greater or the observation time is shorter and indicates that the fluid reacts solidly. The velocity of the fluid is thus decreased in such a way. In the azimuthal direction,

the same behavior can be observed through **Fig. 6.1(b)**. In addition, the thickness of the boundary layer is also significantly reduced. Moreover, **Fig. 6.1(c)** identifies the velocity in axial direction with respect to η. It is noted that the enlargement of $\beta_1 (= 0.05, 0.3, 0.5, 0.7)$ reduces the velocity in the axial direction $H(\eta)$. The behavior of temperature $\theta(\eta)$ of the liquid is presented through **Fig. 6.1(d)**. After examining, it is seen that the fluid temperature $\theta(\eta)$ enhances with the enlargement in $\beta_1 (= 0.05, 0.3, 0.5, 0.7)$. This can be explained physically as the effect of Deborah number of relaxation time on the fluids having a solid-like response. Therefore, the conductive heat transfer rises in solid-like fluid as compared to liquid thereby, the temperature enhances in this manner. On the other hand, **Fig. 6.1(e)** depicts the opposite trend regarding concentration distribution $\phi(\eta)$. In order to view the velocity field variations, thermal and solutal distributions for retardation time parameter β_2, curves are sketched through **Figs. 6.2(a-c)**. The effect of β_2 on azimuthal velocity profile $G(\eta)$ is indicated in **Fig. 6.2(a)**. The curves in this figure noted that the azimuthal velocity improves with the increment in β_2. The function $G(\eta)$ is directly proportional to β_2. This means that fluid flows parallel to the disk, which accelerates with a higher rate of fluid retardation time. **Fig. 6.2(b)** perceives the behavior of liquid temperature on changing values of $\beta_2 (= 0.05, 0.3, 0.5, 0.7)$ by setting default parameters fixed. It is seen that the fluid temperature is raised up by the action of β_2. On the other hand, the solutal distribution $\phi(\eta)$ demonstrates the inverse trend which is depicted in **Fig. 6.2(c)**. Furthermore, in this situation, the concentration boundary layer appears to be thinner.

The effect of thermal relaxation time parameter on $\theta(\eta)$ is discussed along with the other fixed parameters in **Fig. 6.3(a)**. With the enlargement of thermal relaxation time parameter ε_t, there is a reduction in temperature of Oldroyd-B fluid. Physically, for $\varepsilon_t = 0$, the Cattaneo-

Christov model (non-Fourier heat flux model) converts to the classical Fourier's law implying that the heat energy transports in the fluid instantly. As in **Fig. 6.3(a),** for large estimation of non-zero values of ε_t diminishes the thermal distribution $\theta(\eta)$. Because the heat energy rate in the given fluid is controlled by a non-Fourier heat flux model. The influence of homogeneous reaction parameter K_1 on $\phi(\eta)$ is illustrated in **Fig. 6.3(b)**. Increasing the values of K_1 from 0.3 to 7.0 with $\mathrm{Pr} = 5.0 = Sc$, which results to enhance the concentration distribution. Additionally, the thickness of concentration boundary layer becomes thinner when the homogeneous reaction increases. Moreover, the same behavior for the heterogeneous reaction parameter K_2 can be found as stated in **Fig. 6.3(c)**.

The influence of Pr on $\theta(\eta)$ is discussed in **Fig. 6.4(a)**. In this figure, the plot shows a decreasing trend of liquid temperature when different values of $\mathrm{Pr}(= 3.0, 5.0, 7.0, 9.0)$ are taken. Physically, for higher Prandtl number $\mathrm{Pr}(> 1)$, the thermal diffusivity reduces, hence the reduction in the temperature distribution is noted in this situation. Moreover, the change of mass transport against Schmidt number Sc is pictured in **Fig. 6.4(b)**. The result is carried out for Sc in the range (3.0 to 9.0) with respect to η. It is remarked that the mass transport in the fluid is increased by the higher values of Sc [see **Fig. 6.4(b)**].

To watch the change in concentration gradient at the wall $\phi'(0)$ for different physical parameters, results are done in **Figs. 6.5(a-b)**. The effect of K_1 on wall concentration gradient $\phi'(0)$ is analyzed with respect to ω as obtained in **Fig. 6.5(a)**. This profile shows a declining behavior for distinct values of K_1 against ω. Furthermore, when the stretching parameter ω increases, the wall concentration gradient increases. Additionally, **Fig. 6.5(b)** shows the numerical investigation of $\phi'(0)$ on the heterogeneous reaction parameter K_2. From these curves, an increment in $\phi'(0)$ is observed under the action of K_2 and ω, respectively.
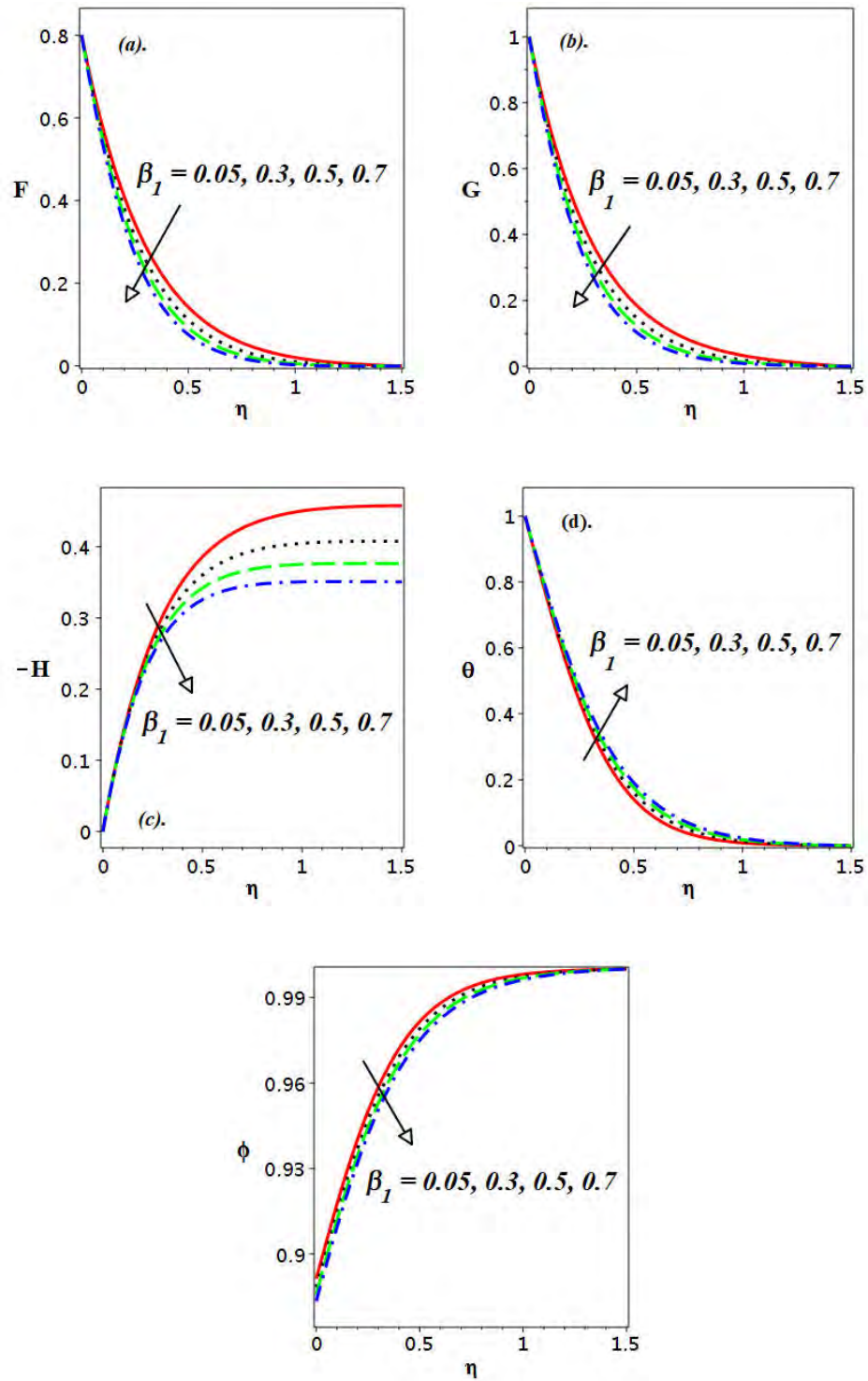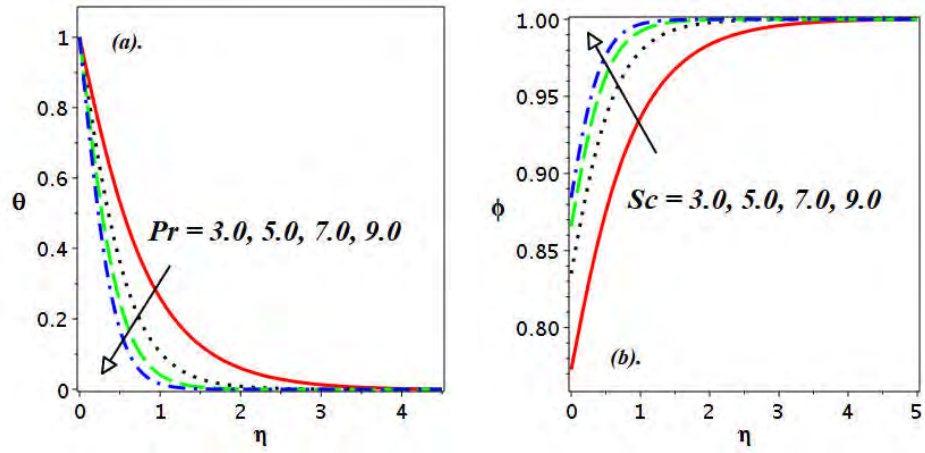
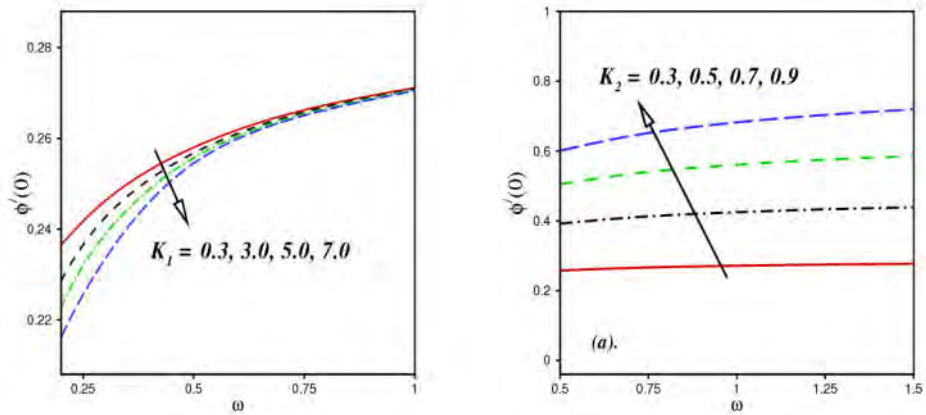**Figs. 6.1**: Impact of β_1 on $F(\eta)$, $G(\eta)$, $H(\eta)$, $\theta(\eta)$ and $\phi(\eta)$.
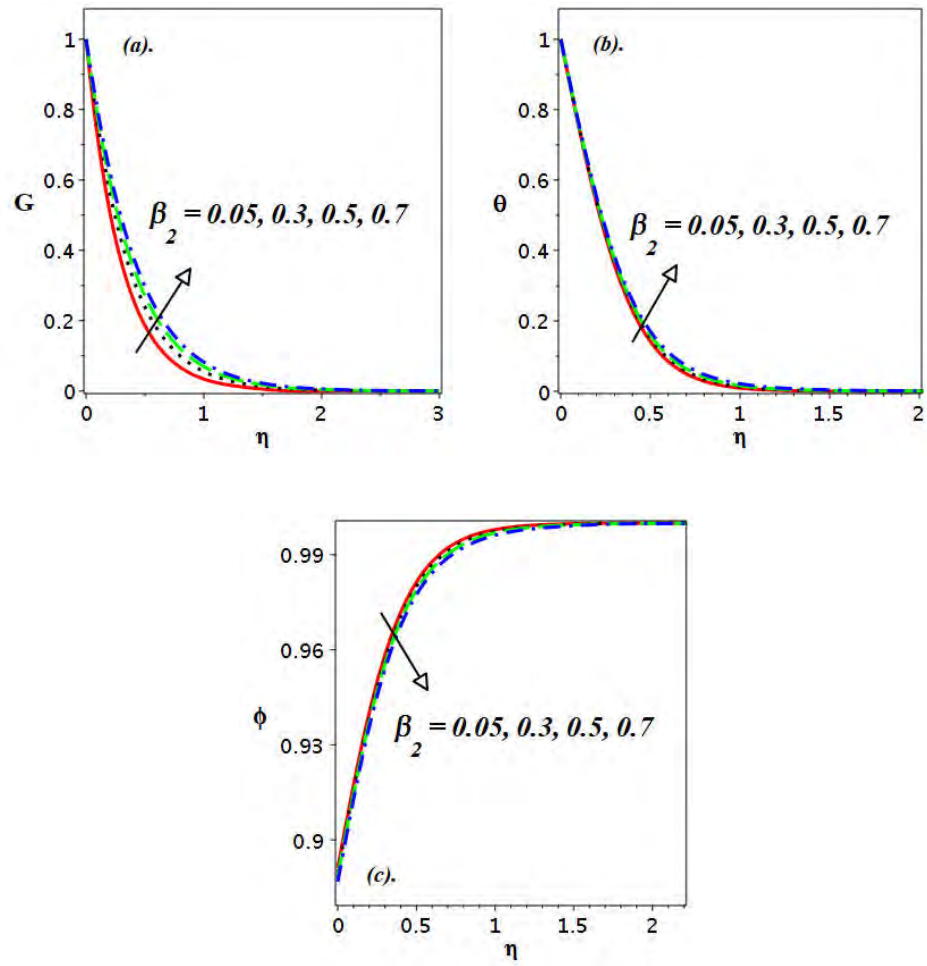
Figs. 6.2: Impact of β_2 on $G\left(\eta\right)$, $\theta\left(\eta\right)$ and $\phi\left(\eta\right)$.
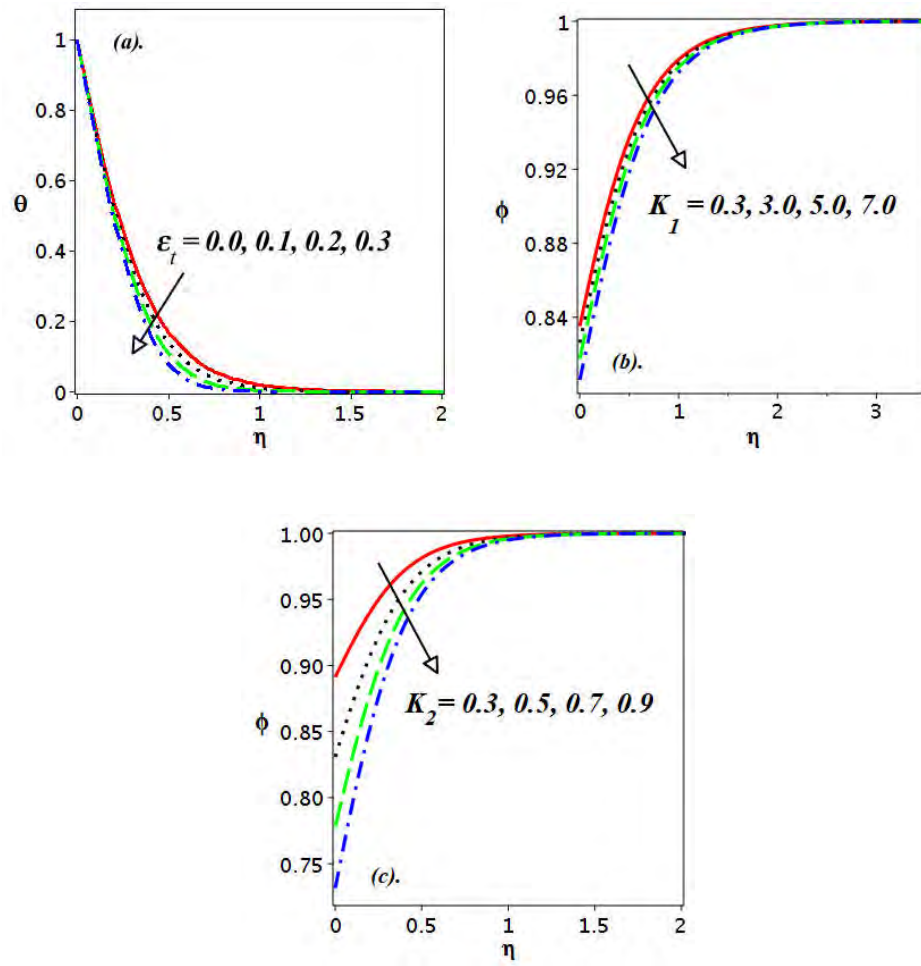
Figs. 6.3: Impact of ε_t on $\theta(\eta)$, impact of K_1 on $\phi(\eta)$ and impact of K_2 on $\phi(\eta)$.

Figs. 6.4: Impact of Pr on $\theta\left(\eta\right)$ and impact of Sc on $\phi\left(\eta\right)$.

Figs. 6.5: Impact of K_1 on $\phi'\left(0\right)$ and impact of K_2 on $\phi'\left(0\right)$.

Chapter 7

Swirling Flow of Oldroyd-B Fluid with Cattaneo-Christov Theory and Heat Generation/Absorption

In this chapter, the analysis of Cattaneo-Christov heat and mass flux theories in the flow of Oldroyd-B fluid over a rotating disk is presented. Additionally, the heat generation/absorption and chemical reaction are also added into heat and mass equations, respectively. Here, the flow phenomenon is due to the rotating as well as stretching of the disk. The system of partial differential equations (PDEs) is converted into non-dimensional ordinary differential equations (ODEs) by utilizing some suitable variables. The analytical solutions are obtained by using the homotopy analysis method (HAM) in Mathematica software. The graphical results are achieved in the form of velocity fields, temperature and concentration distributions. Results show that the temperature of the Oldroyd-B fluid rises when the magnetic field parameter increases in

some specific range. It is noted that the temperature reduces as the thermal relaxation time parameters increases. Additionally, the concentration distribution is seen in decreasing trend by the enlargement of solutal relaxation time parameter.

7.1 Problem Formulation

Let us assume three dimensional magnetized flow of Oldroyd-B fluid due to a rotating and stretching disk. For the formation of heat and mass transport equations, the Cattaneo-Christov heat and mass flux theories are used instead of classical Fourier's and Fix's laws. Moreover, the heat generation/absorption is also added into the heat equation and chemical reaction is included into the concentration equation. The magnetic field is applied perpendicularly to the disk (see **Fig. 2.1,** cf. Chapter **2**). The equations for the given problem are (Eqs. $(2.18 - 2.20)$ cf. Chapter **2**)

$$\frac{\partial u}{\partial r} + \frac{u}{r} + \frac{\partial w}{\partial z} = 0, \tag{7.1}$$

$$
\begin{aligned}
u\frac{\partial u}{\partial r} - \frac{v^2}{r} + w\frac{\partial u}{\partial z} &= \nu\frac{\partial^2 u}{\partial z^2} - \frac{\sigma}{\rho}B_0^2\left[u + \lambda_1 w\frac{\partial u}{\partial z}\right] \\
&- \lambda_1\left[u^2\frac{\partial^2 u}{\partial r^2} + w^2\frac{\partial^2 u}{\partial z^2} + 2uw\frac{\partial^2 u}{\partial r\partial z} - \frac{2uv}{r}\frac{\partial v}{\partial r} - \frac{2vw}{r}\frac{\partial v}{\partial z} + \frac{uv^2}{r^2} + \frac{v^2}{r}\frac{\partial u}{\partial r}\right] \\
&+ \nu\lambda_2\left[-\frac{1}{r}\left(\frac{\partial u}{\partial z}\right)^2 - 2\frac{\partial u}{\partial z}\frac{\partial^2 w}{\partial z^2} + w\frac{\partial^3 u}{\partial z^3} - \frac{\partial u}{\partial r}\frac{\partial^2 u}{\partial z^2} - \frac{\partial u}{\partial z}\frac{\partial^2 u}{\partial r\partial z} + u\frac{\partial^3 u}{\partial r\partial z^2}\right], \tag{7.2}
\end{aligned}
$$

$$u\frac{\partial v}{\partial r} + \frac{1}{r}uv + w\frac{\partial v}{\partial z} = \nu\frac{\partial^2 v}{\partial z^2} - \frac{\sigma}{\rho}B_0^2\left[v + \lambda_1 w\frac{\partial v}{\partial z}\right]$$

$$-\lambda_1\left[u^2\frac{\partial^2 v}{\partial r^2} + w^2\frac{\partial^2 v}{\partial z^2} + 2uw\frac{\partial^2 v}{\partial r\partial z} + \frac{2}{r}uv\frac{\partial u}{\partial r} + \frac{2}{r}vw\frac{\partial u}{\partial z} - \frac{2}{r^2}u^2v - \frac{1}{r^2}v^3 + \frac{1}{r}v^2\frac{\partial v}{\partial r}\right]$$

$$+\nu\lambda_2\left[\begin{array}{c} u\frac{\partial^3 v}{\partial r\partial z^2} - 2\frac{\partial v}{\partial z}\frac{\partial^2 w}{\partial z^2} + w\frac{\partial^3 v}{\partial z^3} - \frac{1}{r}\frac{\partial u}{\partial z}\frac{\partial v}{\partial z} \\ \\ -\frac{\partial v}{\partial r}\frac{\partial^2 u}{\partial z^2} + \frac{1}{r}v\frac{\partial^2 u}{\partial z^2} - \frac{\partial v}{\partial z}\frac{\partial^2 u}{\partial r\partial z} - \frac{1}{r}u\frac{\partial^2 v}{\partial z^2} \end{array}\right], \tag{7.3}$$

$$u\frac{\partial T}{\partial r} + w\frac{\partial T}{\partial z} = \frac{k}{\rho c_p}\frac{\partial^2 T}{\partial z^2} + \frac{Q_0}{\rho c_p}(T - T_\infty) + \varepsilon_0\frac{Q_0}{\rho c_p}\left(u\frac{\partial T}{\partial r} + w\frac{\partial T}{\partial z}\right)$$

$$-\varepsilon_0\left[u^2\frac{\partial^2 T}{\partial r^2} + 2uw\frac{\partial^2 T}{\partial r\partial z} + w^2\frac{\partial^2 T}{\partial z^2} + u\frac{\partial w}{\partial r}\frac{\partial T}{\partial z} + u\frac{\partial u}{\partial r}\frac{\partial T}{\partial r} + w\frac{\partial u}{\partial z}\frac{\partial T}{\partial r} + w\frac{\partial w}{\partial z}\frac{\partial T}{\partial z}\right], \tag{7.4}$$

$$u\frac{\partial C}{\partial r} + w\frac{\partial C}{\partial z} = D_B\frac{\partial^2 C}{\partial z^2} - K_1(C - C_\infty) - \varepsilon_1 K_1\left(u\frac{\partial C}{\partial r} + w\frac{\partial C}{\partial z}\right)$$

$$-\varepsilon_1\left[u^2\frac{\partial^2 C}{\partial r^2} + 2uw\frac{\partial^2 C}{\partial r\partial z} + w^2\frac{\partial^2 C}{\partial z^2} + u\frac{\partial w}{\partial r}\frac{\partial C}{\partial z} + u\frac{\partial u}{\partial r}\frac{\partial C}{\partial r} + w\frac{\partial u}{\partial z}\frac{\partial C}{\partial r} + w\frac{\partial w}{\partial z}\frac{\partial C}{\partial z}\right] \tag{7.5}$$

The boundary conditions are

$$u = cr, \quad v = \Omega r, \quad w = 0, \quad T = T_w, \quad C = C_w \quad \text{at} \ z = 0,$$

$$u \to 0, \quad v \to 0, \quad T \to T_\infty, \quad C \to C_\infty \quad \text{as} \ z \to \infty. \tag{7.6}$$

Here, ε_1 is the solutal relaxation time.

Substituting the transformations (Eq. (2.24) cf. Chapter **2**) into Eqs. (7.1) to (7.5) gives

$$H' + 2F = 0, \tag{7.7}$$

$$F^2 - G^2 + F'H - F'' + \beta_1 \left(F''H^2 + 2FF'H - 2GG'H \right)$$

$$+\beta_2 \left(2F'^2 + 2F'H'' - F'''H \right) + M \left(F + \beta_1 F'H \right) = 0, \tag{7.8}$$

$$2FG + G'H - G'' + \beta_1 \left(G''H^2 + 2 \left(FG' + F'G \right) H \right)$$

$$-\beta_2 \left(G'''H - 2F'G' - 2G'H'' \right) + M \left(G + \beta_1 G'H \right) = 0, \tag{7.9}$$

$$\frac{1}{\text{Pr}} \theta'' - H\theta' - \varepsilon_t \left[H^2\theta'' + HH'\theta' \right] + \gamma\theta + \varepsilon_t\gamma H\theta' = 0, \tag{7.10}$$

$$\phi'' - ScH\phi' - \varepsilon_c Sc \left[H^2\phi'' + HH'\phi' \right] - ScK\phi - Sc\varepsilon_c KH\phi' = 0. \tag{7.11}$$

The boundary conditions are

$$F(\eta) = \omega, \ G(\eta) = 1, \ H(\eta) = 0, \ \theta(\eta) = 1, \ \phi(\eta) = 1 \text{ at } \eta = 0,$$

$$F(\eta) \to 0, \ G(\eta) \to 0, \ \theta(\eta) \to 0, \ \phi(\eta) \to 0 \quad \text{as} \ \eta \to \infty. \tag{7.12}$$

The dimensionless parameters which are as follow:

Here, ε_c the solutal relaxation time parameter and K the chemical reaction parameter. These quantities are defined as

$$\varepsilon_c = \varepsilon_1 \Omega, \ K = \frac{K_1}{\Omega}. \tag{7.13}$$

7.2   Results and Discussion

This study presents the swirling flow of magnetized Oldroyd-B fluid due to a stretching as well as rotating of the disk. The Cattaneo-Christov theory is used to formulate the heat and

mass transport mechanisms. Moreover, the heat generation/absorption and chemical reaction are also taken into heat and mass equations, respectively. The analytical results are expressed graphically to see the physical behavior of the fluid. The findings are given in **Figs. 7.2** to **7.6** against various involved physical parameters. **Tables 7.1** and 7.**2** show the comparison between present results with the past outcomes for a limiting case,.i.e., in the absence of β_1, β_2, M, ω, δ, γ, ε_t and ε_c. These tabulated results are the analytical values of $F'(0)$, $-G'(0)$ and $-\theta'(0)$ compared with those of the previous literature. In **Table 7.1,** a comparison of $-\theta'(0)$ amongst the results by Gregg and Sparrow [58], the numerical results and the results obtained from the present study is given. Furthermore, **Table 7.2** shows a link between the results of the present study, the results obtained by Turkyilmazoglu [54] and the numerical results. These tables show the validity of the present scheme and problem.

Influence of retardation time parameter β_2 on velocity profile, temperature and concentration distributions is presented in **Figs. 7.1(a-e)**. It reveals that the radial velocity $F(\eta)$ shows the reducing behavior by increasing the retardation time parameter β_2 as shown in **Fig. 7.1(a)**. A similar observation can be seen for azimuthal fluid velocity $G(\eta)$ by enlarging $\beta_2(= 0.1, 0.3, 0.5, 0.7)$. Further, to see the influence of β_2 on axial fluid velocity $H(\eta)$, **Fig. 7.1(c)** is sketched. On the other hand, **Fig. 7.1(d)** is drawn to see the effect of β_2 on temperature distribution $\theta(\eta)$ provided that the temperature enhances in the Oldroyd-B fluid flow as β_2 increases in the range 0.1 to 0.7. Additionally, the change in concentration distribution $\phi(\eta)$ is pictured in **Fig. 7.1(e)** with respect to higher retardation time parameter β_2. It is illustrated that the concentration in the Oldroyd-B liquid is enhanced by taking different values of β_2 in positive increasing order.

The impact of M (magnetic field parameter) on velocity fields, temperature and concen-

tration distributions is discussed through **Figs. 7.2(a-e)**. It is stated that the radial velocity diminishes as magnetic field parameter increases in the range $M(= 0.5, 1.0, 1.5, 2.0)$. A similar pattern can be seen for the velocity of azimuthal direction. Additionally, **Fig. 7.2(c)** is sketched to observe the variation of liquid velocity in axial direction. On the other hand, the temperature distribution is discussed via **Fig. 7.2(d)** against different values of magnetic field number M. This profile reveals that $\theta(\eta)$ enhances as M varies from 0.5 to 2.0. A similar behavior is noted for the concentration distribution $\phi(\eta)$ in the flow [see **Fig. 7.2(e)**].

The change in temperature in the liquid with respect to thermal relaxation time parameter ε_t is presented through **Fig. 7.3(a)**. It is depicted that temperature reduces for larger estimations of ε_t. In physical terms, the liquid particles take additional time to pass heat into the neighboring particles by increasing the thermal relaxation time parameter, which allows the temperature to decrease, thereby reducing the temperature in the liquid. On the other hand, by setting $\varepsilon_t(= 0)$, the concept of Cattaneo-Christov converts to the classical Fourier's law, thereby heat is immediately transmitted through the substance so that increases the fluid temperature. Moreover, the curves for concentration distribution are drawn with the influence of ε_c. It is evaluated that with a larger approximation of ε_c, the concentration distribution decreases which is shown in **Fig. 7.3(b)**.

Figs. 7.4(a, b) are presented to exhibit the dependence of the fluid temperature on the heat generation/absorption parameter γ. It is deduced from the plots that the temperature is an increasing function of heat generation parameter $\gamma(> 0)$. Additionally, it is found that the heat absorption parameter $\gamma(< 0)$ falls down the temperature and the thermal boundary layer. **Fig. 7.5** displays the involvement of the K on the concentration distribution. It delineates that the chemical reaction parameter K has a decaying effect on the concentration distribution

102

and concentration boundary layer structures.

Table 7.1: A link between present study and with previous article for the $-\theta'(0)$ on various values of Pr.

Pr	Gregg and Sparrow [58]	Analytical results	Numerical results
1	0.39625	0.3968553	0.39682844
10	1.1341	1.1338514	1.13385776
100	2.6871	2.6867440	2.68677447

Table 7.2: A comparison of the $F'(0)$, $-G'(0)$ and $-\theta'(0)$ on fixed Pr $= 6.2$ with previous published articles.

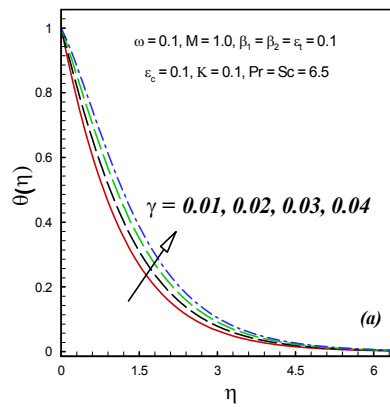|	Turkyilmazoglu [54]	Analytical results	Numerical results
$F'(0)$	0.51023262	0.50007761	0.51011626
$-G'(0)$	0.61592201	0.61852072	0.61584927
$-\theta'(0)$	0.93387794	0.93004605	0.93369411
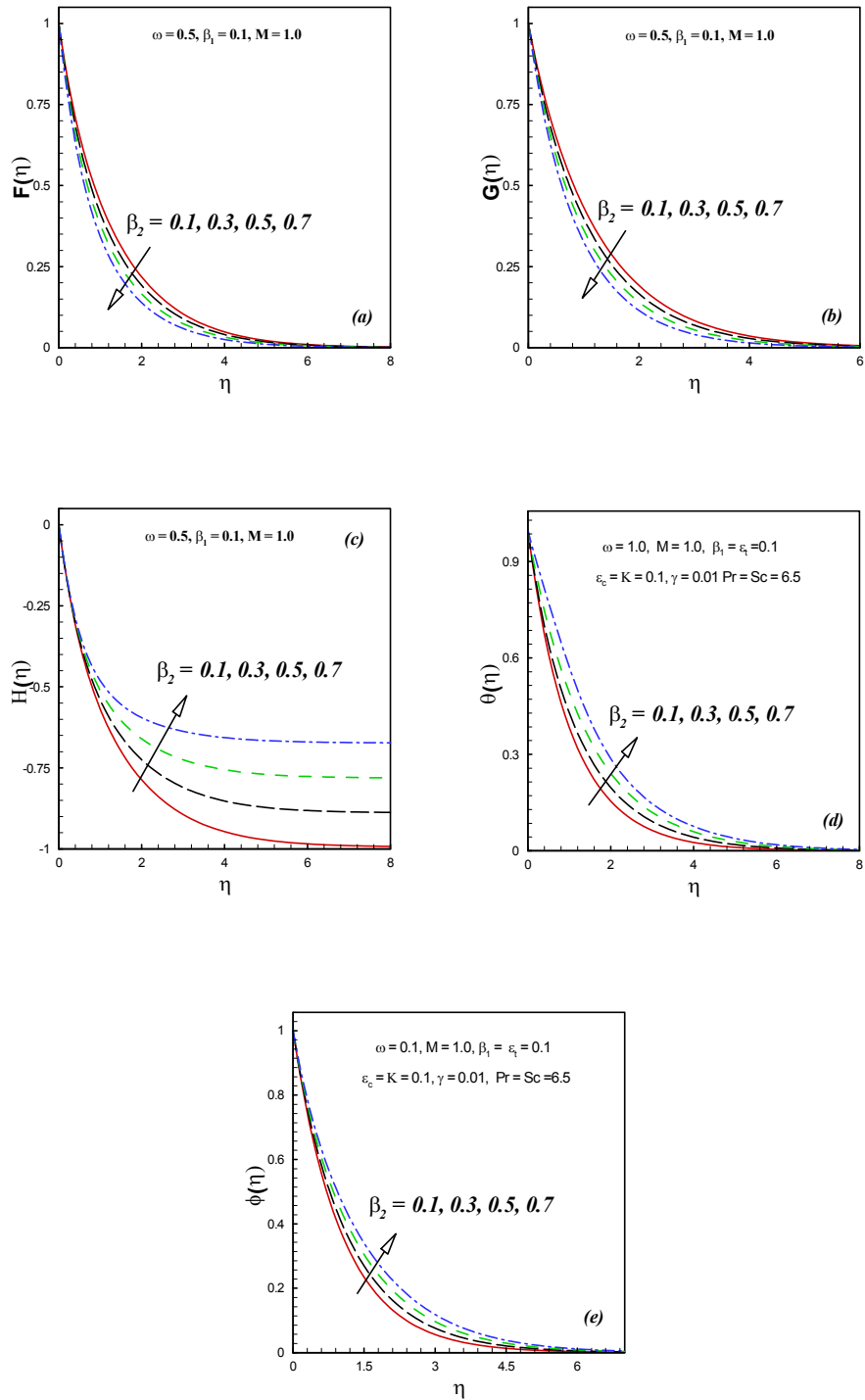
Figs. 7.1: Impact of β_2 on $F(\eta)$, $G(\eta)$, $H(\eta)$, $\theta(\eta)$ and $\phi(\eta)$.
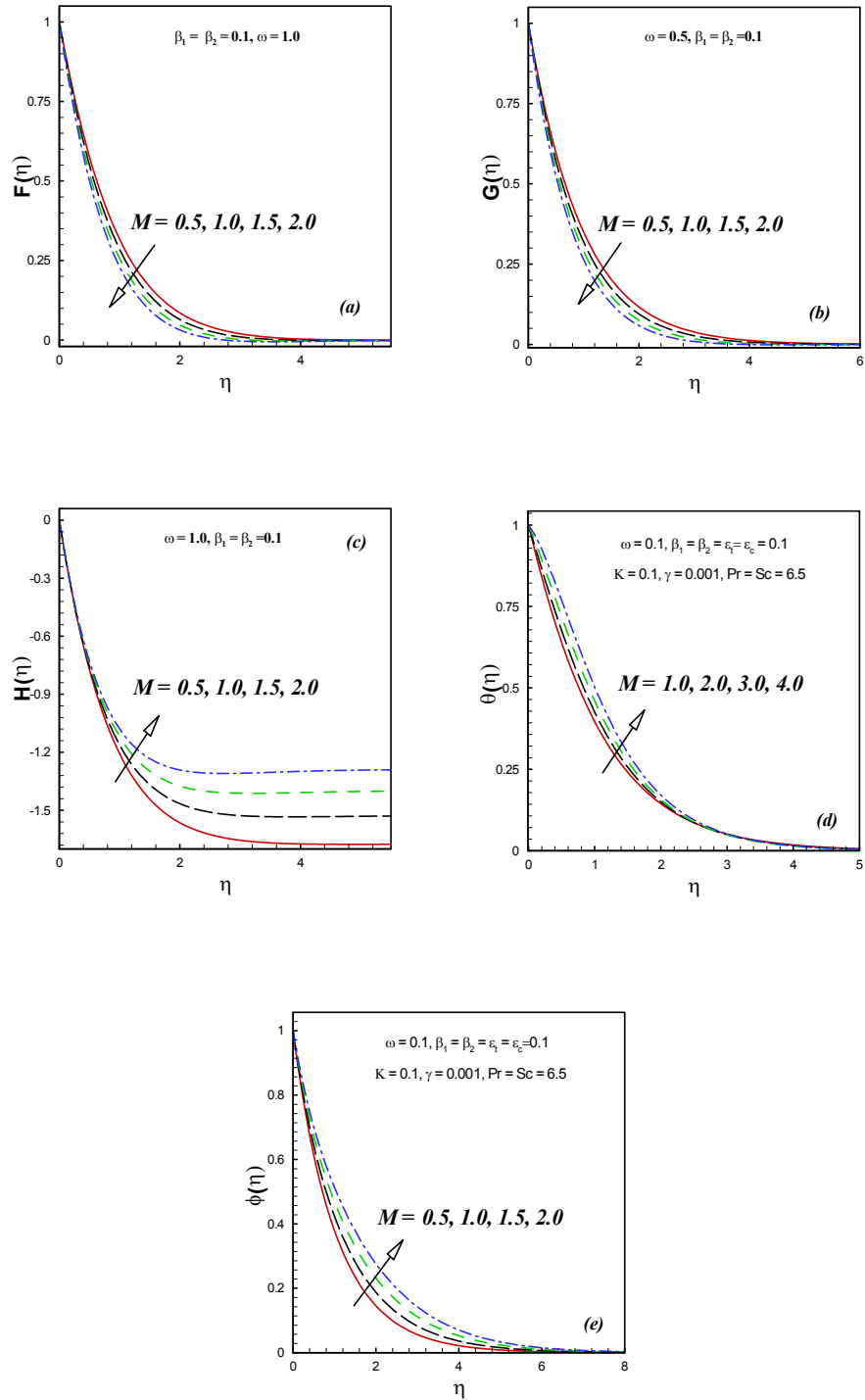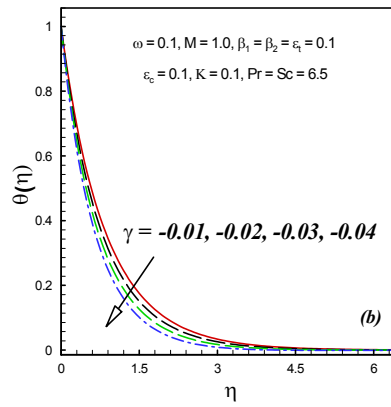
Figs. 7.2: Impact of M on $F(\eta)$, $G(\eta)$, $H(\eta)$, $\theta(\eta)$ and $\phi(\eta)$.
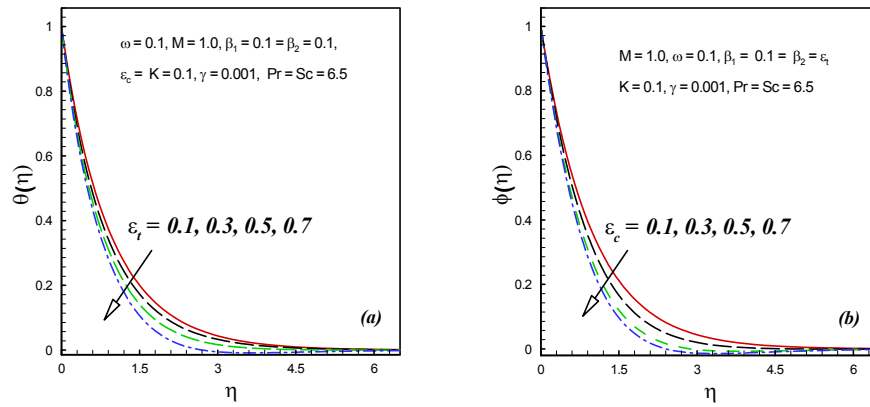
Figs. 7.3: Variation of temperature distribution $\theta\left(\eta\right)$ on ε_t and ε_c.

Figs. 7.4: Variation of $\theta\left(\eta\right)$ on $\gamma > 0$.

The plot shows $\theta(\eta)$ versus η with parameters:

$\omega = 0.1, M = 1.0, \beta_1 = \beta_2 = \varepsilon_t = 0.1$

$\varepsilon_c = 0.1, K = 0.1, Pr = Sc = 6.5$

$\gamma = -0.01, -0.02, -0.03, -0.04$

(b)

Figs. 7.4: Variation of $\theta(\eta)$ on $\gamma < 0$.

The plot shows $\phi(\eta)$ versus η with parameters:

$M = 1.0, \omega = 0.1, \beta_1 = \beta_2 = \varepsilon_t = 0.1$

$\varepsilon_c = 0.1, \gamma = 0.01, Pr = Sc = 6.5$

$K = 0.1, 0.3, 0.5, 0.7$
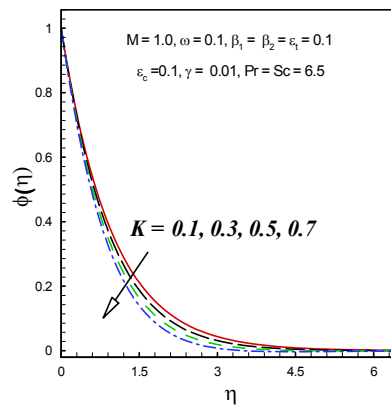
Fig. 7.5: Variation of $\phi(\eta)$ on various values of K.

Chapter 8

Swirling Flow of Oldroyd-B Nanofluid with Cattaneo-Christov Double Diffusion Theory

This chapter presents a swirling flow of the viscoelastic Oldroyd-B fluid in the presence of nanoparticles. A progressive modification is made to the heat and concentration equations of nanofluid by exploiting the Cattaneo-Christov theory. The feature of the Lorentz force due to the magnetic field applied normally to the disk is discussed. A homotopic approach (HAM) is applied for the analysis of the governing nonlinear problem. Results show that temperature as well as concentration distributions are reduced by higher magnitude of thermal and solutal relaxation time parameters, respectively.

8.1 Formulation of Governing Problem

Here, we examine the steady and incompressible von Karman swirling axisymmetric flow of an Oldroyd-B nanofluid. The fluid flow is generated by the rotating and stretching of the disk as displayed in the setup **Fig. 2.1** (cf. Chapter **2**).

For formulation of heat and mass transport in the fluid, the Cattaneo-Christov theory is employed. The Buongiorno model is adopted to study the thermal features of the nanoparticles described by thermophoresis and Brownian motion quantities.

The above assumptions lead the following system of nonlinear governing equations (Eqs. (1.7), (1.19), (1.20) cf. Chapter **1** and (2.18), (2.19), (2.20) cf. Chapter **2**)

$$\frac{\partial u}{\partial r} + \frac{u}{r} + \frac{\partial w}{\partial z} = 0, \tag{8.1}$$

$$
\begin{aligned}
u\frac{\partial u}{\partial r} - \frac{1}{r}v^2 + w\frac{\partial u}{\partial z} &= \nu\frac{\partial^2 u}{\partial z^2} - \frac{\sigma}{\rho}B_0^2\left[u + \lambda_1 w\frac{\partial u}{\partial z}\right] \\
&-\lambda_1\left[u^2\frac{\partial^2 u}{\partial r^2} + w^2\frac{\partial^2 u}{\partial z^2} + 2uw\frac{\partial^2 u}{\partial r\partial z} - \frac{2}{r}uv\frac{\partial v}{\partial r} - \frac{2}{r}vw\frac{\partial v}{\partial z} + \frac{1}{r^2}uv^2 + \frac{1}{r}v^2\frac{\partial u}{\partial r}\right] \\
&+\nu\lambda_2\left[-\frac{1}{r}\left(\frac{\partial u}{\partial z}\right)^2 - 2\frac{\partial u}{\partial z}\frac{\partial^2 w}{\partial z^2} + w\frac{\partial^3 u}{\partial z^3} - \frac{\partial u}{\partial r}\frac{\partial^2 u}{\partial z^2} - \frac{\partial u}{\partial z}\frac{\partial^2 u}{\partial r\partial z} + u\frac{\partial^3 u}{\partial r\partial z^2}\right],
\end{aligned}
\tag{8.2}
$$

$$
\begin{aligned}
u\frac{\partial v}{\partial r} + \frac{1}{r}uv + w\frac{\partial v}{\partial z} &= \nu\frac{\partial^2 v}{\partial z^2} - \frac{\sigma}{\rho}B_0^2\left[v + \lambda_1 w\frac{\partial v}{\partial z}\right] \\
&-\lambda_1\left[u^2\frac{\partial^2 v}{\partial r^2} + w^2\frac{\partial^2 v}{\partial z^2} + 2uw\frac{\partial^2 v}{\partial r\partial z} + \frac{2}{r}uv\frac{\partial u}{\partial r} + \frac{2}{r}vw\frac{\partial u}{\partial z} - \frac{2}{r^2}u^2v - \frac{1}{r^2}v^3 + \frac{1}{r}v^2\frac{\partial v}{\partial r}\right] \\
&+\nu\lambda_2\left[\begin{array}{c} u\frac{\partial^3 v}{\partial r\partial z^2} - 2\frac{\partial v}{\partial z}\frac{\partial^2 w}{\partial z^2} + w\frac{\partial^3 v}{\partial z^3} - \frac{1}{r}\frac{\partial u}{\partial z}\frac{\partial v}{\partial z} \\ -\frac{\partial v}{\partial r}\frac{\partial^2 u}{\partial z^2} + \frac{1}{r}v\frac{\partial^2 u}{\partial z^2} - \frac{\partial v}{\partial z}\frac{\partial^2 u}{\partial r\partial z} - \frac{1}{r}u\frac{\partial^2 v}{\partial z^2} \end{array}\right],
\end{aligned}
\tag{8.3}
$$

109

$$u\frac{\partial T}{\partial r} + w\frac{\partial T}{\partial z} = 2\varepsilon_0\tau\frac{D_T}{T_\infty}\left[u\frac{\partial T}{\partial z}\frac{\partial^2 T}{\partial r\partial z} + w\frac{\partial T}{\partial z}\frac{\partial^2 T}{\partial z^2}\right] + \tau\left[D_B\left(\frac{\partial C}{\partial z}\frac{\partial T}{\partial z}\right) + \frac{D_T}{T_\infty}\left(\frac{\partial T}{\partial z}\right)^2\right]$$

$$+\alpha\frac{\partial^2 T}{\partial z^2} + \varepsilon_0\tau D_B\left[u\frac{\partial^2 C}{\partial r\partial z}\frac{\partial T}{\partial z} + u\frac{\partial C}{\partial z}\frac{\partial^2 T}{\partial r\partial z} + w\frac{\partial^2 C}{\partial z^2}\frac{\partial T}{\partial z} + w\frac{\partial C}{\partial z}\frac{\partial^2 T}{\partial z^2}\right]$$

$$-\varepsilon_0\left[u^2\frac{\partial^2 T}{\partial r^2} + 2uw\frac{\partial^2 T}{\partial r\partial z} + w^2\frac{\partial^2 T}{\partial z^2} + u\frac{\partial w}{\partial r}\frac{\partial T}{\partial z} + u\frac{\partial u}{\partial r}\frac{\partial T}{\partial r} + w\frac{\partial u}{\partial z}\frac{\partial T}{\partial r} + w\frac{\partial w}{\partial z}\frac{\partial T}{\partial z}\right], \quad (8.4)$$

$$u\frac{\partial C}{\partial r} + w\frac{\partial C}{\partial z} = D_B\frac{\partial^2 C}{\partial z^2} + \varepsilon_1\frac{D_T}{T_\infty}\left[u\frac{\partial^3 T}{\partial r\partial z^2} + w\frac{\partial^3 T}{\partial z^3}\right] + \frac{D_T}{T_\infty}\frac{\partial^2 T}{\partial z^2}$$

$$-\varepsilon_1\left[u^2\frac{\partial^2 C}{\partial r^2} + 2uw\frac{\partial^2 C}{\partial r\partial z} + w^2\frac{\partial^2 C}{\partial z^2} + u\frac{\partial w}{\partial r}\frac{\partial C}{\partial z} + u\frac{\partial u}{\partial r}\frac{\partial C}{\partial r} + w\frac{\partial u}{\partial z}\frac{\partial C}{\partial r} + w\frac{\partial w}{\partial z}\frac{\partial C}{\partial z}\right] (8.5)$$

8.2 Boundary Conditions

The BCs of the governing problem are:

(i) On the surface of the disk $(z = 0)$

$$(u, v, w) = (cr, \Omega r, 0), \quad (T, C) = (T_w, C_w). \tag{8.6}$$

(ii) On the free stream $(z \to \infty)$

$$(u, v) \to (0, 0), \quad (T, C) \to (T_\infty, C_\infty), \tag{8.7}$$

where Ω indicates the swirling rate and c the stretching rate.

By substituting the von Kármán similarity transformations (Eq. (2.24)) cf. Chapter **2**) into Eqs. (8.1) to (8.5), we acquire

$$H' + 2F = 0, \tag{8.8}$$

$$F^2 - G^2 + F'H - F'' + \beta_1 \left(F''H^2 + 2FF'H - 2GG'H \right)$$

$$+\beta_2 \left(2F'^2 + 2F'H'' - F'''H \right) + M \left(F + \beta_1 F'H \right) = 0, \tag{8.9}$$

$$2FG + G'H - G'' + \beta_1 \left(G''H^2 + 2 \left(FG' + F'G \right) H \right)$$

$$-\beta_2 \left(G'''H - 2F'G' - 2G'H'' \right) + M \left(G + \beta_1 G'H \right) = 0, \tag{8.10}$$

$$\frac{1}{\text{Pr}} \theta'' - H\theta' + Nb \left[\theta'\phi' + \varepsilon_t \left(H\theta'\phi'' + H\theta''\phi' \right) \right]$$

$$+Nt \left[\theta'^2 + 2\varepsilon_t H\theta'\theta'' \right] - \varepsilon_t \left[H^2\theta'' + HH'\theta' \right] = 0, \tag{8.11}$$

$$\phi'' - ScH\phi' - \varepsilon_c Sc \left[H^2\phi'' + HH'\phi' \right] + \frac{Nt}{Nb} \left[\theta'' + \varepsilon_c H\theta''' \right] = 0, \tag{8.12}$$

with non-dimensional BCs

$$(F, G, H, \theta, \phi) = (\omega, 1, 0, 1, 1) \quad \text{at} \quad \eta = 0,$$

$$(F, G, \theta, \phi) \to (0, 0, 0, 0) \quad \text{as} \quad \eta \to \infty. \tag{8.13}$$

The involved parameters are similar as defined in previous chapters.

8.3 Results and Discussion

To acquire the analytical series solution of the proposed problem (8.8) to (8.12) and (8.13), a homotopy analysis method is implemented. This part is centered around the physical explanation of involved parameters impact on velocity field, temperature and solutal distributions. The von Karman swirling flow of the Oldroyd-B fluid is analyzed in the form of similar solutions. The effect of parameters like magnetic field $0.5 \leq M \leq 2.0$, relaxation time parameter $0.1 \leq \beta_2 \leq 0.7$ are analyzed on velocity profile, thermal and solutal distributions. The impact of thermal relaxation time parameter $0.1 \leq \varepsilon_t \leq 0.7$, thermophoresis parameter $0.1 \leq Nt \leq 0.7$, the Brownian motion parameter $0.1 \leq Nb \leq 0.7$, the Prandtl number $5.0 \leq \mathrm{Pr} \leq 9.0$ on temperature distribution is inspected. Solutal relaxation time parameter $0.1 \leq \varepsilon_c \leq 0.7$, the thermophoresis parameter $0.1 \leq Nt \leq 0.7$, the Brownian motion parameter $0.1 \leq Nb \leq 0.7$ and the Schmidt number $5.0 \leq Sc \leq 9.0$ are examined on concentration distribution.

Figs. 8.1(a-e) depict the effect of the magnetic field parameter M on velocity profile, temperature, and concentration distributions of the liquid. From **Figs.8.1(a)** and **8.1(b)**, the variations in velocity profiles with respect to the magnetic field parameter M are disclosed against η. It is seen that the velocities in the radial and azimuthal directions decline with the influence of M $(0.5 - 2.0)$. Additionally, the magnitude of the velocity profile in the axial direction reduces with the higher impact of M, as shown in **Fig. 8.1(c)**. Physically, the magnetic field is a resistive force which produces resistance to the motion of the liquid and thus a reduction in the motion of the fluid is noticed. The impact of magnetic field parameter M on the temperature distribution $\theta(\eta)$ is plotted in **Fig. 8.1(d)**. It is stated that the temperature is enhanced by higher values of M. Due to the presence of the magnetic field, the Lorentz

force (the resistive force) appears in the motion of fluid. A higher magnetic field corresponds to a stronger Lorentz force that enhances the temperature of the liquid. Furthermore, the concentration distribution $\phi(\eta)$ is enhanced by taking a large estimation of the magnetic field (see **Fig. 8.1(e)**).

To see the effect of the retardation time parameter β_2 on the velocity of the fluid, temperature and concentration distributions, the curves are plotted via **Figs. 8.2(a-e)**. It is observed that the velocity in the radial $F(\eta)$ and azimuthal $G(\eta)$ directions decrease as β_2 changes from 0.1 to 0.7. Moreover, the velocity in the axial direction is affected by the retardation time parameter, as shown in **Fig. 8.2(c)**. To analyze the influence of β_2 on the temperature and concentration distributions, the results are sketched in **Figs. 8.2(d)** and **8.2(e)**, respectively. From these figures, it is observed that a stronger rate of the retardation time parameter β_2 leads to increase the temperature and concentration distribution of the Oldroyd-B liquid (see **Figs. 8.2(d)** and **8.2(e)**).

The variations of the temperature distribution $\theta(\eta)$ with respect to thermal relaxation time parameter ε_t are plotted in **Fig. 8.3(a)**. In this figure, the temperature declines with the enlargement of ε_t. In fact, for higher values of ε_t, the fluid particles take more extra time to transport heat into the adjoining particles, which causes a decrease in the temperature. Moreover, **Fig. 8.3(b)** shows the effect of the solutal relaxation time parameter ε_c on the $\phi(\eta)$. It reveals that the concentration distribution $\phi(\eta)$ and the boundary layer thickness fall down as the ε_c increases from 0.1 to 0.7.

Figs. 8.4(a) and **8.4(b)** elucidate the influence of Nt on the temperature and concentration distributions, respectively. The temperature as well as concentration of the liquid enhance with Nt. Physically, higher values of Nt increase the thermophoretic force which leads to increase

the transportation of heat and mass in the fluid flow.

Figs. 8.5(a) and **8.5(b)** show the influence of Nb on the temperature $\theta(\eta)$ and concentration $\phi(\eta)$ distributions, respectively, in the Oldroyd-B fluid flow. It shows that the temperature rises with respect to $Nb\,(0.1 - 0.7)$. It is because of the fact that a higher rate of Nb causes an increase in the diffusion rate which leads to the maximum in collision between the fluid particles. Therefore, the temperature of the fluid increases. The change in the solutal distribution on Nb is discussed in **Fig. 8.5(b)**. It is stated that higher values of Nb reduce the concentration distribution. Basically, a higher rate of Nb causes more collision between the fluid particles. So, for that reason, the mass transfers at a very low rate and consequently, a reduction in the concentration distribution is noticed.

Fig. 8.6(a) delineates the effect of Pr on the temperature distribution. The temperature reduces as Pr changes from 5.0 to 9.0. Additionally, the impact of Sc on the concentration distribution is sketched in **Fig. 8.6(b)**. It is obvious that increasing values of Sc tend to diminish the concentration distribution . Since the Schmidt number is inversely proportional to the diffusion coefficient. So, enlarging the Schmidt number leads to a decrease in the concentration of nanoparticles.
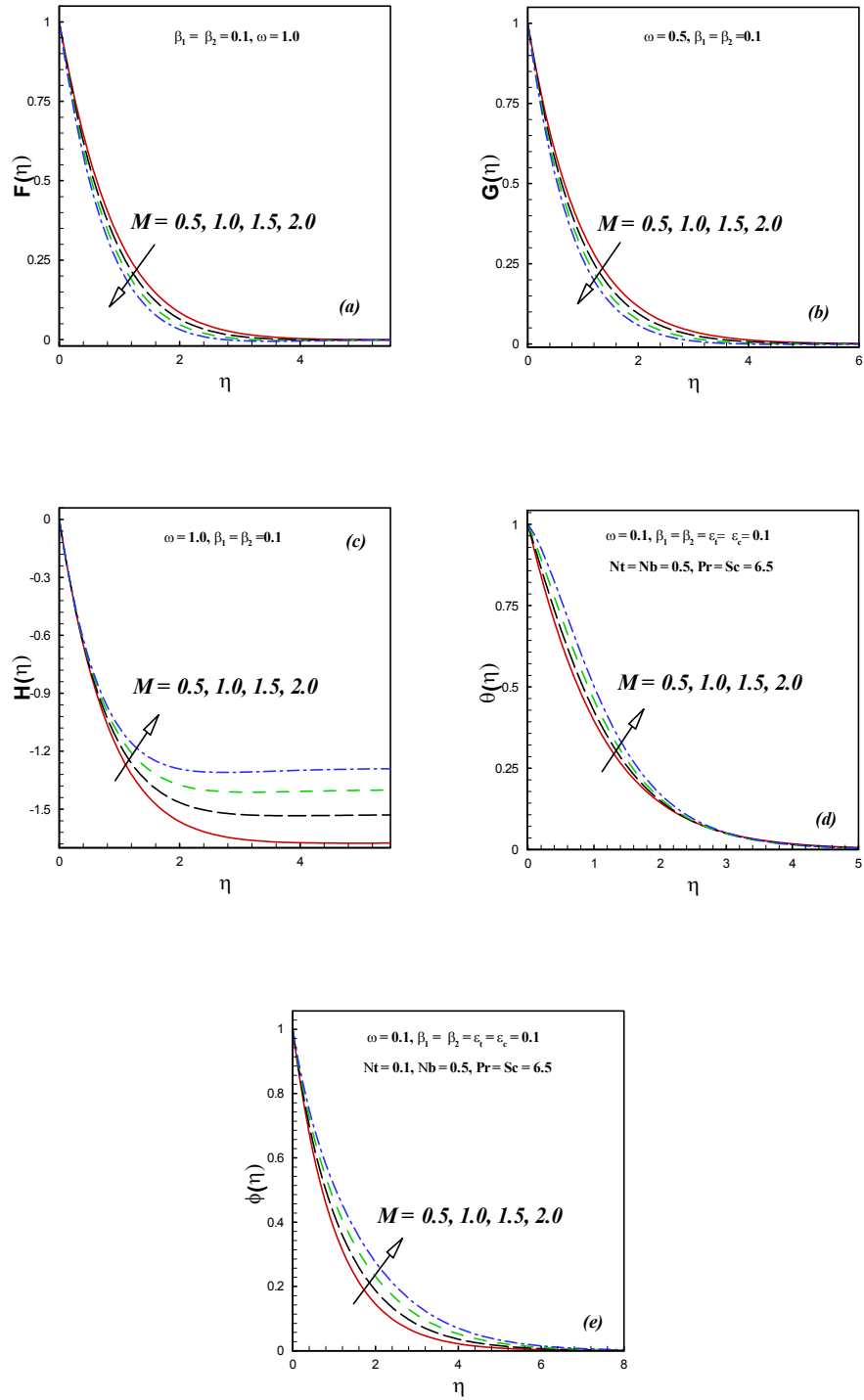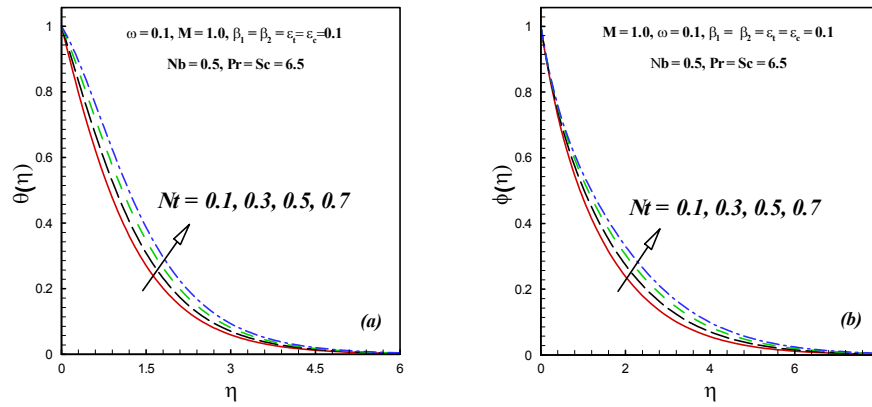
Figs. 8.1: Effect of M on $F(\eta)$, $G(\eta)$, $H(\eta)$, $\theta(\eta)$ and $\phi(\eta)$.
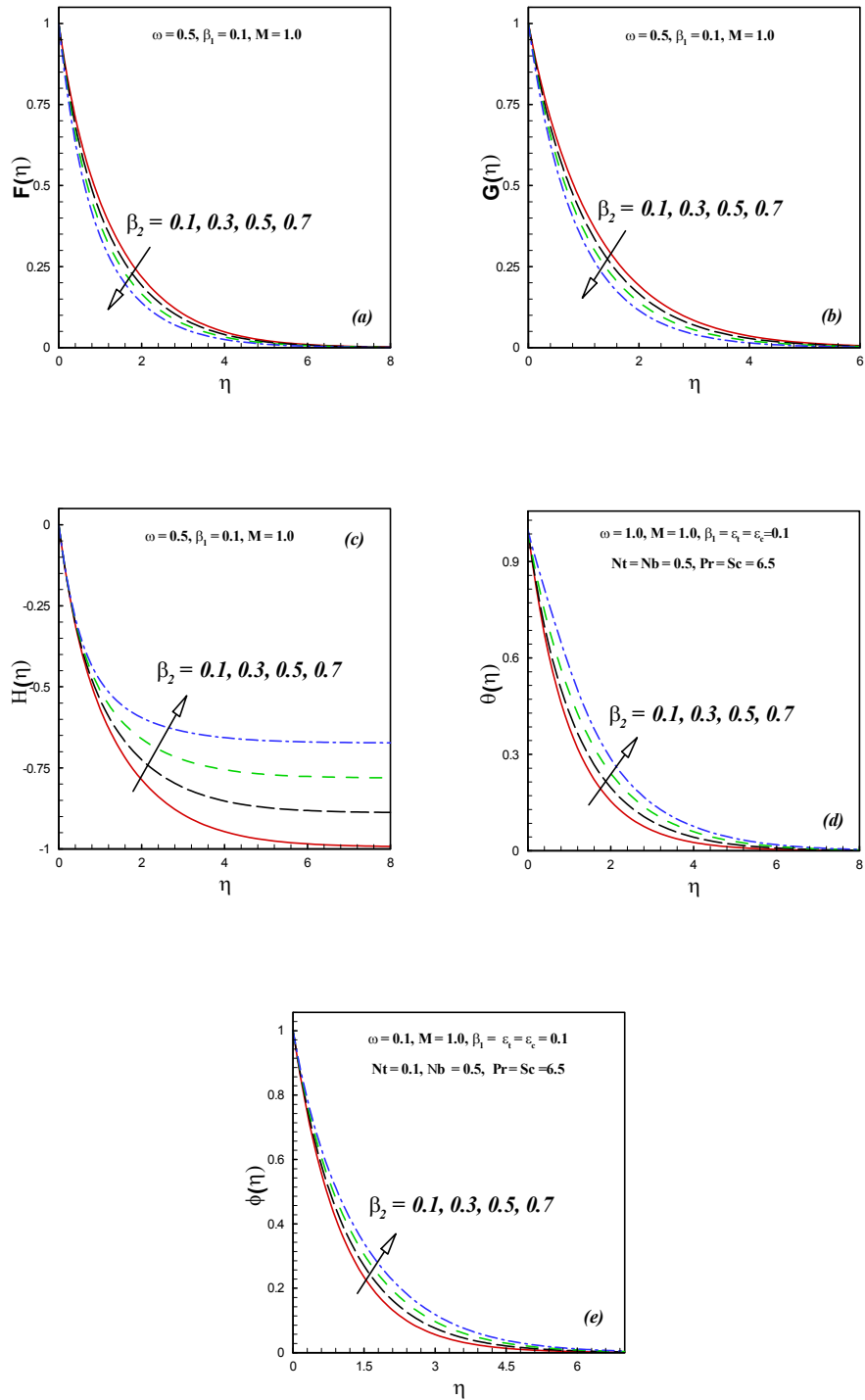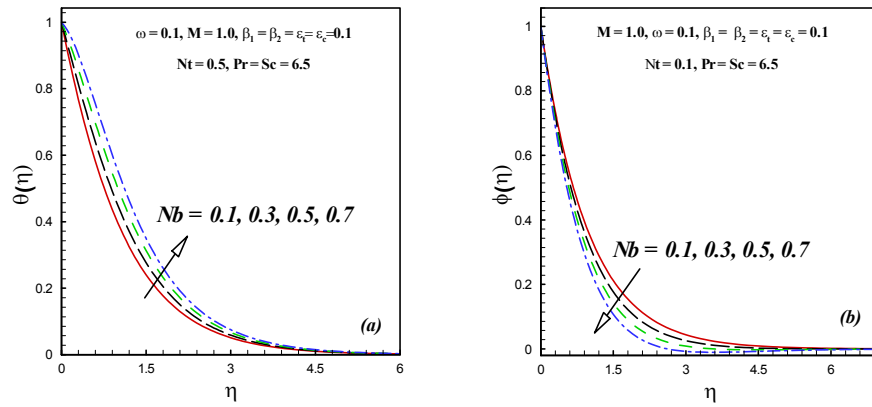
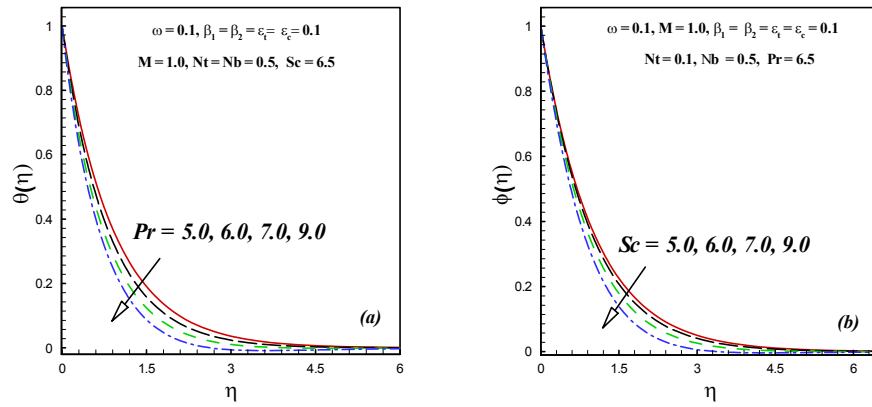**Figs. 8.2**: Effect of β_2 on $F(\eta)$, $G(\eta)$, $H(\eta)$, $\theta(\eta)$ and $\phi(\eta)$
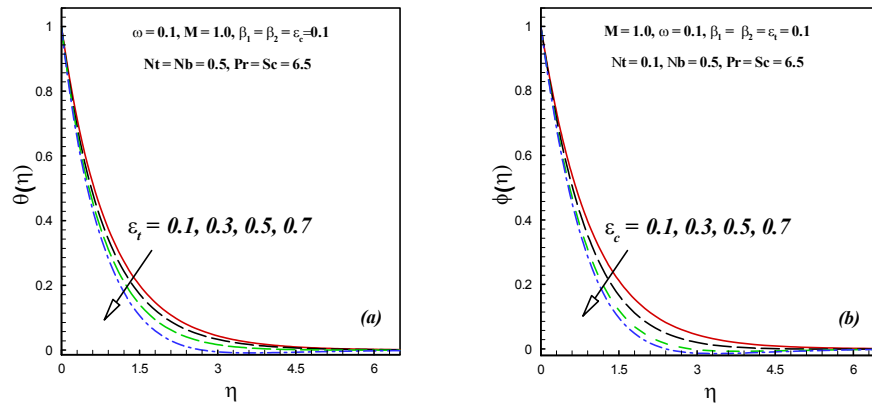
Figs. 8.3: Effect of ε_t on $\theta(\eta)$ and effect of ε_c on $\phi(\eta)$.

Figs. 8.4: Effect of Nt on $\theta(\eta)$ and $\phi(\eta)$.

Figs. 8.5: Effect of Nb on $\theta(\eta)$ and $\phi(\eta)$.

Figs. 8.6: Effect of Pr on $\theta(\eta)$ and effect of Sc on $\phi(\eta)$.

Chapter 9

Conclusion and Future Work

The aim of research work presented in this thesis is to study the swirling motion of a non-Newtonian Oldroyd-B fluid caused by rotating disk geometry. For the required purpose, the mathematical formulation of the swirling flow of Oldroyd-B fluid over a rotating disk is developed. Additionally, the transportation of heat and mass is studied with different physical aspects. The von Karman transformations are utilized to convert the governing partial differential equations (PDEs) into non-linear ordinary differential equations (ODEs). The system of ODEs is then solved by using the numerical and semi analytical approaches which are bvp midrich scheme and homotopy analysis method. The validity of obtained results proved through the comparison with results of the published literature.

9.1   Concluding Remarks

In this thesis, we compile some significant findings achieved in the preceding chapters as:

- Both the radial and azimuthal fluid velocity components were declined by stronger rate

of magnetic force.

- It was seen that by the higher values of stretching parameter, the radial velocity was enhanced while a contrary effect was seen in the case of azimuthal velocity.

- Significant variation was observed in the velocity and temperature of fluid against mass transfer parameter.

- It was deduced from the results that the temperature was an increasing function of the heat generation parameter while, for the heat absorption parameter, the temperature and thermal boundary layers were noticed in decreasing trend.

- The temperature and solutal distributions were diminished against increasing trend of relaxation time parameter and boosted for retardation time parameter.

- The occurrence of radiative heat flux enhanced the thermal profile efficiently.

- It was revealed that the thermal distribution was boosted by the increasing values of Brownian motion parameter and reduced the solutal distribution.

- The temperature and concentration distributions were found to be reduced by the thermal and solutal relaxation time parameters, respectively.

- The temperature as well as concentration distributions were increased due to increment in thermophoresis parameter.

- It was concluded that the solutal distribution was enhanced with the increasing impact of activation energy.

- For the solutal distribution, a declining trend was noticed as homogeneous reaction parameter change the values in increasing manner.

9.2 Future Work

Here in this study, the numerical and analytical investigations of non-Newtonian Oldroyd-B fluid flow are focused. The mathematical formulations were developed with heat and mass transfer over a rotating disk geometry. However, there are further directions that can be made to the Oldroyd-B fluid flow to extend the current work. Some suggestions in this regards will be pursued in the future research as follows:

- The current mathematical model can be extended to an Oldroyd-B fluid flow over a rotating sphere.

- This work may also be extended on flows over a rotating cylinder in future.

- The transient thin film flows of Oldroyd-B fluid over a rotating geometries can also be studied.

- Regarding the numerical solutions, it may be interesting to discuss the proposed problems with the help of different advanced numerical schemes such as finite difference method, finite volume method and lattice Boltzmann method etc.

Bibliography

[1] J.G. Oldroyd, On the formulation of rheological equations of state, *Proc. R. Soc. Lond. Ser.A*, **200** (1950), 523-541.

[2] M. Sajid, Z. Abbas, T. Javed, and N. Ali, Boundary layer flow of an Oldroyd-B fluid in the region of a stagnation point over a stretching sheet, *Canadian J. Phys.*, **88**, (2010) 635-640.

[3] S.A. Shehzad, S. Ali, A. Alsaedi, T. Hayat and M. S. Alhuthali, Three-dimensional flow of an Oldroyd-B fluid with variable thermal conductivity and heat generation/absorption, *PLOS ONE*, **8**, (2013) e78240.

[4] T. Hayat, T. Muhammad, S. A . Shehzad and A. Alsaedi, An analytical solution for magnetohydrodynamic Oldroyd-B nanofluid flow induced by a stretching sheet with heat generation/absorption, *Int. J. Therm. Sci.*, **111** (2017) 274-288.

[5] B. Mahanthesh, B.J. Gireesha, S.A. Shehzad, F.M. Abbasi, and R.S.R. Gorla, Nonlinear three-dimensional stretched flow of an Oldroyd-B fluid with convective condition, thermal radiation, and mixed convection, *Appl. Math. Mech.*, **38**, (2017) 969-980.

[6] K. Kumar, K. Ganesh, G. K. Ramesh, B. J. Gireesha, and R. S. R. Gorla, Characteristics of Joule heating and viscous dissipation on three-dimensional flow of Oldroyd B nanofluid with thermal radiation, *Alex. Eng. J.*, **57** (2018) 2139-2149.

[7] P. Liang, S. Wang and M. Zhao, Numerical study of rotating electroosmotic flow of Oldroyd-B fluid in a microchannel with slip boundary condition, *Chinese J. Phys.*, **65** (2020) 459-471.

[8] T.V. Karman, Uberlaminare und turbulente Reibung, *Z. Angew. Math. Mech.* (ZAMM), **1** (1921) 233-252.

[9] W.G. Cochran, The flow due to a rotating disk, *Proc. Camb. Phil. Soc.*, **30** (1934) 365-375.

[10] M. Turkyilmazoglu, Three dimensional MHD stagnation flow due to a stretchable rotating disk, *Int. J. Heat Mass Transf.*, **55** (2012) 6959-6965.

[11] M. Turkyilmazoglu, Effects of uniform radial electric field on the MHD heat and fluid flow due to a rotating disk, *Int. J. Eng. Sci.*, **51** (2012) 233-240.

[12] M. Turkyilmazoglu, Nanofluid flow and heat transfer due to a rotating disk, *Comput. Fluids*, **94** (2014) 139-146.

[13] M.M. Rashidi, N. Kavyani and S. Abelman, Investigation of entropy generation in MHD and slip flow over a rotating porous disk with variable properties, *Int. J. Heat Mass Transf.*, **70** (2014) 892-917.

[14] R. Ellahi, M.H, Tariq, M. Hassan and K. Vafai, On boundary layer nano-ferroliquid flow under the influence of low oscillating stretchable rotating disk, *J. Mol. Liq.*, **229** (2017) 339-345.

[15] B. Mahanthesh, B.J. Gireesha, S.A. Shehzad, A. Rauf and P.B.S. Kumar, Nonlinear radiated MHD flow of nanoliquids due to a rotating disk with irregular heat source and heat flux condition, *Phys. B: Cond. Matt.*, **537** (2018) 98-104.

[16] M. Gholinia, K. Hosseinzadeh, H. Mehrzadi, D.D. Ganj and A.A. Ranjbar, Investigation of MHD Eyring–Powell fluid flow over a rotating disk under effect of homogeneous–heterogeneous reactions, *Case Stud. Therm. Eng.*, **13** (2019) 100356.

[17] J. Ahmed, M. Khan and L. Ahmad, Stagnation point flow of Maxwell nanofluid over a permeable rotating disk with heat source/sink, *J. Mol. Liq.*, **287** (2019) 110853.

[18] J. Ahmed, M. Khan and L. Ahmad, MHD von Kármán swirling flow in the Maxwell nanofluid with nonlinear radiative heat flux and chemical reaction, *Heat Transf. Res.*, **51** (2020) 377-394.

[19] S. Choi and J.A. Eastman, Enhancing thermal conductivity of fluids with nanoparticles, *ASME Int. Mech. Eng. Congr. Exposition, San Francisco* (1995).

[20] J. Buongiorno, Convective transport in nanofluids, *ASME J. Heat Transf.*, **128** (2006) 240-250.

[21] W. Khan and I. Pop, Boundary-layer flow of a nanofluid past a stretching sheet, *Int. J. Heat Mass Transf.*, **53**, (2010) 2477-2483.

[22] Hashim, A. Hafeez, A.S. Alshomrani and M. Khan, Multiple physical aspects during the flow and heat transfer analysis of Carreau fluid with nanoparticles, *Scientific Reports*, **8**, (2018) 1-14.

[23] M. Jafaryar, M. Sheikholeslami, Z. Li and R. Moradi, Nanofluid turbulent flow in a pipe under the effect of twisted tape with alternate axis, *J. Therm. Analy. Calor.*, **135**, (2019) 305-323.

[24] A. Hamid, Hashim, A. Hafeez, M. Khan, A.S. Alshomrani and M. Alghamdi, Heat transport features of magnetic water-graphene oxide nanofluid flow with thermal radiation: stability test, *Euro. J. Mech.-B/Fluids*, **76**, (2019) 434-441.

[25] T. Hayat, T. Muhammad, A. Alsaedi and M.S. Alhuthali, Magnetohydrodynamic three-dimensional flow of viscoelastic nanofluid in the presence of nonlinear thermal radiation, *J. Mag. Mag. Mater.*, **385** (2015) 222-229.

[26] A. Ahmed, M. Khan, J. Ahmed and A. Hafeez, Von Kármán rotating flow of Maxwell nanofluids featuring the Cattaneo-Christov theory with a Buongiorno model, *Appl. Math. Mech.*, **41** (2020) 1195-1208.

[27] H. Alfvén, Existence of electromagnetic-hydrodynamic waves, *Nature*, **150**, (1942) 405-406.

[28] J. Zhao, L. Zheng, X. Zhang, and F. Liu, Convection heat and mass transfer of fractional MHD Maxwell fluid in a porous medium with Soret and Dufour effects, *Int. J. Heat Mass Transf.*, **103** (2016) 203-210.

[29] M. Sheikholeslami and H.B. Rokni, Simulation of nanofluid heat transfer in presence of magnetic field: a review, *Int. J. Heat Mass Transf.*, **115** (2017) 1203-1233.

[30] M. Sheikholeslami, and S.A. Shehzad, CVFEM for influence of external magnetic source on Fe_3O_4-H_2O nanofluid behavior in a permeable cavity considering shape effect, *Int. J. Heat Mass Transf.*, **115** (2017) 180-191.

[31] S.R. Sheri and T. Thumma, Numerical study of heat transfer enhancement in MHD free convection flow over vertical plate utilizing nanofluids, *Ain Shams Eng. J.*, **9** (2018) 1169-1180.

[32] A. Tassone, M. Nobili and G. Caruso, Numerical study of the MHD flow around a bounded heating cylinder: Heat transfer and pressure drops, *Int. Commun. Heat Mass Transf.*, **91** (2018) 165-175.

[33] A. Ahmed, M. Khan, M. Irfan and J. Ahmed, Transient MHD flow of Maxwell nanofluid subject to non-linear thermal radiation and convective heat transport, *Appl. Nanosci.*, **10** (2020) 5361-5373.

[34] K. Hiemenz, The boundary layer on a straight circular cylinder immersed in the uniform flow of liquid, *Dinglers Polytech. J.*, **326** (1911) 321-324.

[35] T.C. Chiam, Stagnation-point flow towards a stretching plate, *J. Phys. Soci. Jpn.*, **63** (1994) 2443-2444.

[36] T.C. Chiam, Heat transfer with variable conductivity in a stagnation-point flow towards a stretching sheet, *Int. Commun. Heat Mass Transf.*, **23** (1996) 239-248.

[37] T.R. Mahapatra and A.S. Gupta, Heat transfer in stagnation point flow towards a stretching sheet, *Heat Mass Transf.*, **38** (2002) 517-521.

[38] A. Ishak, K. Jafar, R. Nazar and I. Pop, MHD stagnation point flow towards a stretching sheet, *Physica A: Stat. Mech. Appl.*, **388** (2009) 3377-3383.

[39] M. Mustafa, T. Hayat, I. Pop, S. Asghar, and S. Obaidat, Stagnation-point flow of a nanofluid towards a stretching sheet, *Int. J. Heat Mass Transf.*, **54** (2011) 5588-5594.

[40] S.S. Motsa, Y. Khan and S. Shateyi, A new numerical solution of maxwell fluid over a shrinking sheet in the region of a stagnation point, *Math. Prob. Eng.*, **2012** (2012) 290615.

[41] K. Bhattacharyya, S. Mukhopadhyay and G.C. Layek, Slip effects on boundary layer stagnation-point flow and heat transfer towards a shrinking sheet, *Int. J. Heat Mass Transf.*, **54** (2011) 308-313.

[42] M. Khan, Hashim and A. Hafeez, A review on slip-flow and heat transfer performance of nanofluids from a permeable shrinking surface with thermal radiation: dual solutions, *Chem. Eng. Sci.*, **173** (2017) 1-11.

[43] A. Hamid, Hashim, M. Khan and A. Hafeez, Unsteady stagnation-point flow of williamson fluid generated by stretching/shrinking sheet with ohmic heating, *Int. J. Heat Mass Transf.*, **126** (2018) 933-940.

[44] J.B.J. Fourier, Theorie Analytique de la Chaleur, Didot, Paris, (1822) 499-508.

[45] C. Cattaneo, Sulla conduzione del calore, *Atti Sem. Mat. Fis. Univ. Modena*, **3** (1948) 83-101.

[46] C.I. Christov, On frame indifferent formulation of the Maxwell-Cattaneo model of finite speed heat conduction, *Mech. Res. Commun.*, **36** (2009) 481-486.

[47] M. Ciarletta and B. Straughan, Uniqueness and structural stability for the Cattaneo-Christov equations, *Mech. Res. Commun.*, **37** (2010) 445-447.

[48] B. Straughan, Thermal convection with the Cattaneo–Christov model, *Int. J. Heat Mass Transf.*, **53** (2010) 95-98.

[49] S. Han, L. Zheng, C. Li and X. Zhang, Coupled flow and heat transfer in viscoelastic fluid with Cattaneo-Christov heat flux model, *Appl. Math. Lett.*, **38** (2014) 87-93.

[50] A. Rauf, S.A. Shehzad, Z. Abbas and T. Hayat, Unsteady three-dimensional MHD flow of the micropolar fluid over an oscillatory disk with Cattaneo-Christov double diffusion, *Appl. Math. Mech.*, **40** (2019) 1471-1486.

[51] A. Rauf, Z. Abbas and S.A. Shehzad, Utilization of Maxwell-Cattaneo law for MHD swirling flow through oscillatory disk subject to porous medium, *Appl. Math. Mech.*, **40** (2019) 837-850.

[52] F.A. Sulti, Impact of Cattaneo–Christov Heat Flux Model on Stagnation-Point Flow Toward a Stretching Sheet With Slip Effects, *J. Heat Transf.*, **141** (2019) 022003.

[53] N. Bachok, A. Ishak and I. Pop, Flow and heat transfer over a rotating porous disk in a nanofluid, *Phys. B*, **406** (2011) 1767-1772.

[54] M. Turkyilmazoglu, Nanofluid flow and heat transfer due to a rotating disk, *Comput. Fluids*, **94** (2014) 139-146.

[55] N. Kelson and A. Desseaux, Note on porous rotating disk flow, *Aust. N. Z. Ind. Appl. Math. J.* (ANZIAM J), **42** (2000) 837-855.

[56] S. Rosseland, Astrophysik und Atom-Theoretische Grundlagen, Springer Verlag, Berlin, (1931) 41–44.

[57] J.H. Merkin, A model for isothermal homogeneous-heterogeneous reactions in boundary-layer flow, *Math. Comp. Model.*, **24** (1996) 125-136.

[58] J.L. Gregg and E.M. Sparrow, Heat transfer from a rotating disk to fluids of any Prandtl number, *ASME J. Heat Transf.*, **81** (1959) 249-251.

Turnitin Originality Report

Swirling Flow of an Oldroyd-B Fluid over a Rotating Disk   by Abdul Hafeez .

From CL QAU (DRSML)

- Processed on 10-Feb-2022 08:52 PKT
- ID: 1759002370
- Word Count: 22265

Similarity Index
16%
Similarity by Source

Internet Sources:
    7%
Publications:
    12%
Student Papers:
    6%

---

sources:

---

1 1% match (student papers from 30-Jun-2021)
Submitted to Higher Education Commission Pakistan on 2021-06-30

---

2 1% match (publications)
Jawad Ahmed, Masood Khan, Latif Ahmad, Abdullah K. Alzahrani, Metib Alghamdi. "Thermally radiative flow of Maxwell nanofluid over a permeable rotating disk", Physica Scripta, 2019

---

3 1% match (publications)
A. Ahmed, M. Khan, J. Ahmed, A. Hafeez. "Von Kármán rotating flow of Maxwell nanofluids featuring the Cattaneo-Christov theory with a Buongiorno model", Applied Mathematics and Mechanics, 2020

---

4 1% match (publications)
Jawad Ahmed, Masood Khan, Latif Ahmad, Abdullah Khamis Alzahrani, Metib Alghamdi. "Thermally radiative flow of Maxwell nanofluid over a permeable rotating disk", Physica Scripta, 2019

---

5 1% match (Internet from 16-Dec-2021)
https://www.amm.shu.edu.cn/CN/Y2020/V41/I7/1083

---

6 < 1% match (student papers from 02-May-2018)
Submitted to Higher Education Commission Pakistan on 2018-05-02

---

7 < 1% match (student papers from 16-Dec-2021)
Submitted to Higher Education Commission Pakistan on 2021-12-16

---

8 < 1% match (student papers from 07-Aug-2017)
Submitted to Higher Education Commission Pakistan on 2017-08-07

Flow of Oldroyd-B fluid caused by a rotating disk featuring the Cattaneo-Christov theory with heat generation/absorption

Abdul Hafeez [*], Masood Khan

Department of Mathematics, Quaid-i-Azam University, Islamabad 44000, Pakistan

ABSTRACT

This article presented the Cattaneo-Christove heat and mass flux theories in the flow of Oldroyd-B fluid over a rotating disk. The flow configuration is due to the rotating as well as stretching of the disk. The heat generation/absorption and chemical reaction are also considered. For the formulation of heat and mass equations, the Cattaneo-Christov theories are used rather than Fourier's and Fick's laws. The von Karman's transformations are used to convert the partial differential equations into non-dimensional ordinary differential equations. The analytical series solutions are obtained by utilizing the homotopy analysis method (HAM) in Mathematica software. The graphical results are achieved in the form of velocity fields, temperature and concentration distributions. Results show that the temperature of the Odroyd-B fluid rises when the magnetic field parameter increases in some specific range. Further, the velocities show a reducing behavior against magnetic field parameter. It is observed that the temperature reduces as thermal relaxation time parameter increases. It is also be mentioned that the solutal relaxation time parameter is influenced on concentration distribution in decreasing trend.

1. Introduction

It is well understood that in many engineering applications, fluid flows through a rotating disk geometry has a crucial significance. This form of geometry is commonly used in the energy production, aerodynamics and rotating machinery industries. Due to these applications, the similarity variables were initially developed by von Karman [1] for the axisymmetric hydrodynamic flow of viscous fluid over a rotating disk and using the integral approach to obtain the approximate solution of the problem. Further, Cochran [2] was utilized the von Karman variables and obtained asymptotic solutions for the steady hydrodynamic problem. Further, Zandbergen et al. [3,4] were described the von Kármán flow problem to obtain the numerical and the analytical solutions. Moreover, the works on the flow by a rotating disk was done by various researches. For instance, nanofluid flow and heat transfer due to a rotating disk was investigated by Bachok et al. [5]. Three dimensional stagnation flow by a stretchable rotating disk was disclosed by Turkyilmazoglu [6] and obtained numerical solution of the problem. The MHD flow over a rotating permeable disk with entropy generation was studied by Rashidi et al. [7] and used the Karman's transformations to convert the partial differential equations into non-dimensional ordinary

differential equations. Yin et al. [8] discussed the fluid flow of nanofluids through a rotating disk with uniform stretching rate in the radial direction and homotopy analysis method (HAM) is utilized to acquire the analytical solutions for the problem. Additionally, fluid flow between two stretchable rotating disk with the influence of the thermal radiation is discovered by Zangooee et al. [9]. Additionally, flow and heat transfer of Oldroyd-B nanofluid over a rotating disk is examined by Hafeez et al. [10] and obtained the numerical solutions with the help of bvp midrich scheme in Maple programming. Additionally, flow of viscoelastic fluid caused by a rotating disk was disclosed by Hafeez et al. [11]. In their study they used the Cattaneo-Christov heat flux theory for the formulation of heat equation. Khan et al. [12] scrutinized the swirling flow of non-Newtonian fluid and considered the rotating disk geometry for the motion of the fluid. In their investigation, the thermal analysis is performed in the presence of non-linear thermal radiation and heat absorption/generation. Additionally, some recent articles about fluid flows due to a rotating disk are presented via Refs. [13–18].

This research shows an analytical survey of the flow of viscoelastic Oldroyd-B fluid over a rotating disk. The magnetic field effect is applied normal to the disk. In order to observe the heat and mass transfer processes in the liquid, the Cattaneo-Christov heat and mass flux theories